THE DEVELOPMENT OF AN IN-VITRO IMMATURE ANIMAL MODEL FOR PREDICTING PEDIATRIC FEMUR FRACTURE STRENGTH

by

Fernando Aguel

B.S. in Bioengineering, University of Pittsburgh, 2000

Submitted to the Graduate Faculty of

The School of Engineering in partial fulfillment

of the requirements for the degree of

Master of Science in Bioengineering

University of Pittsburgh

2004

UNIVERSITY OF PITTSBURGH

SCHOOL OF ENGINEERING

This thesis was presented

by

Fernando Aguel

It was defended on

September 22, 2004

and approved by

Mary Clyde Pierce, M.D.,
Associate Professor, Departments of Pediatrics, Rehabilitation Science and Technology

Richard Debski, Ph.D.,
Assistant Professor, Departments of Bioengineering, Orthopedic Surgery

Thesis Advisor: Gina Bertocci, Ph.D.,
Associate Professor, Departments of Bioengineering, Rehabilitation Science and Technology, and Pediatrics

THE DEVELOPMENT OF AN IN-VITRO IMMATURE ANIMAL MODEL FOR PREDICTING PEDIATRIC FEMUR FRACTURE STRENGTH

Fernando Aguel, M.S.

University of Pittsburgh, 2004

Fractures are the second most common presentation of child abuse, soft tissue injury being the most common. Femurs are the most common long-bone fractured in inflicted injury. When a child presents to the emergency department, a clinician must judge if the child's fracture matches the account provided by the caregiver. An objective tool is needed to aid in the assessment of injury plausibility. Predicting femur fracture strength is key to developing this tool. Immature porcine femurs are widely used to model pediatric human femurs. This study investigated immature porcine femur fracture load, energy to failure and stiffness in three-point bending, torsion and axial compression, with and without soft tissue intact and at different displacement rates.

Significant differences exist between three point bending with soft tissue intact (n=6) and devoid of soft tissue (n=6) for stiffness (means=1607.9 lbf/in. and 1981.9 lbf/in, respectively, p=0.046) and energy to failure (means=36.9 in-lbf and 25.0 in-lbf, respectively, p=0.046). Torsion tests show significant differences in the fracture torque between groups tested at 0.167 degrees/sec (n=7) and 90 degrees/sec (n=7, means=30.69 in-lbf and 46.13 in-lbf, respectively, p=0.018). Axial compression experiments at 0.04 in/sec (n=5) resulted in fracture load, energy to failure and stiffness of 273.4 lbf, 70.7 in-lbf and 829.4 lbf/in, respectively, while axial compression experiments at 2 in/sec (n=2) resulted in higher fracture loads, energy to failure and stiffness (441 lbf, 154.2 in-lbf and 1894 lbf/in, respectively).

Three-point bending tests resulted in oblique or transverse fractures, torsion and axial compression tests resulted in spiral and growth plate fractures, respectively. Correlations between bone mineral density and structure geometry showed promise as a predictive model for femur fracture response in all loading mechanisms. Multivariable regression modeling resulted in high R^2 values (0.62 – 0.74) for femurs tested with soft tissue intact in three-point bending, but low values (0.22 – 0.29) for femurs tested devoid of soft tissue in three-point bending; relatively high R^2 values (0.66 – 0.78) for fracture torque in torsion and low R^2 values (0.22 – 0.47) for energy to failure in torsion. Further investigation with a larger sample is needed to reliably predict immature femur fracture response.

TABLE OF CONTENTS

LIST OF TABLES

LIST OF FIGURES

ACKNOWLEDGEMENTS

I would like to acknowledge the Whitaker Foundation and the Children's Hospital of Pittsburgh for funding this research and I would also like to acknowledge the NSF IGERT training grant without which I would never have been able to finish this thesis. I would like to thank Dr. Pierce for providing the inspiration for this line of research for me and helped me understand the clinical aspects of this research, and Dr. Bertocci for her guidance and for making it possible for me to do this research and mentoring me. I would like to thank Dr. Debski and the students and the staff at the MSRC for allowing me to use their lab and equipment; your ideas and training have really helped me tremendously. I would like to thank BC Deemer for his help in my research. In addition, I would like to thank all the rest of the students, staff and faculty in the Bioengineering department at the University of Pittsburgh for their support, in particular Dr. Redfern who advised me as an undergraduate here and Dr. Borovetz to whom I could always go to with any concern or question about my studies.

My Family has always supported me in everything I have done, never more than in my graduate studies. I would like to thank my mom and dad, who offered words of wisdom at crucial times and always helped me remember to take things one step at a time during my times of crisis and to work hard so as to not have any regrets in what I do. I would like to thank my brother, Felipe, for all of his support and suggestions regarding my graduate work and help whenever I needed it. You were all critical to my success in my studies and my life and without you, I would have never gotten this far. And finally, I would like to thank my friends for listening to my problems, special thanks to John Bendick who listened to me throughout my studies and to Susan Frayte who helped me organize my work for the experimental work and during the writing of this document.

1.0 INTRODUCTION

Child abuse and neglect is the leading cause of trauma related death in children 4 years of age and younger (1). Every year nearly 2,000 children die, 18,000 become disabled and 150,000 are seriously injured in the United States alone (*2*). In 1999, over 166,000 cases of physical child abuse were identified(1). In 2002, 896,000 children were victims of abuse and neglect in the United States, almost 179,000 suffering physical abuse (*3*). The highest rates of abuse and neglect occurred in children three years and younger (*4*). Children who were victimized are three times as likely to be victimized again (*2*).

Fractures are the second most common presentation of child abuse and are an indication that the child is being subjected to potentially life threatening trauma (1,5). Long-bone fractures have been identified as the most common fracture seen in inflicted injury (6-9). The most common long-bone fractured from abusive trauma is the femur (10,11). Femur fractures in children younger than 1 year are highly suspect for abuse (7,12-14). In fact, 65% of femur fractures in children younger than 1 year were the result of abuse (15). Transverse fractures of the femur are one of the most common fractures observed in child abuse cases, occurring 3 to 4 times as often as the classic metaphyseal fracture in abused children (12,16).

Fracture type alone however is not enough to determine whether a femur fracture was accidental or caused by inflicted trauma. Low bone strength can make a fracture caused by an

ordinarily benign accident seem dramatic enough to conclude that the injury was inflicted. An objective tool is needed to aid in the assessment of whether a specific femur fracture is the result of accidental or inflicted trauma.

When a child presents to the emergency department (ED), a clinician must make a judgment on whether or not the child's fracture was caused by the account provided by the caretaker or if the fracture was a result of abusive circumstances. Understanding the levels of energy and force required to cause a fracture aids in the assessment of whether the fracture is compatible with the reported cause.

The forces and mechanisms necessary to generate a specific fracture type have not been well studied in the pediatric population. Understanding how the loading mechanism affects fracture type and resulting fracture load and fracture energy is critical to aid a clinician in determining between whether a fracture may have been caused by accidental and inflicted trauma.

When an injured child presents to the emergency department, the caregiver provides an account explaining how the injury occurred. The physician must then judge whether the story matches the child's injury. An objective tool to aid in making this decision would reduce the chances of misdiagnosing child abuse (both false positives and false negatives). This tool would consist of determining the load characteristics associated with common falsely reported accidents and determining the loads necessary to cause fractures. If the expected load characteristics of the specifically reported fall match the loads required to cause the observed fracture, then the physician may conclude that the account of the scenario does match the injury and biomechanical compatibility exists. No further biomechanical investigation is required. However, additional aspects of the case must be evaluated to complete the diagnostic process. If

the expected loads of the accident scenario do not match the load characteristics of the observed fracture, then the physician would pursue a formal comprehensive investigation with children and youth services (figure 1-1).

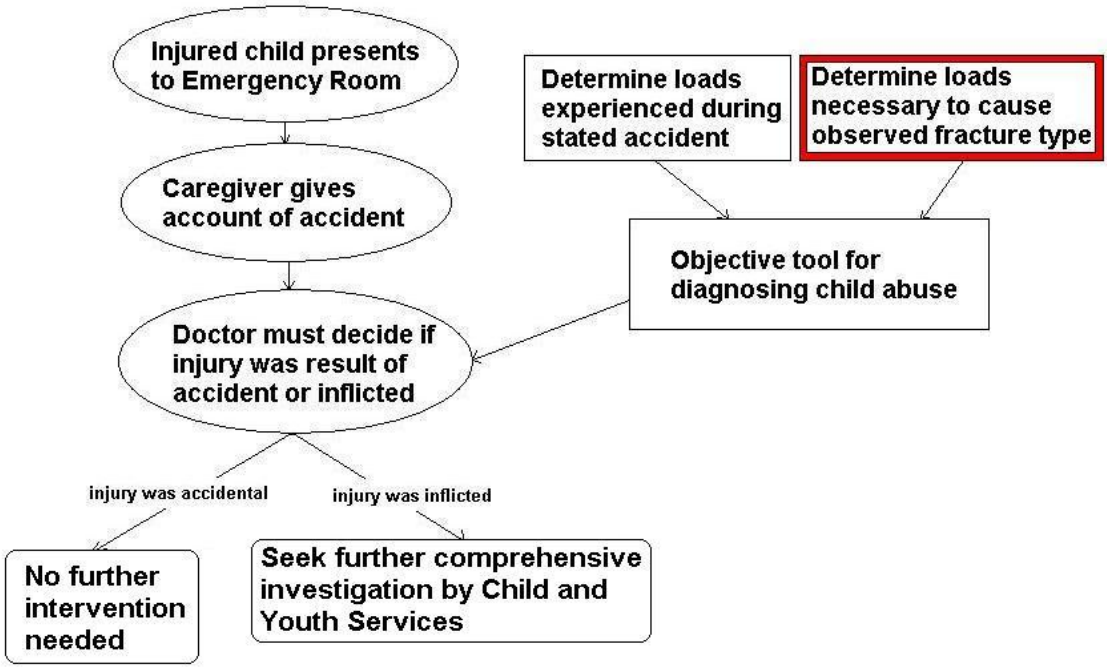

Figure 1-1 Flow chart demonstrating scenario where predicting femur fracture load aids in diagnosing child abuse

2.0 BACKGROUND

2.1 PREVIOUS RESEARCH

A predictor of fracture strength, or femur structural capacity, is key to developing a tool to aid the clinician in determining whether a fracture was caused by accidental or inflicted trauma. When studying any structure (eg. Steel beam, femur), one must consider several factors such as the geometry of the structure (eg, the cross sectional area and shape), as well and the material which makes up the structure. Measurements of femoral geometry could be obtained by measuring the radiographs taken in two anatomical positions (medial-lateral and antero-posterior). An indicator of bone strength, bone mineral density (BMD) can be measured by performing dual energy x-ray absorptiometry (DEXA) scans. DEXA is a technique by which the mineral content of a bone is calculated from measuring the absorption of x-rays by the bone. BMD measured from a DEXA scan is calculated in grams per square centimeter (areal density rather than volumetric).

In attempting to develop a predictor of femur fracture strength, one must first begin with an animal model before proceeding to human tests. Animals have been used extensively when investigating long-bone strength (17-21). Several studies have investigated bone mineral density

(BMD) as a bone strength predictor, and investigated the relation between BMD and bone cross sectional area to bone strength. In these studies, investigators succeeded in correlating mature (porcine, bovine, canine and rat) femoral bone strength to the BMD (using DEXA, qCT and ultrasound methods) and cross sectional area (17-21). Both qCT and ultrasound speed of sound measurements of BMD have been found to have strong correlations to DEXA measures of BMD (17,19).

2.1.1 Bone Mineral Density Deficiency Studies

DEXA scans measure bone mineral content (BMC) and BMD (areal density) which are indicators of bone strength (17,22-26). DEXA scans were performed on frozen femurs dissected both with and without soft tissue intact (if specimen was to be tested without soft tissue, it was DEXA scanned without soft tissue and vice versa).

Mice and rats have been used as models of osteogenesis imperfecta and evaluation of the effect of diet on bone strength (18,27-29). Three of these studies utilized DEXA scans for measuring bone mineral density and bone mineral content (BMC) when evaluating bone strength in three-point bending and found BMD to be a significant indicator of bone strength (18,27,28).

Saban investigated the strain of mouse that exhibits the osteogenesis imperfecta (oim) phenotype. The mice were grouped by genotype, that is there was a homozygous oim group, a homozygous non-oim group and a heterozygous oim group (30). Femurs of the mice of each group were tested in four-point bending at a displacement rate of 0.5 millimeters per minute and were shown to have statistical differences between all groups in ultimate load, energy to failure

and stiffness (p=0.001), except when comparing the stiffness of the femurs of the heterozygous oim group to the non-oim group (30).

Calero investigated the effect of BMD (acquired by ultrasound measurements) on resistance to torsion (17). Calero et al. compared the resistance to fractures caused by torsional loading in healthy rats with ooforectomized (surgical removal of one or both ovaries) rats in order to study the effect of BMD on fractures caused by torsional loading. Four groups of 12 week old rats were studies, two groups were controls which were used to compare to the ooforectomized rats three weeks after surgery and six weeks after surgery (controls underwent surgical trauma but were not ooforectomized). The rat femurs (n=74) were dissected, analyzed by DEXA scans, ultrasound speed of sound measurement and tested to failure in torsion (10 degrees per minute) (17). The femurs of each pair of groups showed statistically significant differences between DEXA obtained BMD (BMD_{DEXA}), ultrasound speed of sound (SOS) and torque to fracture (p=0.001, 0.05 and 0.05 respectively) (17). This study found correlations between BMD_{DEXA} and SOS (r=0.39, p=0.0008) showing that SOS compares well to DEXA methods for evaluating BMD; and BMD_{DEXA} and the failure torque of the femur (r=0.31, p=0.03), showing that the torque to failure increases as BMD of the femur increases (17).

Pierce et al. investigated the failure strength of immature porcine femurs (n=22, age: 3 to 12 months, weight: 3.6 to 7 kg) and their correlation to BMD, BMC and geometric measures (inner and outer diameter, length) (1). Three point bending was performed (n=15) to failure at a displacement rate of 1 millimeter per second (1). Torsion testing to failure was also performed (n=7) at displacement rates of 1 degree per second (1). Three point bending fracture load was found to range from 530 N to 1024 N (mean=726 N, SD=138 N) (1). Torsion fracture torque was found to range from 1383 N-mm to 3559 N-mm (mean=2703 N-mm, SD=826 N-mm) (1).

Statistical regression was used to determine an empirically derived parameter (BPAR= function of BMD, BMC, mass, length, length between growth plates, inner diameter, outer diameter) to correlate to failure load, failure moment and energy to failure in bending (r^2=0.84, r^2=0.92, r^2=0.88; $p<0.001$, $p<0.00005$, $p<0.05$ respectively) (1).

2.1.2 Effect of Displacement Rate on Fracture Load

Another study investigated the relation between BMD and bone longitudinal cross sectional area with fracture load in three-point bending of immature porcine femurs and humeri (25). Koo et al. tested the long bones at two different displacement rates (0.1 millimeters per second and 1millimeters per second) to investigate the effect of displacement rate on fracture load (25). This study utilized DEXA scans to measure BMD but rather than use the bone cross sectional area, the investigators used the bone longitudinal cross sectional area (ie. the area of the shadow produced by shining a light perpendicular to the axis of the bone) (25). This study found strong correlations between bone mineral density and the energy to failure, moment at failure and flexural stiffness for the long bones tested (25). However, based on engineering principles, structural resistance to fracture is more likely related to the cross sectional area of the femur, and not the longitudinal bone area.

2.2 BEAM THEORY

Though bones are biologic tissue, they can be considered an engineering solid and engineering solid mechanics can be applied to the analysis of bone response to loading in various fracture modes. Classic beam theory states that the strength of a solid structure is a function of the cross sectional area of the structure (31). This theory takes on different forms for each mode of loading.

2.2.1 Bending

In bending, the applicable function of cross sectional area is called the area moment of inertia. The area moment of inertia, I, is a measure of a beam's resistance to bending. The area moment of inertia for hollow rod of concentric circular cross section that can be used to approximate a long bone is given in equations 1 and 2 where r_o is the outer radius, r_i is the inner radius, D_o is outer diameter and D_i is inner diameter (31).

$$I = \frac{\pi}{4}\left(r_o^{\,4} - r_i^{\,4}\right) \qquad (1)$$

or

$$I = \frac{\pi}{64}\left(D_o^{\,4} - D_i^{\,4}\right) \qquad (2)$$

The area moment of inertia can be normalized to the outer radius of the beam resulting in equation 3 and 4 (31). This normalized parameter is called the section modulus, Z.

$$Z = \frac{\pi}{4r_o}\left(r_o{}^4 - r_i{}^4\right) \qquad (3)$$

or

$$Z = \frac{\pi}{32D_o}\left(D_o{}^4 - D_i{}^4\right) \qquad (4)$$

2.2.2 Torsion

The polar moment of inertia is a measure of a beam's resistance to torsion. This is also the case with a long bone. The polar moment of inertia, J, for a hollow rod of concentric circular cross section is given in equations 5 and 6 where r_o is the outer radius, r_i is the inner radius, D_o is outer diameter and D_i is inner diameter (31).

$$J = \frac{\pi}{2}\left(r_o{}^4 - r_i{}^4\right) \qquad (5)$$

or

$$J = \frac{\pi}{32}\left(D_o{}^4 - D_i{}^4\right) \qquad (6)$$

2.2.3 Buckling

In axial compressive loading, buckling is what would normally be of concern in traditional beam theory. However, what is typically referred to as a buckle fracture (in bone) is a result of axial compression, but not a result of beam buckling, but rather beam compression fracture. Beam buckling states that in an axially compressed beam, the beam will bow out at or near half the

length of the beam and cause failure ultimately from the bending that is induced. In the case of immature porcine femurs in axial compression, a buckle or impaction (or compression) fracture is what actually results from axial compression testing. This is because the slenderness ratio of the immature porcine femur does not exceed the strength limit for the material and therefore should be considered a short column (*32*). Mechanics of materials states that the key factors of the measure of resistance is the material which constitutes the beam and the cross sectional area of the beam (31). The cross sectional area, CSA, for hollow rod of concentric circular cross section is given in equations 7 and 8 where r_o is the outer radius, r_i is the inner radius, D_o is outer diameter and D_i is inner diameter (31).

$$CSA = \pi\left(r_o^{\,2} - r_i^{\,2}\right) \qquad (7)$$

or

$$CSA = \frac{\pi}{4}\left(D_o^{\,2} - D_i^{\,2}\right) \qquad (8)$$

3.0 OBJECTIVE AND SPECIFIC AIMS

3.1 OBJECTIVE

The objective of this project was to develop an in vitro animal model for predicting pediatric femur fracture strength. This model must account for bone developmental progress. Towards this objective, immature femurs were mechanically tested to various loading conditions (tested using different displacement rates and both with and without soft tissue intact). Relationships between fracture strength, stiffness, strain energy to failure and bone geometry, bone mineral content (BMC) and bone mineral density (BMD) were also investigated.

3.2 SPECIFIC AIMS

Specific Aim #1: Investigate the effect of loading rate on fracture load, stiffness and strain energy to failure of immature porcine femurs.

Hypothesis #1: Faster loading rates will increase the fracture load, stiffness and strain energy to failure.

Specific Aim #2: Investigate the effect of soft tissue presence on fracture load, stiffness and strain energy to failure of immature porcine femurs.

Hypothesis #2: The presence of soft tissue will have no effect on the stiffness or fracture load while increasing the strain energy to failure.

Specific Aim #3: Develop a model for predicting the fracture load, stiffness and strain energy to failure of immature porcine femurs based on BMC and BMD data from DEXA scans and bone geometry measured from radiographs.

Hypothesis #3: Femur fracture load and strain energy to failure will be correlated with DEXA and radiograph data.

4.0 METHODS

Immature porcine femurs were tested in three loading mechanisms, three point bending, torsion and axial compression. Femurs tested in three point bending were divided into two groups: femurs tested with soft tissue intact (n=6) and femurs tested devoid of soft tissue (n=6). Both groups tested in three point bending were tested at a displacement rate of 2 inches per second. Femurs tested in torsion were separated into two groups as well: femurs tested at a displacement rate of 0.167 degrees per second (n=7) and femurs tested at a displacement rate of 90 degrees per second (n=7). The immature porcine femurs tested in axial compression were similarly separated into two groups: femurs tested at 0.04 inches per second (n=5) and femurs tested at a displacement rate of 2 inches per second (n=2). Specimens tested in torsion and axial compression were tested devoid of soft tissue while leaving the periosteum intact. Research performed was approved by the University of Pittsburgh's Institute for Animal Care and Use Committee protocol number 0304451.

4.1 SPECIMEN

Porcine legs were obtained (Thomas D. Morris Inc., Towson MD 21286) and shipped frozen, packed with ice. The porcine legs were immediately put in freezers at -20^{o}C. The porcine legs were thawed by removing them from the freezer and placing them in a room temperature setting. After thawing (approximately 30 hours), the hind legs were disarticulated at both the hip joint and the knee joint. During dissection for disarticulation, the femurs were separated at the hip by severing the iliofemoral ligaments, the pubofemoral ligament and the ligamentum teres carefully to avoid cutting the periosteum and the bone. The knee was disarticulated by dissecting away the patella and severing the ligaments of the knee, including the anterior cruciate ligament, the posterior cruciate ligament, the medial collateral ligament and the lateral collateral ligament. The meniscus was also carefully removed without cutting into the bone or the periosteum.

4.1.1 Three Point Bending test specimen preparation

Twelve femurs were disarticulated at the hip and knee for testing in three point bending. The femurs were then divided into two groups of six with one femur from each piglet assigned to a group and the contralateral femur assigned to the other group. The femurs in one group were left unaltered with all soft tissue intact, including the skin (group 1, n=6). The femurs in the other group were dissected free of all soft tissue except for the periosteum (group 2, n=6). Once prepared, the femurs were wrapped in physiologic saline solution (0.9% saline) soaked gauze to avoid dehydration of the bone and frozen at -20^{o} C.

4.1.2 Torsion test specimen preparation

Fourteen femurs were disarticulated at the hip and knee in the previously described fashion. All femurs which were tested in torsion were dissected free of soft tissue, leaving the periosteum intact. Femurs were divided into two groups of seven with one femur from each piglet assigned to one group (Group 3: femurs which were tested in torsion at an angular displacement rate of 0.167 degrees per second) and the contralateral femur assigned to the other group (Group 4: femurs which were tested in torsion at an angular displacement rate of 90 degrees per second). Once prepared, the femurs were wrapped in physiologic saline solution (0.9% saline) soaked gauze to avoid dehydration of the bone and frozen at -20^{o} C.

4.1.3 Axial Compression test specimen preparation

Fourteen femurs were disarticulated at the hip and knee as previously described. All femurs which were tested in axial compression were dissected free of soft tissue, leaving the periosteum intact. Femurs were then divided into two groups, one group of femurs (group 5, n=5) was tested at a displacement rate of 0.04 inches per second and the other group (group 6, n=2) was tested at a displacement rate of 2 inches per second. Once prepared, the femurs were wrapped in physiologic saline solution (0.9% saline) soaked gauze to avoid dehydration of the bone and frozen at -20^{o} C.

4.2 RADIOGRAPHY

Once the prepared specimens were ready to be tested, the frozen femurs underwent dual-energy x-ray absorptiometry (DEXA) scans to measure the bone mineral content (BMC) and bone mineral density (BMD) of each femur. Following DEXA scans, the femurs were then allowed to thaw by placing them in a cold room kept at constant temperature of 4^{o} C for no more than 24 hours. Once thawed, the femurs were radiographed in the medial-lateral (M-L) and antero-posterior (A-P) directions. The femurs were tested within 2 hours of being x-rayed.

DEXA scans were conducted using a Lunar Prodigy scanner (GE Lunar Corp., Madison Wisconsin, USA). DEXA scans measure areal bone mineral content (BMC) and bone mineral density (BMD), and are readily available at most hospitals. DEXA scanners can be used to scan whole bodies or portions of patients, as well as research specimens such as immature porcine femurs. Each femur was analyzed individually for BMC and BMD.

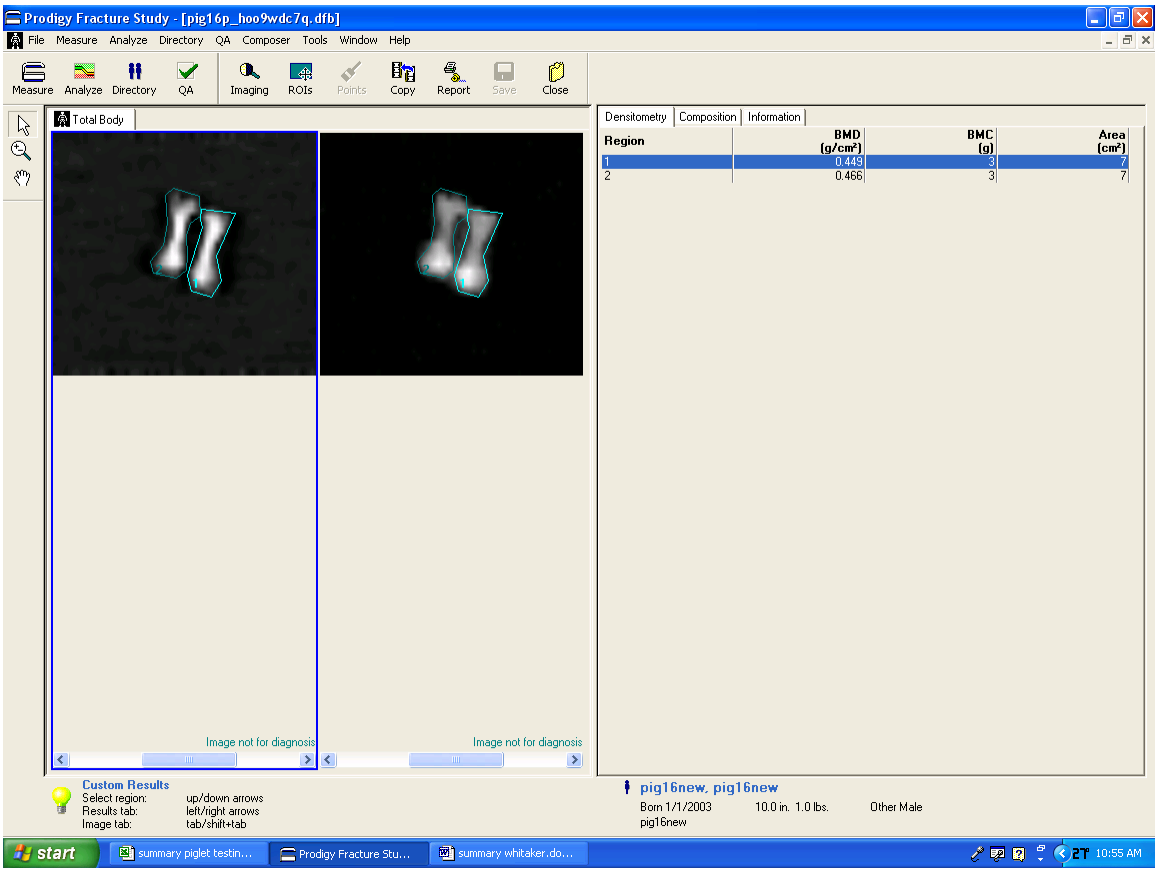

Figure 4-1 Lunar enCORE software (GE Lunar Corp., Madison Wisconsin, USA) utilized in analyzing DEXA scans of immature porcine femurs

X-rays of the immature porcine femurs were taken just before being tested. M-L x-rays were taken as well as A-P x-rays. From each view, measurements of diaphysis outer diameter (OD), diaphysis inner diameter (ID) and length between growth plates (GPL) were taken using hand calipers (accurate to 0.01 inches, product code: MEASECALIPER, General Graphics, Kaysville UT 84037) at the location of the minimum aspect ratio of the femur. Since the femur diaphysis is generally considered to have a circular cross section, the measurements taken from each view was averaged to obtain a good representation of the actual size of the femurs.

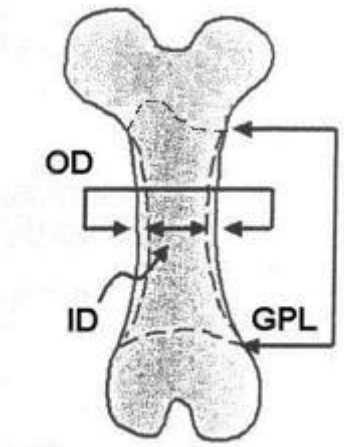

Figure 4-2 Femoral geometric data measured from radiographs in A-P and M-L views

4.3 TESTING APPARATUS

All Femurs were tested using an Instron model # 8251 (Canton, MA, 02021) servo-hydraulic universal testing system (UTS). The UTS consists of a single actuator which is driven by hydraulics which applies a load from above the specimen and a stationary platform where the load cell is mounted. The actuator can move in two degrees of freedom, translational motion along the axis of the actuator and rotation about the longitudinal axis of the actuator. The load cell (Lebow model # 6467, Troy MI, 48084) is a two degree of freedom load cell and can measure force in the direction of motion of the actuator, as well as moments about the rotational axis of the actuator. The load cell is capable of measuring loads of up to ±5,000 lbf and ±1000 in-lbf. Load cell resolution was 0.25 lbs. and 0.025 ft-lbs.

4.4 DATA ACQUISITION

A universal data acquisition program was designed and coded for use in all tests performed for this project. The data acquisition system was developed using Labview (Version 6.0, National Instruments Corporation, Austin, Texas) to measure and collect femoral loads, moments and translational and angular displacements during testing and log the data to a file. Data acquisition rates were user selected in order to accommodate different loading/displacement rates. The data acquisition rates were selected so that the data points would accurately capture the fracture load and the complete loading data. The data acquisition rate for all three-point bending tests was chosen to be 2000 Hz. The data acquisition rate for torsion tests were selected on the basis of the displacement rate, the data for specimens tested at the higher displacement rate (90 degrees per second) were collected at 2000 Hz, while the data for specimens tested at the lower displacement rate were collected at 100 Hz. Data for specimens tested in axial compression were collected at 2000 Hz.

4.5 THREE POINT BENDING

The disarticulated immature porcine femurs were separated into two groups, femurs with soft tissue still attached (group 1, n=6) and femurs devoid of soft tissue (group 2, n=6). Both groups were tested at displacement rates of 2 inches per second. Femurs were placed on the three point bending supports oriented such that the middle support (actuator) applies the load to the posterior

of the femur (figure 4-3). In cases where the femurs were tested with soft tissue intact, the femoral head and condyles were dissected in order for the outer supports of the three-point bending test jigs to be in contact with the femoral head and condyles, while leaving all other soft tissue present, including the soft tissue on which the middle support acted. In all cases, the outer supports were separated one inch and three quarters. This separation represents a distance equal to three quarters the distance between the growth plates (cartilage between the epiphysis and metaphysic where the longitudinal growth of the bone takes place) on average across all femurs. The femurs were supported inside of the growth plates to reduce the potential for shearing at the growth plates. The outer supports of the three point bending test jigs were attached to the UTS load cell in order to measure the load applied normal to the femur during three-point bending. The femur was placed onto the two supports and the middle support of the three-point bending test jig was attached to the UTS actuator, acting downward onto the femur.

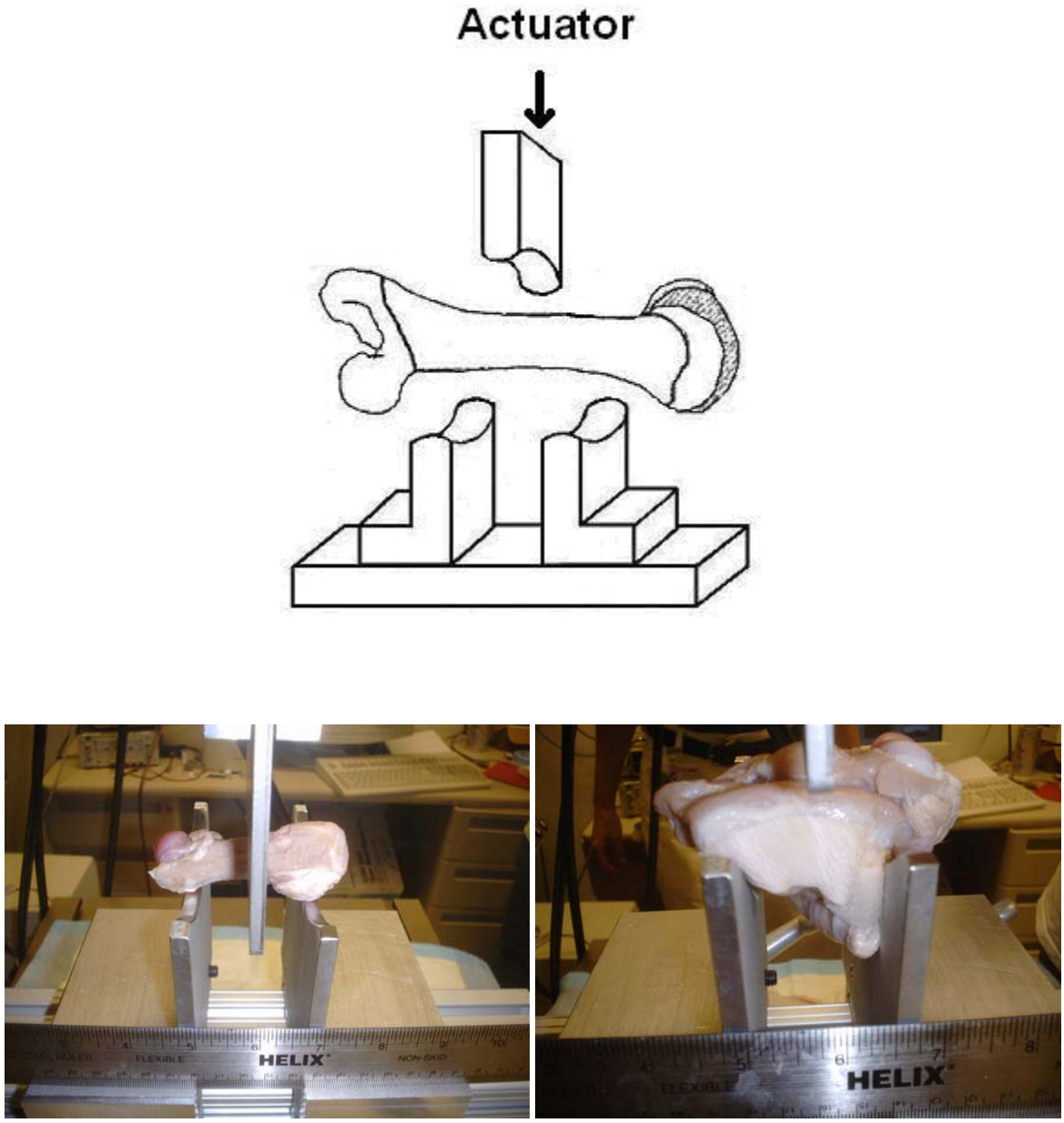

Figure 4-3 Illustration and pictures of three-point bending testing jig

4.6 TORSION

Torsion testing jigs manufactured and one potting block was attached to the actuator via a universal joint, and the other potting block was attached to the load cell via a second universal joint. Torsion test jigs incorporated the use of universal joints (Steel Pin & Block Single U-Joint with Keyway, part no. 8285K33, McMaster-Carr, Los Angeles, CA 90670) to minimize artifact bending caused by improper alignment and the natural curvature of the femur. The potting blocks were manufactured using one half inch thick aluminum plate and the internal measurements (potting volume) were 2in x 2in x 2in. Potting material (Bondo automotive body filler, Bondo Corp., Atlanta GA 30331) and hardener was mixed according to product specifications and potted before hardening. Since the potting material heats during hardening, the block was kept cool by running cool water over it. The potting material and pins (1/16 inch diameter steel rods inserted into the diaphyses of the femur within one quarter inch of the growth plate of the femurs and submerged in the potting material) were used to pot the femur ends to apply the torque. Pins were utilized to aid in fixing the femoral head and condyles in the potting material because the periosteum and small amount of soft tissue (no more than 1/16 inch of tissue left to prevent cutting into periosteum or bone) remained on the femur thus the potting material could not rigidly bond to the femur ends. The use of inserted pins allowed for the potting material to bond to the pins themselves and use the pins to apply the motion to the femur. Small holes (3/64 inch diameter) were drilled into the bone where the pins were inserted making sure to make the drilled holes slightly smaller than the pins that were inserted into these holes. Two groups of femurs were tested in torsion, one group tested at an angular displacement rate of 0.167 degrees per second (n=7) and the other group was tested at an angular displacement rate of 90 degrees per second (n=7). Post-test radiographs were inspected to check if the fracture

originated at the pin insertion. Had any fractures originated at the pin insertion, the test results would have been discarded due to the uncertainty of whether or not the fracture resulted from the stress riser created by the inserted rod. Torsion test jigs are illustrated in figure 4-4. The potting block with the distal end of the femur (femoral condyles) was attached to the UTS load cell in order to measure the torque applied to the femur during loading.

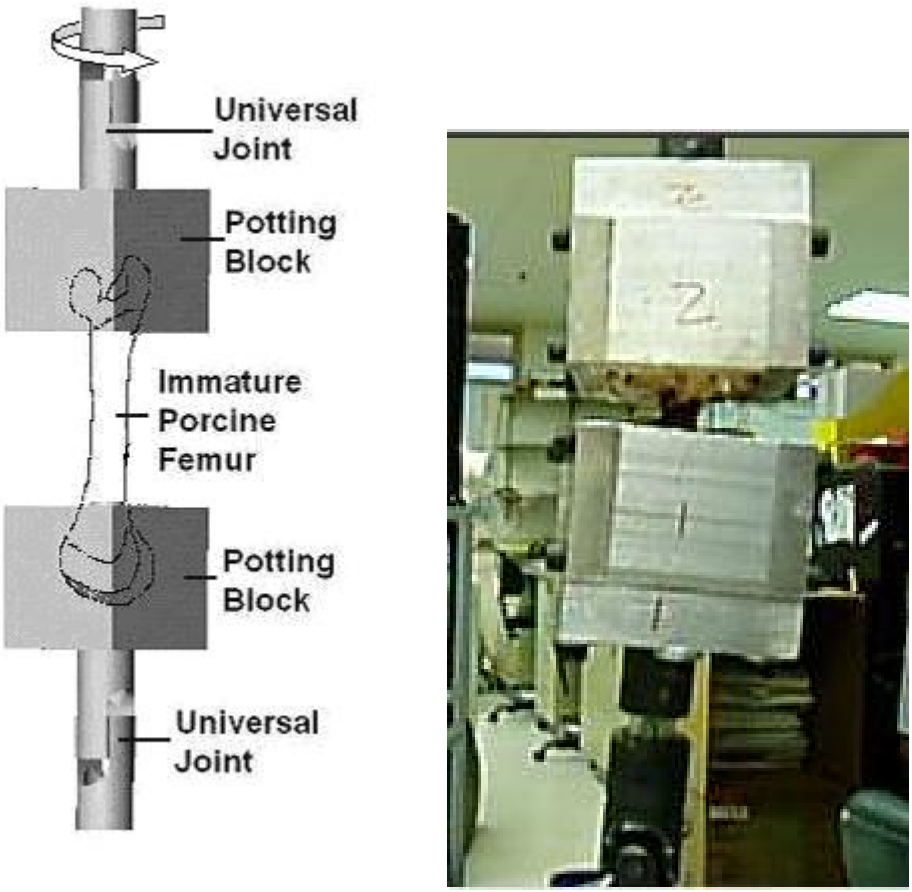

Figure 4-4 Illustration and picture of torsion testing jig

4.7 AXIAL COMPRESSION

Axial compression test jigs included a single potting block in which the proximal end of the femur (femoral head) was potted. Femurs were potted in the block using Bondo auto body filler and were aligned by visual inspection (the femur was aligned using a straight edge rule to ensure that the midline of the femoral shaft was properly aligned) to minimize bending on the femur. The potting block with the proximal end of the femur was attached to the actuator and loaded onto the femoral condyles. The femoral condyles were partially potted (only half of the condyles were submerged in the potting material) in order to prevent lateral slipping of the condyles on the flat surface onto which the femurs were compressed. The potting block containing the distal end of the femur (condyles) was mounted onto the load cell of the UTS to prevent lateral motion of the potting block (preventing bending) and measure the force applied to the femur.

Femurs were tested in axial compression at displacement rates of 0.04 inches per second (group 5, n=5) and 2 inches per second (group 6, n=2) to identify any effect that loading rate may have on the fracture load, stiffness and strain energy to failure of the femur uneven number of specimens were tested in this manner due to the limited number of specimens and since the specimens were failing at the growth plate, the slower displacement rate was chosen to investigate the axial compression tests in a more controlled manner.

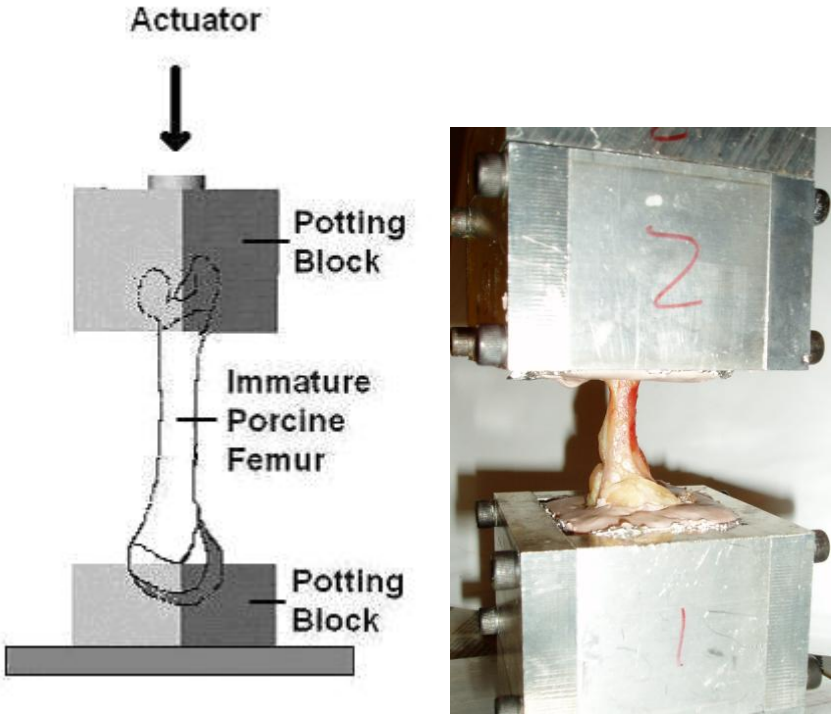

Figure 4-5 Illustration of axial compression testing jig

4.8 DATA ANALYSIS

Data was processed post testing to determine bone fracture load, stiffness and strain energy to failure. Measured variables associated with the slower strain rates were compared to those from the higher strain rates in specimens tested under torsion and axial loading. Variables measured from femurs tested with and without soft tissue were compared to determine the effect of soft tissue when specimens are subjected to bending loads. A mathematical model for predicting fracture strength based on bone geometry, BMC and BMD was developed.

Fracture load, energy to failure and stiffness were evaluated for each loading curve (force vs displacement) using Excel spreadsheet software (Microsoft Office XP, Microsoft Corp.,

Redmond WA 98052). Fracture load was defined as the highest load of the loading curve. The stiffness of each specimen was calculated by curvefitting a line to the linear portion of the force vs displacement curve (typically, from half the fracture load to 90% of the fracture load). Strain energy to failure was calculated using the trapezoid rule to measure the area beneath the force vs displacement curve until the point of fracture.

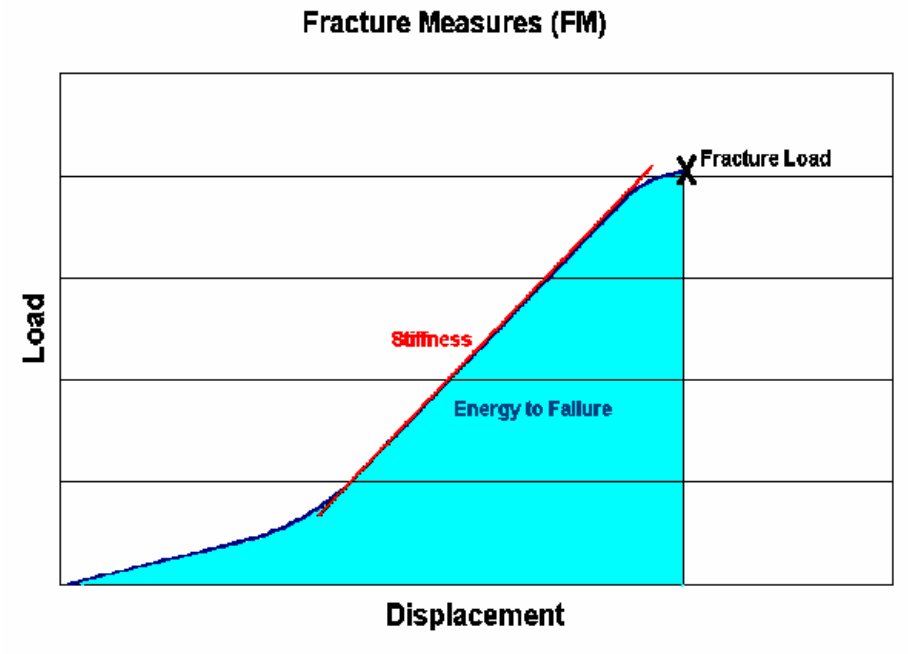

Figure 4-6 Determination of fracture measures

Distribution analysis, comparison of means, correlation and regression analyses were performed using SPSS software (version 10.0, Chicago IL 60606). Kurtosis and skewness of the fracture load distribution, stiffness distribution and energy to failure distribution were calculated in order to check for normality. Wilcoxon matched-pairs signed-ranks tests were performed to detect statistically significant differences in fracture load, stiffness and strain energy to failure between groups tested in three-point bending with and without attached soft tissue structure intact, between groups tested in torsion at displacement rates of 10 degrees per minute (0.167

deg/sec) and 5400 degrees per minute (90 deg/sec) and between groups tested in axial compression at displacement rates of 0.04 inches per second and those tested at 2 inches per second. Non-parametric statistical analysis was performed to study the relation between femur radiographic measures (BMD, BMC, Z) with fracture load, stiffness and strain energy to failure. Correlation coefficients (Spearman's rho) were evaluated for variables and parameters under each loading condition as illustrated in table 4-1.

Table 4-1 Correlations evaluated between fracture measures and geometric and radiographic data

	I	BMD	I*BMD	I*BMD*BMC
Fracture Load	x	x	x	x
Stiffness	x	x	x	x
Strain Energy to Failure	x	x	x	x

In order to more quantitatively describe the relationship between the fracture measures and the radiographic and geometric measures, a regression model was developed to predict the fracture measures. Multivariable regressions were performed entering the variables as a block (enter method) for each fracture measure (fracture load, stiffness and energy to failure) to the geometric and radiographic data (BMD, BMC and I or J or CSA) for both loading conditions in three point bending tests and both loading conditions in torsion tests. The models developed utilized the unstandardized coefficients in the regression model equations which are reported in the results section.

5.0 RESULTS

Fracture load, stiffness and energy to failure were calculated for each specimen (Stiffness was not calculated for torsion tests due to the non-linearity of the loading curve). The data for each loading mechanism (three point bending, torsion and axial compression) was separated into 2 groups (with and without soft tissue for the three-point bending loading mechanism and low and high displacement rates for the torsion and axial compression mechanisms). The Fracture measures (fracture load, stiffness and energy to failure) were compared between groups to detect statistically significant differences between the groups. Fracture measures were correlated to bone densitometry data and geometry data in order to develop a model for predicting femur fracture strength. Multivariable regressions of several different forms were explored, including linear models of several different forms and exponential models. It was determined that the linear models were the best fit for this data.

5.1 THREE POINT BENDING

The immature porcine femurs tested in three point bending were groups by whether they still had soft tissue intact (group 1, n=6) or whether the soft tissue had been removed from the femur (group 2, n=6). Fracture load, energy to failure and stiffness were calculated for each specimen.

Table 5-1 Summary of radiographic and geometric parameters in three point bending tests

	Average Inner Radius(in)	Average Outer Radius (in)	Growth Plate Length (in)	Z (in^3)	BMC (g)	BMD (g/cm^2)
Group 1, n=6						
Mean	0.110	0.220	2.244	0.008	4.31	0.51
Range	0.095 – 0.131	0.211 – 0.232	2.178 – 2.327	0.007 – 0.009	3.87 – 5.21	0.422 – 0.567
S.D.	0.013	0.008	0.057	0.001	0.488	0.053
Group 2, n=6						
Mean	0.110	0.206	2.317	0.006	5.04	0.57
Range	0.094 – 0.130	0.192 – 0.218	2.203 – 2.386	0.005 – 0.007	3.33 – 6.68	0.481 – 0.690
S.D.	0.015	0.011	0.072	0.001	1.092	0.073

A representative load deformation curve is shown in figure 5-1. As previously mentioned, the fracture load can be seen as the highest point on this curve and the stiffness can be observed as the linear region of the upward sloping part of the curve. The energy to failure is the area under this curve up to the fracture point. Load vs deformation curves for group 1 are shown in appendix A and for group 2 in Appendix B.

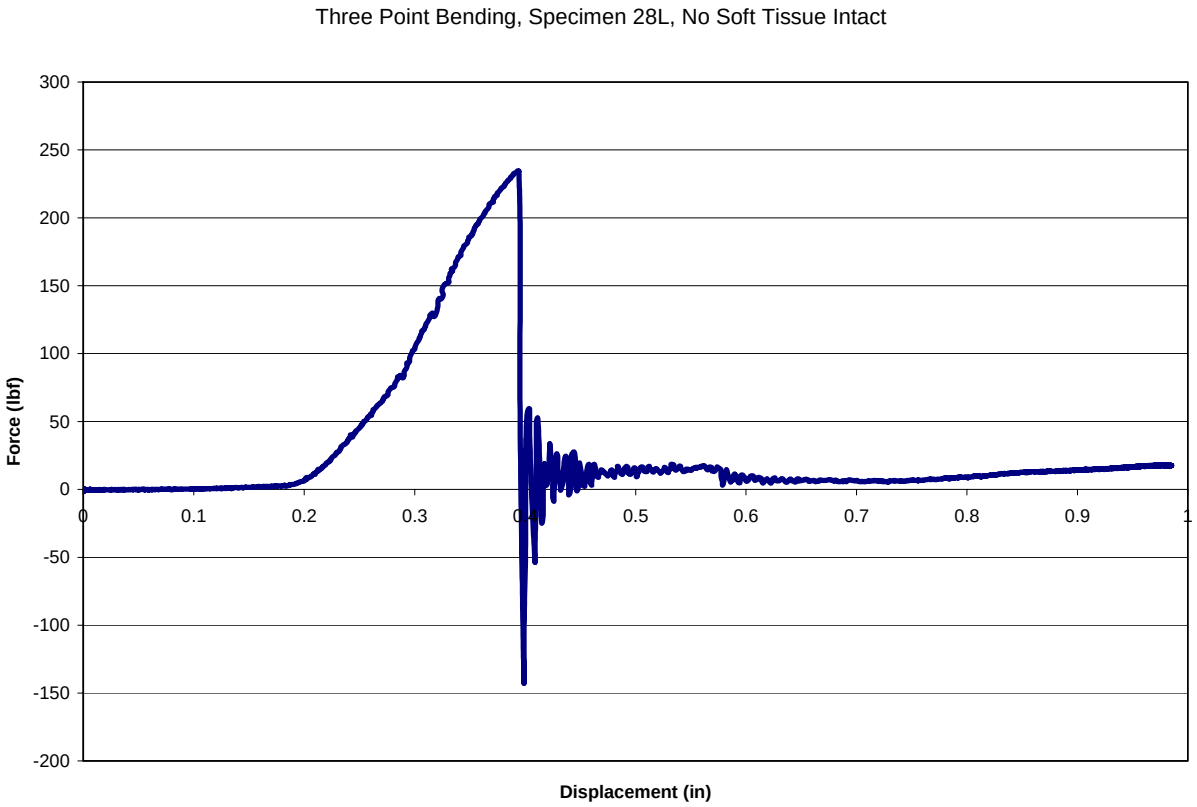

Figure 5-1 Load – deformation curve for specimen 28L, tested in three point bending devoid of soft tissue

5.1.1 Fracture Morphology (Three Point Bending)

Radiographs were taken post testing of each specimen and showed that all specimens failed with oblique fractures or transverse fractures. Furthermore, all specimens in group 2 showed transverse fractures whereas four of the femurs in group 1 showed transverse fractures and the other two specimens showed oblique fractures. All fractures, whether transverse or oblique occurred at the mid diaphysis of the femur as shown in figure 5-1.

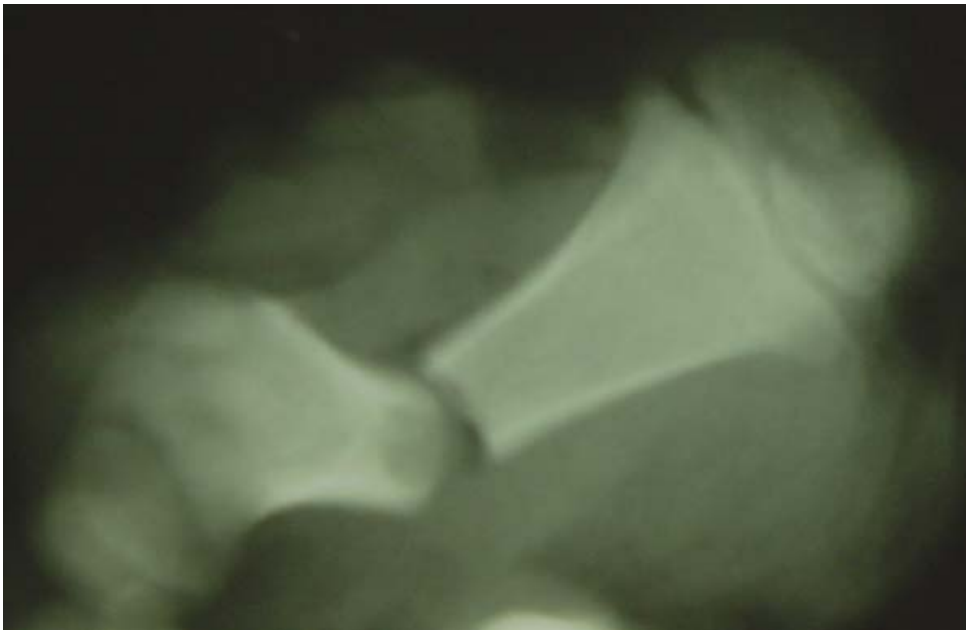

Figure 5-2 X-ray showing transverse fracture of femur tested in three-point bending with soft tissue intact

5.1.2 Statistical Analysis (Three Point Bending)

Statistical analysis was performed on the data in order to test the hypotheses 2 and 3. The fracture load, energy to failure and stiffness were determined and are summarized in table 5-1.

Table 5-2 Summary of fracture measures in three-point bending

	Fracture Load (lbf)	Stiffness (lbf/in.)	Energy to failure (lbf*in.)
Group 1 (Soft tissue intact, n=6)			
Mean	290.2	1607.9	36.9
Range	252.9-321.9	1218.8-2125.2	26.9-49.4
Standard Dev.	27.5	402.9	8.3
Group 2 (No soft tissue, n=6)			
Mean	286.0	1981.9	25.0
Range	234.7-321.0	1540.5-2278.3	21.4-29.4
Standard Dev.	30.6	268.2	2.9

The data from two groups of data were analyzed using SPSS software (SPSS Inc., Chicago, IL). A one-sample Kolmogorov-Smirnov test was used to compare the data from each group to a normal distribution. In both cases the data indicates that a normal distribution can not be assumed. Therefore non-parametric statistics were used to compare the means of the fracture measures of the two groups and both parametric and non-parametric techniques were used to determine correlations between the fracture measures of each specimen and radiographic data.

5.1.2.1 Comparison of means (Three Point Bending) A Wilcoxon matched-pairs signed-ranks test was used to compare whether the fracture load, stiffness and strain energy to failure had statistically significant differences between the groups. The data indicates that there is no statistically significant difference between the fracture load of each group ($p=0.917$), though there was statistically significant differences between groups for stiffness and strain energy to failure ($p=0.046$ and $p=0.046$ respectively).

5.1.2.2 Correlations (Three Point Bending) Fracture loads, stiffnesses and energies to failure for each group were correlated with BMD, Z, BMD*Z, BMD*BMC*Z. The results for each group are shown in the table below. In the cases where the immature porcine femurs were tested with soft tissue intact, the correlations show that fracture load are weakly correlated to BMD*BMC*Z (spearman's rho = 0.371) and stiffness has a strong correlation to BMD*BMC*Z (spearman's rho = 0.714) while energy to failure is weakly correlated to Z (spearman's rho = 0.314). In the cases where the immature porcine femurs were tested without soft tissue intact, the correlations show that fracture load has a strong indirect correlation to BMD*Z (spearman's rho = -0.714) and stiffness has a weak indirect correlation to BMD*Z (spearman's rho = -0.371) while energy to failure has a very strong indirect correlation to BMD (spearman's rho = -0.943, $p<0.01$).

Table 5-3 Correlations coefficients of fracture measures and radiographic and geometric data in three-point bending

	BMD	Z	BMD * Z	BMD * BMC * Z
Group 1 (Soft tissue intact, n=6)				
Fracture Load	0.143	-0.086	0.029	0.371
Stiffness	0.543	-0.086	0.314	0.714
Energy to failure	-0.257	0.314	0.086	-0.086
Group 2 (No soft tissue intact, n=6)				
Fracture Load	-0.657	-0.371	-0.714	-0.486
Stiffness	-0.371	0.029	-0.371	-0.029
Energy to failure	-0.943**	0.429	-0.314	-0.429

** Significant at 0.01 level

5.1.2.3 Multivariable Regression (Three Point Bending) Multivariable Regression was performed on the data in order to develop a predictive model for fracture load, energy to failure and the stiffness for both groups tested in three point bending. The regressions produced the following equations for predicting the fracture load, energy to failure and stiffness of immature porcine femurs when tested in three-point bending with all soft tissue intact (group 1).

$$FxLoad = 20.2 * BMC - 428.5 * BMD - 12434.4 * Z + 518.2 \quad (9)$$

$$Energy = 2.8 * BMC - 113.6 * BMD + 3725.6 * Z + 53.5 \quad (10)$$

$$Stiffness = 591.5 * BMC - 4078 * BMD - 96083.5 * Z + 1885.8 \quad (11)$$

The values calculated from three point bending are plotted to the values calculated from the models and the coefficient of determination (R^2) is reported for each.

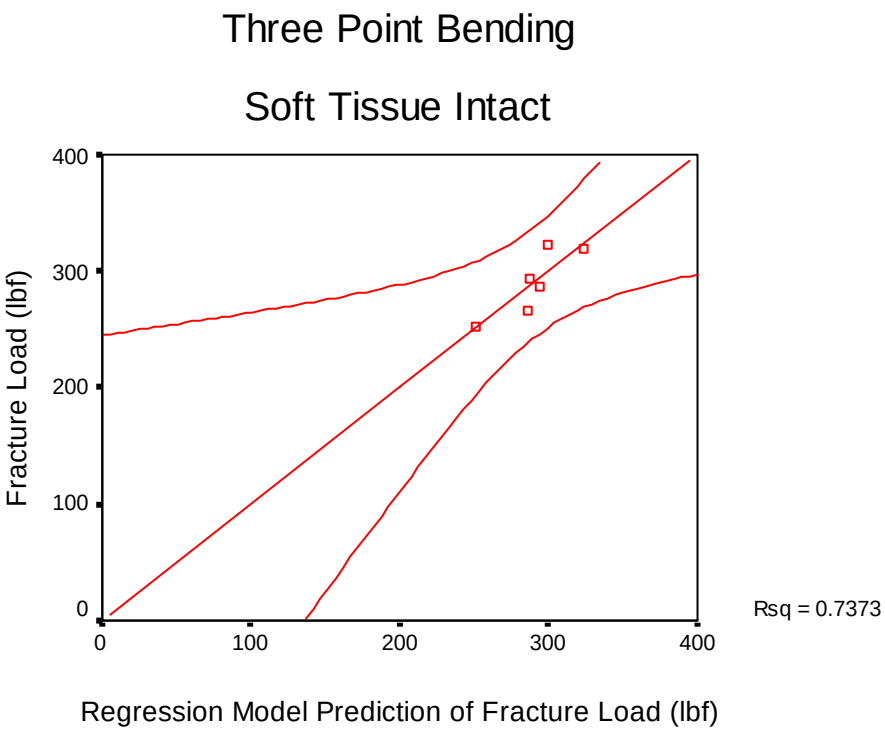

Figure 5-3 Comparison of regression model and experimentally determined fracture load for group 1

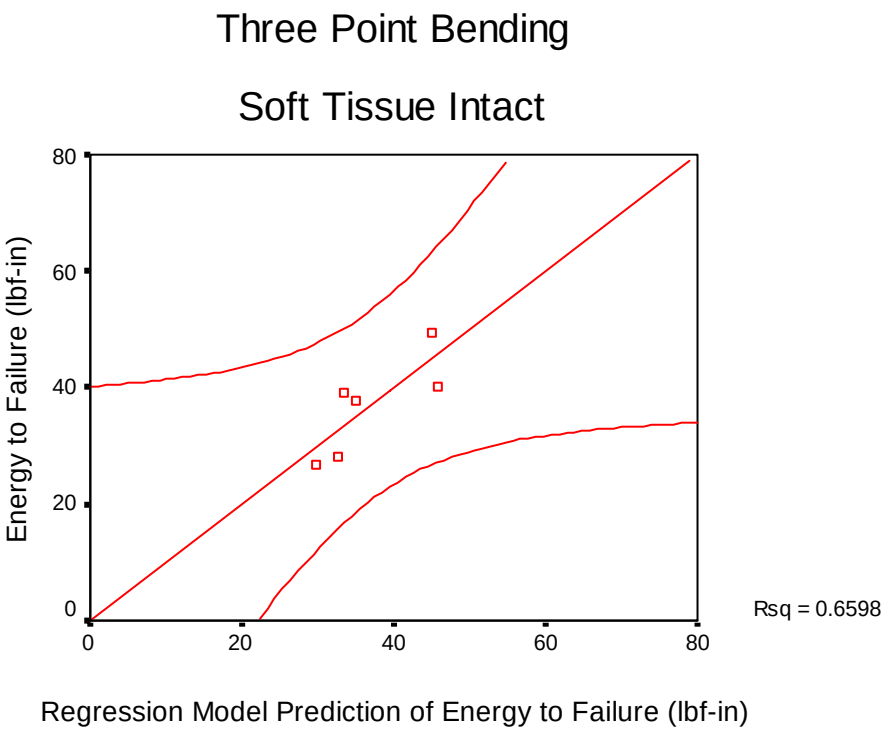

Figure 5-4 Comparison of regression model and experimentally determined energy to failure for group 1

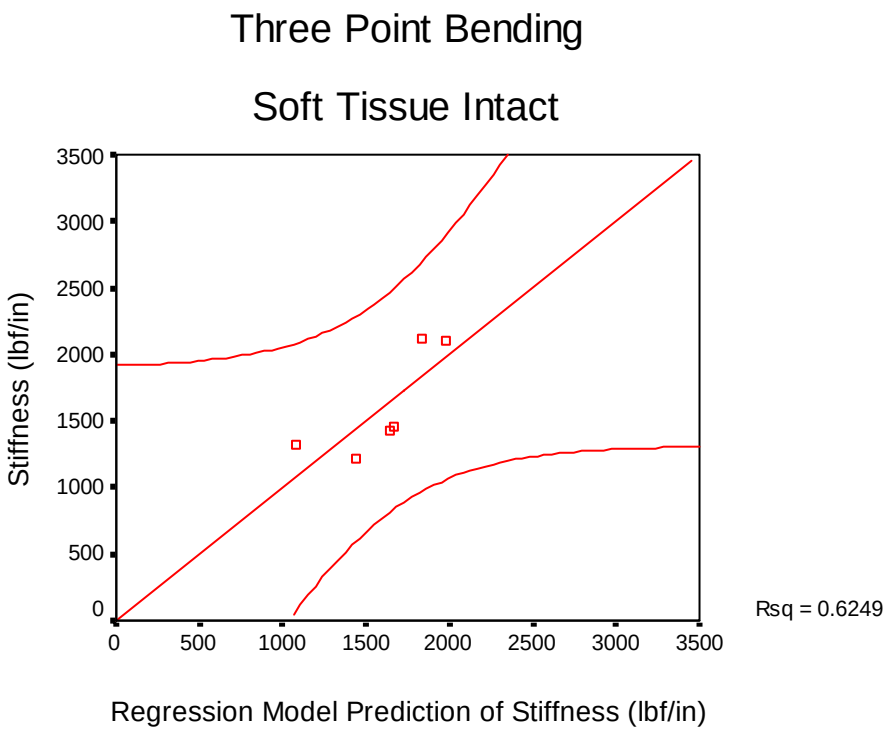

Figure 5-5 Comparison of regression model and experimentally determined stiffness for group 1

The regression models for predicting the fracture measures of immature porcine femurs tested in three-point bending without soft tissue (group 2) are expressed below.

$$FxLoad = 8.1 * BMC + 97.9 * BMD + 16078 * Z + 87.7 \quad (12)$$

$$Energy = -3.1 * BMC + 39.9 * BMD + 78.3 * Z + 17.6 \quad (13)$$

$$Stiffness = 99.6 * BMC + 712.8 * BMD + 144502.8 * Z + 161.1 \quad (14)$$

Plots comparing the measured experimental values to the regression model predictions are shown below for each fracture measure (R^2 values are reported on each graph).

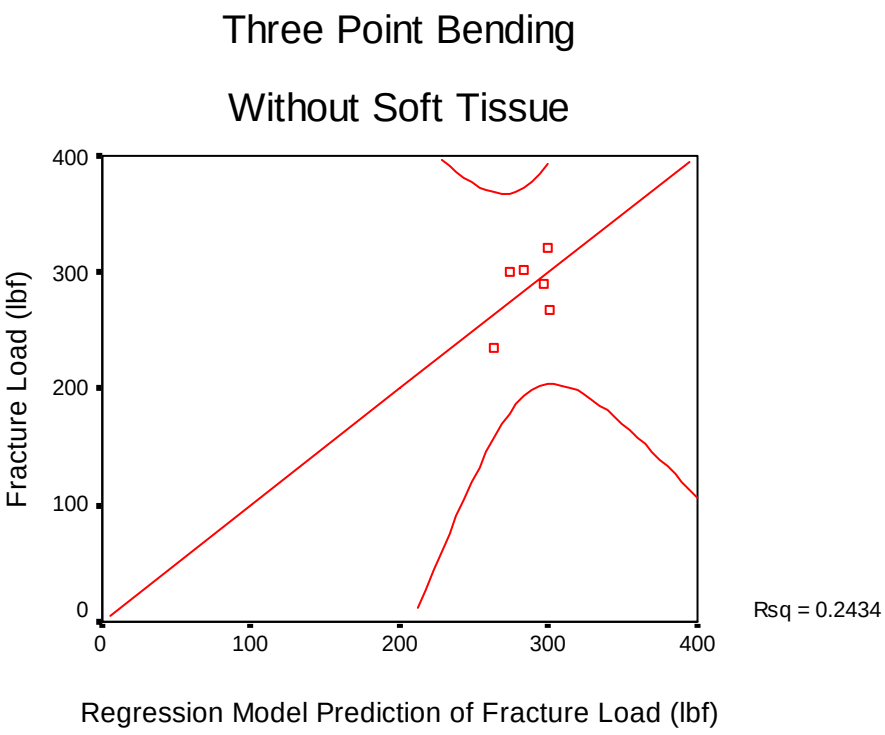

Figure 5-6 Comparison of regression model and experimentally determined fracture load for group 2

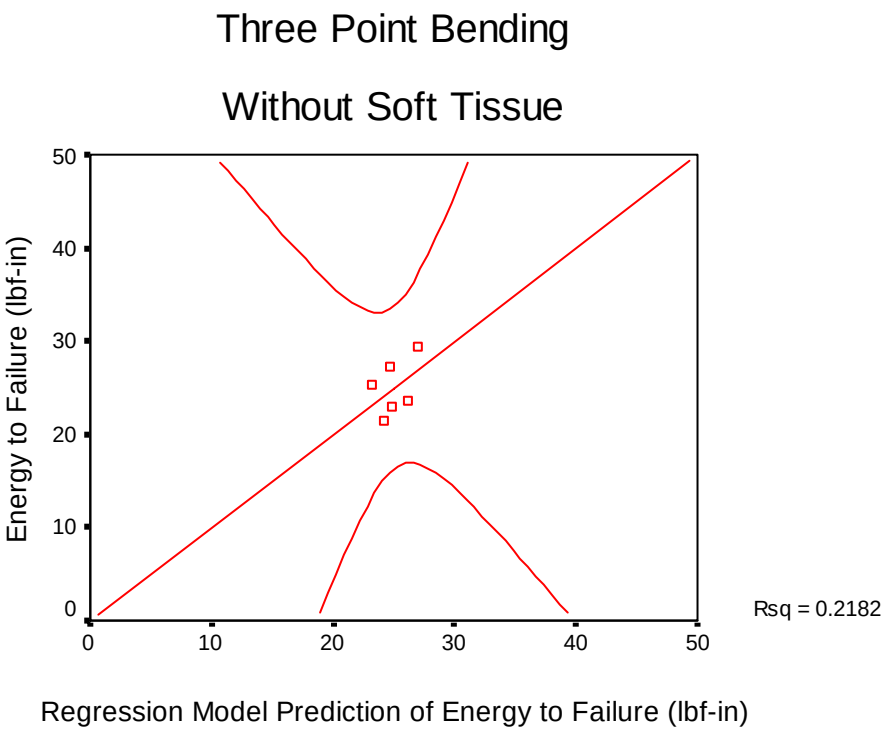

Figure 5-7 Comparison of regression model and experimentally determined energy to failure for group 2

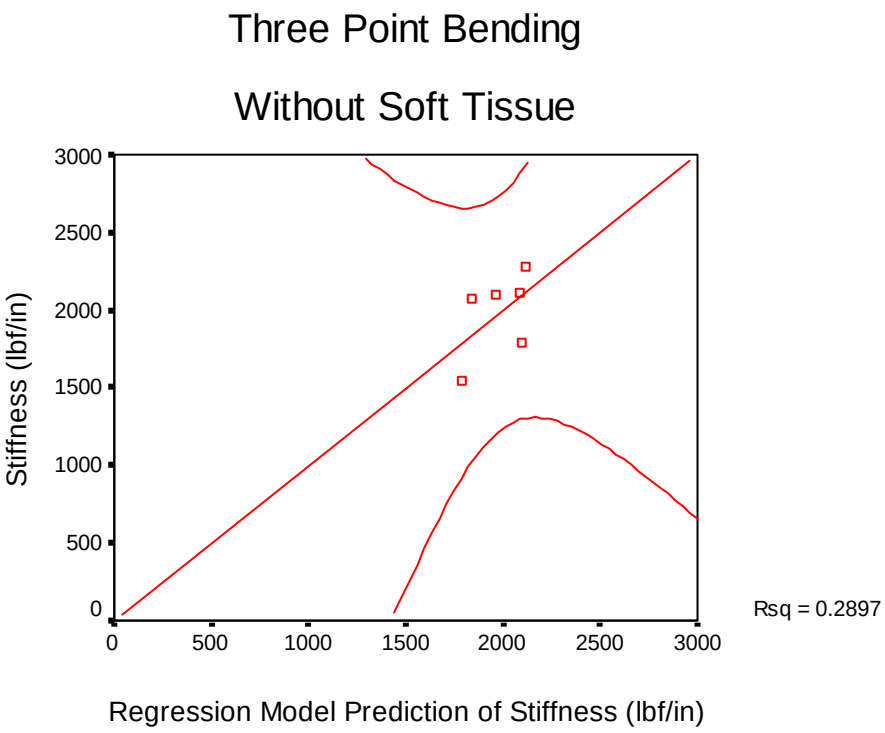

Figure 5-8 Comparison of regression model and experimentally determined stiffness for group 2

5.2 TORSION

The immature porcine femurs tested in torsion were grouped according to the angular displacement rate used to test the specimens. Specimens tested at an angular displacement rate of 0.167 degrees per second were designated group 3 (n=7) and specimens tested at an angular displacement of 90 degrees per second were designated group 4 (n=7). Fracture Load and

energy to failure were calculated for each specimen. The torsion stiffness was not calculated for torsion tests because the torque vs angular displacement curves did not show a linear region.

Table 5-4 Summary of radiographic and geometric parameters for torsion tests

	Average Inner Radius(in)	Average Outer Radius (in)	Growth Plate Length (in)	J (in^4)	BMC (g)	BMD (g/cm2)
Group 3, n=7						
Mean	0.104	0.169	2.325	0.001	3.57	0.448
Range	0.083 – 0.115	0.150 – 0.193	2.12 – 2.54	0.001 – 0.002	3 - 5	0.412 – 0.499
S.D.	0.012	0.013	0.136	0.0001	0.787	0.032
Group 4, n=7						
Mean	0.103	0.170	2.338	0.001	3.57	0.460
Range	0.080 – 0.120	0.145 – 0.190	2.15 – 2.56	0.001 – 0.002	2 – 5	0.407 – 0.511
S.D.	0.016	0.014	0.125	0.002	0.976	0.041

A representative load deformation curve is shown in figure 5-9. As previously mentioned, the fracture load can be seen as the highest point on this curve and the energy to failure is the area under this curve up to the fracture point. Load vs deformation curves for group 3 are shown in appendix C and for group 4 in Appendix D.

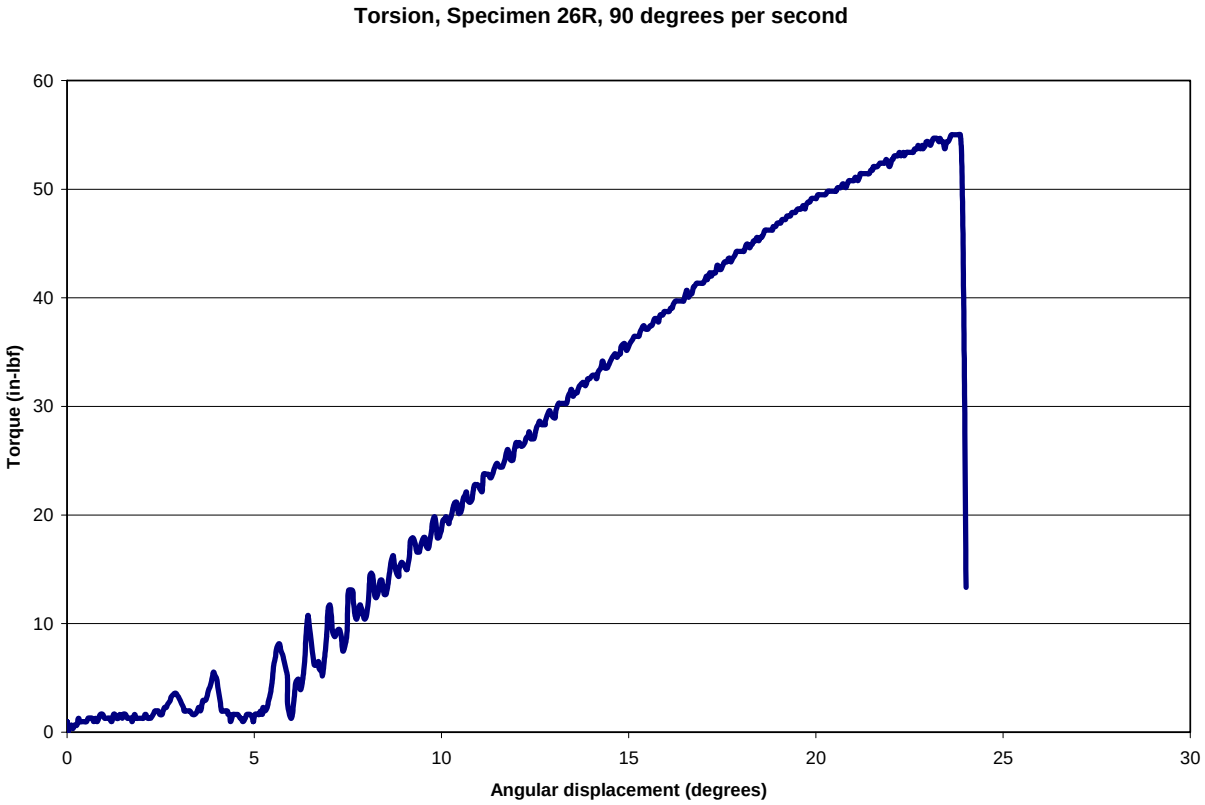

Figure 5-9 Torque – angular displacement curve for specimen 26R, tested in torsion at 90 deg/sec

5.2.1 Fracture Morphology (Torsion)

Radiographs were taken post testing of each specimen and showed that all specimens failed with spiral fractures. It was not evident that any of the spiral fractures originated at the pin insertions of the femur. Another important result was that none of the femurs resulted in shearing of the growth plates.

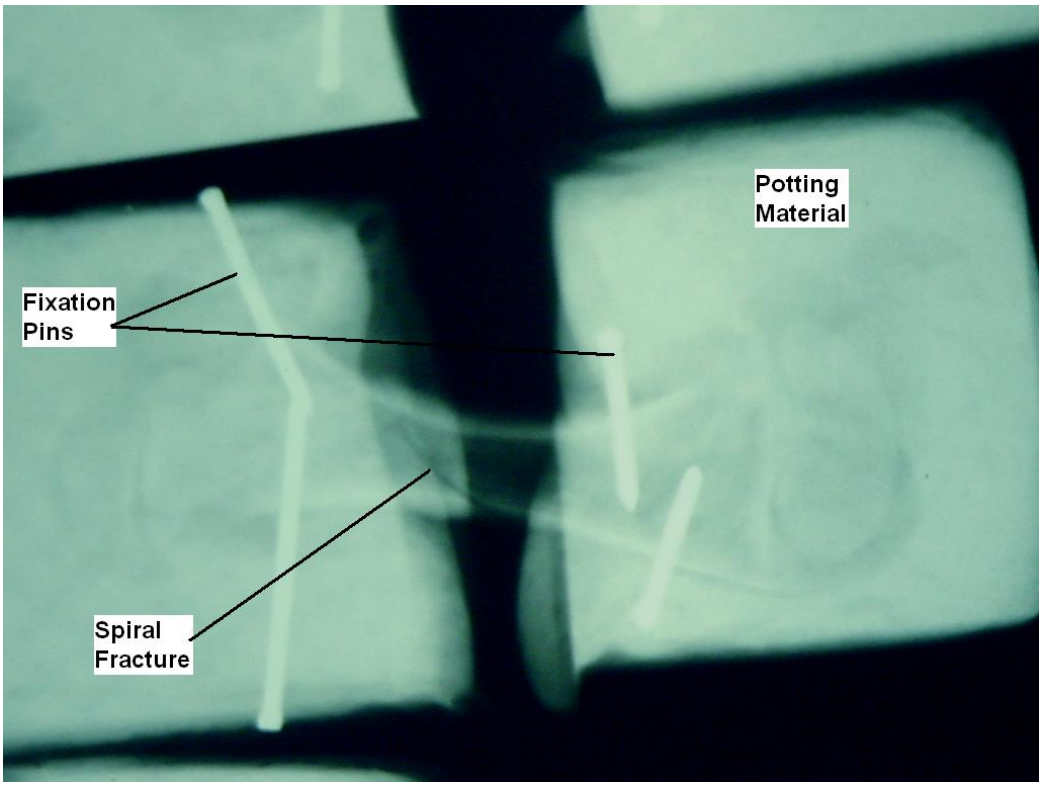

Figure 5-10 Spiral fracture resulting from torsion loading mechanism applied to immature porcine femur

5.2.2 Statistical Analysis (Torsion)

Statistical analysis was performed on the data in order to test the hypotheses 1 and 3. The fracture load and energy to failure were determined and are summarized in table 5-3.

Table 5-5 Summary of fracture measures in torsion

	Fracture Torque (in-lbf)	Energy to Failure (in-lbf)
Group 3 (0.167degrees/s, n=7)		
Mean	30.7	16.7
Range	26.0-37.1	9.4-24.7
Standard Dev.	4.6	5.9
Group 4 (90 degrees/sec, n=7)		
Mean	46.1	15.4
Range	29.6-55.0	8.5-34.5
Standard Dev.	9.4	8.8

The data from two groups of data were analyzed using SPSS software (SPSS Inc., Chicago, IL). One-sample Kolmogorov-Smirnov test was used to compare the data from each group to a normal distribution. As a result, normal distributions could not be assumed for either group and non-parametric comparison of means was used to test hypothesis one. Hypothesis three however was tested using both parametric and non-parametric techniques to investigate the correlations between the fracture measures and radiographic data.

5.2.2.1 Comparison of means (Torsion) A Wilcoxon matched-pairs signed-ranks test was used to compare whether the fracture torque and strain energy to failure had statistically significant differences between the groups. The data indicates that there is a statistically significant difference between the fracture torque of each group ($p=0.018$) though there was no statistically significant differences between groups when evaluating strain energy to failure ($p=0.499$).

Angular displacement to failure was also compared between groups three and four. Wilcoxon matched pairs signed ranks test showed no statistically significant differences in the angular displacement to failure of the femurs tested in torsion ($p<0.05$).

Table 5-6 Summary of angular displacement to fracture in torsion

	Angular Displacement (degrees)
Group 3 (0.167degrees/s, n=7)	
Mean	48.2
Range	31.3 – 78.8
Standard Dev.	17.6
Group 4 (90 degrees/sec, n=7)	
Mean	33.8
Range	19.8 – 62.3
Standard Dev.	16.0

5.2.2.2 Correlations (Torsion) Correlations between fracture torques and energies to failure calculated for each group and BMD, J, BMD*J, BMD*BMC*J were explored. The results for each group are shown in the table below. In the cases where the immature porcine femurs were tested at low displacement rate (0.167 degrees per second), the correlations show that fracture torque has a strong correlation to BMD*BMC*J (spearman's rho = 0.730) and energy to failure has a weak correlation to BMD (spearman's rho = 0.214). In the cases where the immature porcine femurs were tested at the higher displacement rate (90 degrees per second), the correlations show that fracture torque has a very strong correlation to BMD*J (spearman's rho = 0.857, $p<0.05$) and energy to failure is moderately correlated to BMD (spearman's rho = 0.500).

Table 5-7 Correlations coefficients of fracture measures and radiographic and geometric data in torsion

	BMD	J	BMD * J	BMD * BMC * J
Group 3 (0.167degrees/s, n=7)				
Fracture Torque	-0.318	0.430	0.430	0.730
Energy to failure	0.214	-0.286	-0.107	0.071
Group 4 (90 degrees/sec, n=7)				
Fracture Torque	-0.429	0.821*	0.857*	0.786*
Energy to failure	0.500	-0.679	-0.571	-0.571

* Significant at 0.05 level

5.2.2.3 Multivariable Regression (Torsion) Multivariable Regression was performed on the data in order to develop a predictive model for fracture torque and energy to failure for immature

porcine femurs tested in groups 3 and 4. The regressions produced the following equations for predicting the fracture torque and energy to failure of the specimen in group 3.

$$FxTorque = 2.6 * BMC + 9.1 * BMD + 7679.1 * J + 11.3 \quad (15)$$

$$Energy = 0.46 * BMC + 99.0 * BMD + 6359.9 * J - 34.5 \quad (16)$$

Graphs comparing the experimental data to the data from the regression model are presented below. The coefficient of determination for the fit is reported with each graph.

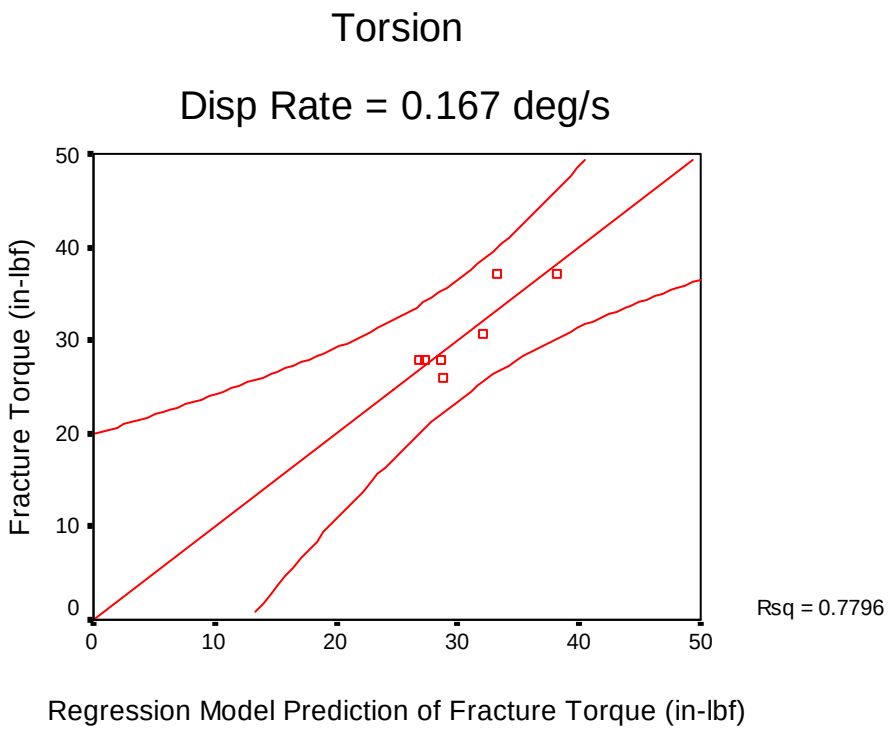

Figure 5-11 Comparison of regression model and experimentally determined fracture torque for group 3

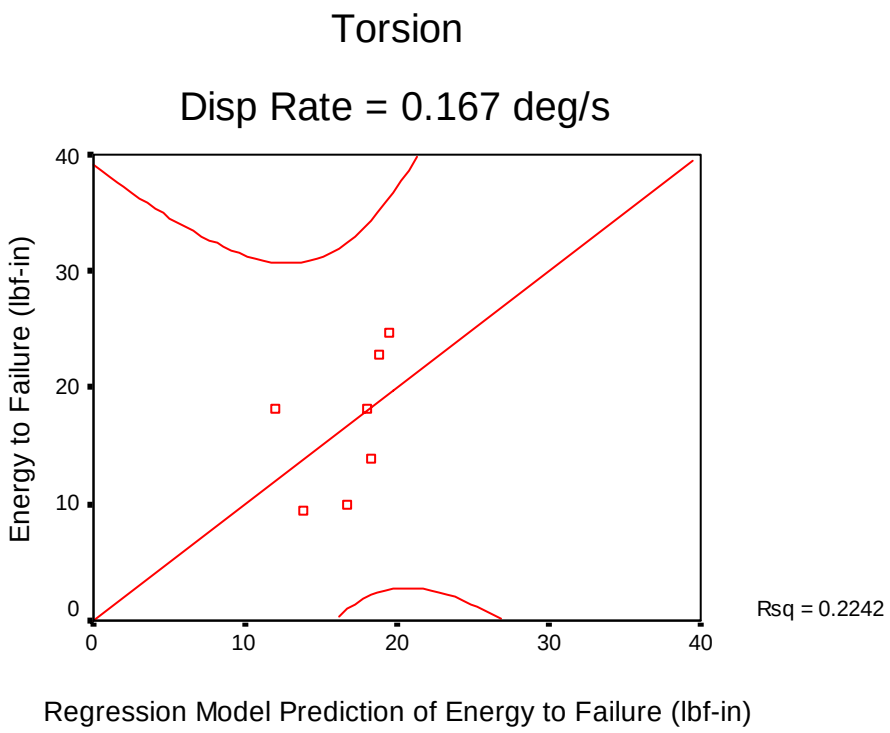

Figure 5-12 Comparison of regression model and experimentally determined energy to failure for group 3

The regression models developed for the fracture torque and energy to failure for specimens in group 4 are expressed below.

$$FxTorque = 9.4 * BMC - 199.6 * BMD + 8308.1 * J + 96.8 \qquad (17)$$

$$Energy = 4.7 * BMC + 8.3 * BMD - 5210.5 * J - 0.48 \qquad (18)$$

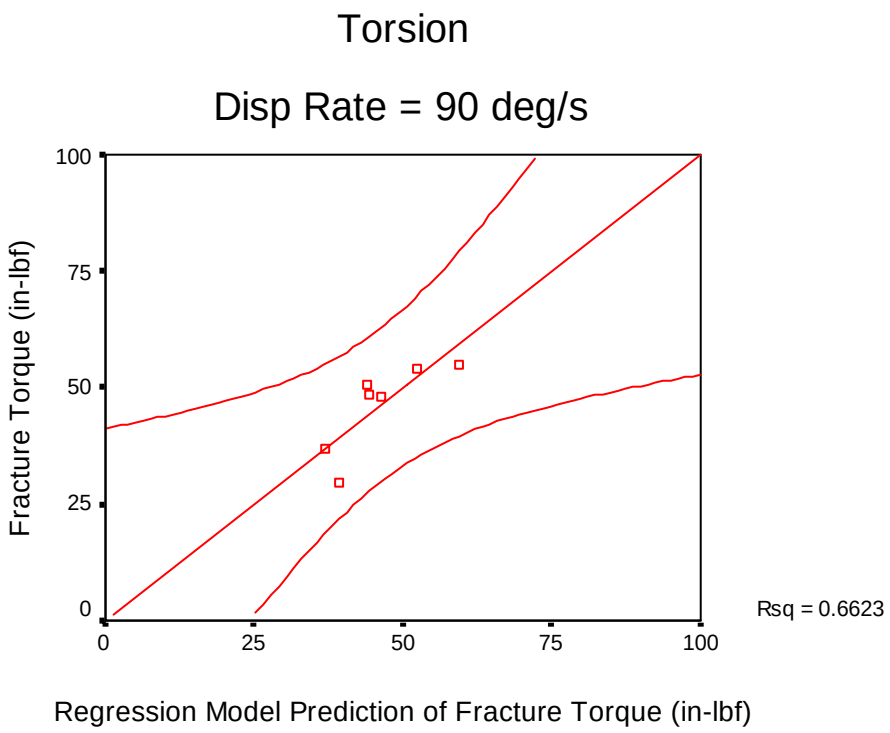

Figure 5-13 Comparison of regression model and experimentally determined fracture torque for group 4

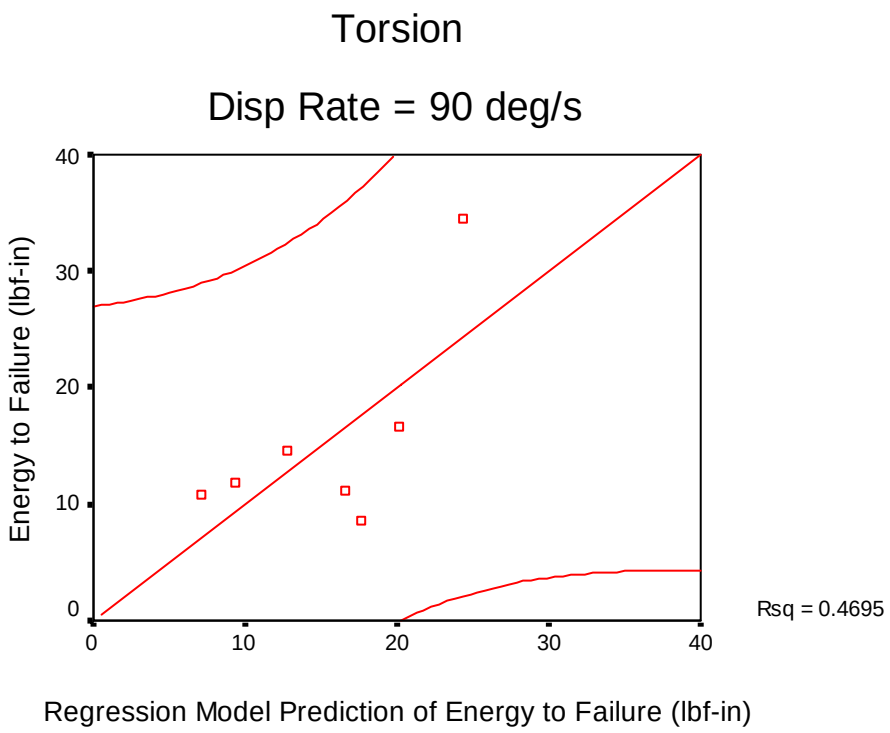

Figure 5-14 Comparison of regression model and experimentally determined energy to failure for group 4

5.3 AXIAL COMPRESSION

The immature porcine femurs tested in axial compression were grouped by the displacement rate at which they were tested. Group 5 (n=5) was tested at a displacement rate of 0.04 inches per second and group 6 (n=2) was tested at a displacement rate of 2 inches per second.

Table 5-8 Summary of radiographic and geometric parameters for axial compression tests

	Average Inner Radius(in)	Average Outer Radius (in)	Growth Plate Length (in)	CSA (in^2)	BMC (g)	BMD (g/cm2)
Group 5, n=5						
Mean	0.097	0.161	2.237	0.052	3.2	0.443
Range	0.083 – 0.113	0.130 – 0.178	2.14 – 2.38	0.030 – 0.066	2 - 4	0.403 – 0.464
S.D.	0.013	0.022	0.098	0.015	0.837	0.024
Group 6, n=2						
Mean	0.101	0.155	2.323	0.044	3	0.429
Range	0.093 – 0.110	0.140 – 0.170	2.265 – 2.38	0.035 – 0.053	2 – 4	0.377 – 0.480
S.D.	0.012	0.021	0.081	0.013	1.414	0.073

A representative load deformation curve is shown in figure 5-15. The fracture load is the highest point on this curve as determined from the slight decrease in load followed by a second ramping phase during which the growth plate of the femur was already fractured (this second part of the curve showing a second ramping was omitted for clarity). The stiffness can be observed as the linear region of the upward sloping part of the curve. The energy to failure is the area under this curve up to the fracture point. Load vs deformation curves for group 5 are shown in appendix E and for group 6 in Appendix F.

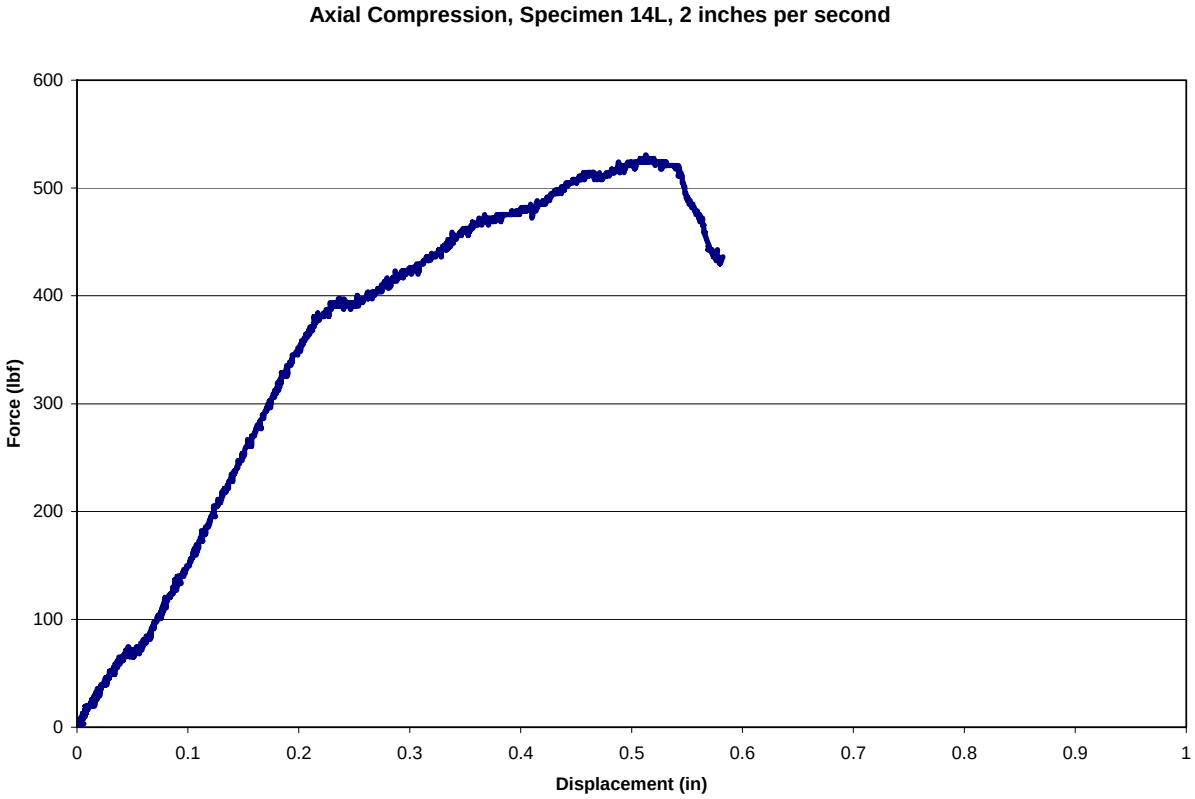

Figure 5-15 Load – deformation curve for specimen 14L, tested in axial compression at 2 in/sec

5.3.1 Fracture Morphology (Axial Compression)

Radiographs were taken post testing of each specimen and showed that all specimens failed at the condylar growth plate. The condyles failed at the growth plate with the condyles sliding to the posterior of the femur.

Figure 5-16 Fracture at growth plate resulting from axial compression

5.3.2 Statistical Analysis (Axial Compression)

Statistical analysis was performed on the data in order to test the hypotheses 1 and 3. The fracture load and energy to failure were determined and are summarized in table 5-5.

Table 5-9 Summary of fracture measures in axial compression

	Fracture Load (lbf)	Stiffness (lbf/in.)	Energy to failure (lbf*in.)
Group 5 (0.04 in / sec, n=5)			
Mean	273.4	829.4	70.7
Range	211.6-390.6	529-1173	29.9-132.5
Standard Dev.	68.4	248.1	38.9
Group 6 (2 in / sec, n=2)			
Mean	441.1	1894	154.2
Range	351.6-530.6	1894-1894	134-174.4
Standard Dev.	126.6	0	28.6

The data from two groups of data were analyzed using SPSS software (SPSS Inc., Chicago, IL). A one-sample Kolmogorov-Smirnov test was used to compare the data from each group to a normal distribution and data indicates that a normal distribution can not be assumed.

5.3.2.1 Comparison of means (Axial Compression) Comparison of group means for femurs loaded in axial compression was not performed because of the sample size of the group 6 (specimens tested at a displacement rate of 2 inches per second, n=2). Since group 6 has such a small sample size, one can not make a conclusive determination about the mean at all.

5.3.2.2 Correlations and Multivariable Regressions (Axial Compression) Correlations and multivariable regressions were not calculated for the axial compression due to the fact that the measures to which fracture load , stiffness and energy to failure were to have been correlated to describe the bone substance of the femur and not the growth plate where the fractures occurred. That is, when deciding what factors (independent variables) to correlate and use in the regression analysis, these variables should be previously determined to have an effect on the dependent variable. Since Bone mineral content and bone mineral density are not a measure associated with the growth plate, they should not be used as independent variables in the correlations or regression analyses.

5.4 CROSS MECHANISM COMPARISON

In order to compare the results of the three loading mechanisms tests, the energy to failure of each specimen loaded in each mechanism was averaged. The average energy to failure of specimens tested in three-point bending was 31.0 lbf-in. The average energy to failure of specimens tested in torsion was 16.1 lbf-in, just over half of the energy for the specimens tested in three-point bending. The average energy to failure for specimens tested in axial compression is 94.6 lbf-in, just over 300% of the energy calculated for specimens tested in three-point bending.

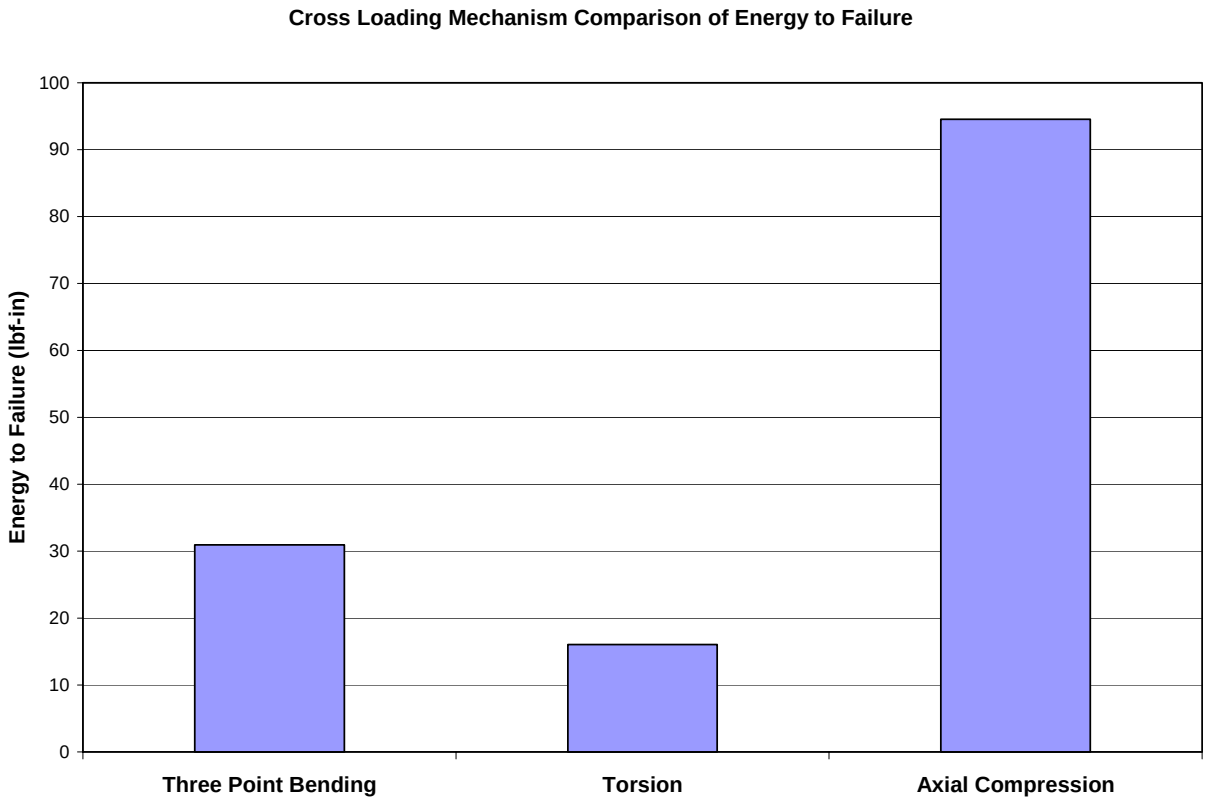

Figure 5-17 Cross Mechanism Comparison of Energy to Failure

6.0 DISCUSSION

Correlation coefficients were determined for fracture measures (fracture load, stiffness and energy to failure) to radiographic (bone mineral density and bone mineral content) and geometric variables (section moduli, etc). This model was chosen because bone mineral density (BMD) and bone mineral content (BMC) are indicators of bone material properties and the geometric variables are characteristics of the structural capacity of any structure. Carter and Hayes reported high correlation of bone strength to the square of bone mineral density (33).

6.1 THREE POINT BENDING

No statistically significant differences in fracture load were observed in three-point bending across groups tested both with and without soft tissue intact . The fact that the presence of soft tissue does not affect fracture load might be explained by the way fracture was defined, which for both groups was the fracture of the femur (and in no way encompassed the soft tissue). Power analysis was performed to determine the necessary sample size in order to detect statistically significant differences in the data. It was calculated that the sample size of each group would have to be 750, meaning that based on the standard deviations observed, no

statistically significant differences in fracture load exist. The differences in stiffness and energy to failure were also expected since soft tissue is less stiff than bone and when tested together, the lower stiffness of the soft tissue lowers the overall stiffness of the specimen; similar to testing two springs in series. Specimens tested with soft tissue intact also showed higher energy to failure which is consistent with the premise that soft tissue shows energy absorption during impacts.

Results of the three-point bending tests showed that statistically significant differences exist between femurs tested with soft tissue intact and femurs tested devoid of soft tissue in stiffness and energy to failure of immature porcine femurs. Three-point bending resulted in fracture loads about twice as high as values reported by Pierce et al., 726 N (163.2 lbf) (1). Higher values may be due to the higher displacement rates in this study, the fact that the periosteum was left intact and the loading alignment (Pierce tested femurs in medial-lateral direction) (1).

Pierce found fracture moments to range from approximately 4500 N-mm (39.8 in-lbf) to approximately 8000 N-mm (70.8 in-lbf) (1). These values were slightly lower than values determined in this study (mean = 125.1 in-lbf) for femurs tested devoid of soft tissue. Koo et al reported the mean failure moment for femurs tested in three point bending at displacement rate of 1 mm/s (0.04 inches per second) to be 10.8 N-m (99.5 in-lbf) (25). These values are all similar and slightly higher values may be due to testing at displacement rate of 2 inches per second in this study where as Pierce and Koo tested at 1 mm per second (0.04 inches per second) (1,25). Also, Pierce tested femurs in three-point bending in the medial lateral direction, where as femurs in this study were tested in the antero-posterior direction, the same anatomical direction tested by Koo (1,25). However, comparing these failure moments to data collected for a child's

femur reported by Sturtz et al (52 Nm or 460 in-lbf), shows that there is almost a four fold increase between the child's femur fracture moment and that of the immature porcine femurs in this study (34). This however, might be the result of Sturtz's data reporting the fracture moment of a segment of the child's femur, rather than of the entire femur (34).

Energy to failure in three point bending for femurs tested devoid of soft tissue (mean = 25.0 in-lbf) were similar to values reported by Pierce et al for failure energy, ranging from about 0.75 J (6.6 in-lbf) to approximately 2.4 J (21.2 in-lbf) and Koo with a mean value of 1.575 N-m (13.9 in-lbf) (1,25). Slightly higher values found in this study may be due to higher displacement rates, two inches per second contrary to Pierce and Koo's 0.04 inches per second (1,25).

Energy available during a fall is a common way to evaluate potential injury risk and therefore is important in evaluating the plausibility of a fracture occurring from a specific fall. Mechanisms similar to three point bending occur relatively frequently during child falls in which the upper leg of the child strikes on object upon landing. The immature porcine femurs tested in three-point bending with soft tissue intact are representative of impacts which occur in these types of falls. Higher values of energy to failure determined for femurs tested with soft tissue intact means that these femurs are more resistant to fracture and that more energy will be required to cause fracture when compared to bone without soft tissue. It is deduced that the soft tissue provides this energy absorption mechanism during impacts.

Femurs tested devoid of soft tissue showed weaker correlations when compared to the correlations determined for femurs tested with soft tissue intact. Correlations between femurs tested with soft tissue intact showed best correlations of fracture load and stiffness to BMD*BMC*Z (Spearman's rho = 0.371 and 0.714 respectively) as expected. The energy to

failure however was weakly correlated to BMD (Spearman's rho = 0.314). This is counter intuitive and may be due in part to the relatively low sample size as well as the lack of a term to describe the energy absorption capacity of the soft tissue.

Correlations between femurs tested devoid of soft tissue showed negative correlations for fracture load and stiffness to BMD*Z (Spearman's rho = -0.714 and -0.371 respectively). The energy to failure however was best correlated to BMD (Spearmn's Rho = -0.943, $p<0.01$). This may be due in part to the fact that BMD is proportional to bone brittleness and as BMD decreases, the femur is more compliant and may therefore absorb more energy.

Multivariable regression analysis indicates that the correlation coefficients (constants of the terms BMC, BMD, Z) did not have statistical significance. This means that though the coefficients were calculated optimize the model, the values can not be conclusively stated (that is, these values may change with further experiments). The Regression model for fracture load of group 1 (femurs tested with soft tissue intact) had an R^2 value of 0.74 which indicates that this model accounts for 74% of the variability of the fracture load data for this group. The model for stiffness and energy to failure for group 1 indicate that 62% and 66% of the variability of each fracture measure is explained by the model respectively. R^2 values for the regression models determined for group 2 (femurs tested without soft tissue) were determined to be 0.24, 0.29 and 0.22 for fracture load, stiffness and energy to failure respectively. The higher R^2 values for femurs tested with soft tissue intact shows promise for the use of such a model in a clinical setting.

Fracture patterns in specimens tested in three point bending were expected to be transverse and oblique fractures. Three point bending tests of specimens in group 1 resulted in 4 transverse fractures and 2 oblique factures. The testing of group 2 resulted in all specimens

failing with transverse fractures. This indicates that femurs with soft tissue intact (group 1) can absorb more energy and results in similar fracture patterns to those of group 2 when tested in three point bending. Fracture patterns observed in this study are consistent with those observed by Kress et al. in human cadaver three point bending (impact) tests on femurs and tibias (35).

6.2 TORSION

Statistically significant differences in fracture torque between groups 3 and 4 were observed for immature porcine femurs tested in torsion. This difference may be due to viscoelastic properties that bone exhibits. Viscoelastic models predict that as the (angular) displacement rate of a specimen increases, the failure load (torque) will also increase (36). No statistically significant differences were observed in energy to failure. Power analysis was performed to determine the necessary sample size in order to detect statistically significant differences in the data. It was calculated that the sample size of each group would have to be 520, meaning that based on the standard deviations observed, no statistically significant differences in energy to failure were observed in torsion.

Torsion tests performed at an angular displacement rate of 0.167 degrees per second resulted in fracture torques (mean = 30.69 in-lbf) greater than values reported by Pierce et al., 2703 N-m (23.9 in-lbf) (1). Values lower than those of Pierce were expected since Pierce tested at a higher angular displacement rate (1 degree per second) (1). Pierce's mean fracture torque was calculated from data which included specimens whose fracture mode was not consistent, but

rather, 5 of the 7 specimen experienced shearing at the growth plates (1). Therefore it is not appropriate to make a direct comparison. Therefore, comparing the highest fracture torque value reported by Pierce shows a more comparable value for the expected trend based on angular displacement rate (3559 N-mm or 31.5 in-lbf) (1). Pierce's slightly higher maximum value for fracture torque compared to the mean of the fracture toque in determined here may be due to piglet preparation in that this study left the periosteum of the femur intact whereas Pierce did not leave the periosteum intact (1). Femurs tested at a higher angular displacement rate (90 degrees per second) in this study showed a mean fracture torque of 46.13 in-lbf consistent with the hypothesis that fracture torque would be higher when tested at a higher angular displacement rate.

Energy to failure in torsion did not show statistically significant differences between the two groups tested (angular displacement rates: 0.167 degrees per second and 90 degrees per second).

Mechanisms consistent with torsional loading occur relatively frequently during child falls in which the child's torso is rotating and the foot of the child is fixed without rotation. Case studies indicate that spiral fractures are commonly associated with children who twist when running (37). Higher values of failure torque determined for femurs tested at a higher displacement rate shows fracture load is rate dependent and therefore exhibits viscoelastic properties.

When investigating correlations between biomechanical response and material properties and geometric parameters, fracture torque was found to have strong correlations to BMD*BMC*J at both displacement rates (0.73 for group 3 and 0.786 for group 4). At the higher displacement rate (group 4), fracture load had very strong correlations to J and BMD*J (0.82 and

0.857 respectively). Similarly, Calero found a linear correlation (r=0.31, p=0.03) between fracture torque in rat femurs and BMD (17). Calero's results support the results obtained in piglets in this study that fracture torque can be correlated to radiographic measures.

Battaglia et al investigated the relationship between ash content of mice femora and torsional fracture measures such as fracture torque and energy to failure (38). A displacement rate of 1 degree per second was used and the fracture torque exhibited a good fit to ash content (R^2=0.68) (38). Energy to failure however, did not show any correlation to ash content (R^2=0.01) (38). Similarly, this study found strong correlations for radiographic and geometric parameters to fracture torque, but weak correlation for energy to failure.

Multivariable regression models for fracture torque fit the data for fracture torque accounting for 78% and 66% of the data variability for angular displacement rates of 0.167 degrees per second and 90 degrees per second respectively. The regression models for energy to failure accounted for less that 50% of the variability of the data at both displacement rates (R^2=0.22 and for an angular displacement rate of 0.167 and R^2=0.47 for an angular displacement rate of 90 degrees per second).

Investigating the fracture patterns of torsion tests, the only fracture types observed were spiral fractures. This suggests that torsion loading, no matter what the displacement rate is, will result in a spiral fracture.

6.3 AXIAL COMPRESSION

Fractures resulting from axial compression all resulted in shearing of the condylar growth plate. The fracture load, stiffness and energy to failure all show trends of increasing value with higher displacement rates. Lochmuller et al performed axial compression tests of discs cut from the distal end of the radius of mature human specimens (39). A displacement rate of 0.8 millimeters per second was utilized in the testing and fracture load was measured (39). DEXA obtained measurements of BMC were taken to correlate to fracture load (39). It was found that fracture load and BMC correlated strongly (r=0.84) (39).

Carter and Hayes studied human trabecular bone in compression as a two-phase porous structure (40). They compresses cylinders of human trabecular bone from the femoral condyles and tibial plateau and removed the marrow from half their specimens (40). They found that at low strain rates from 0.001 per second to 1.0 per second (corresponding to displacement rates of 0.0005 mm/s to 0.5 mm/s) showed no statistical significance between specimens tested with and without marrow, but at a strain rate of 10 per second (5 mm/s), they discovered that specimens tested with and without marrow present displayed statistically significant differences in compressive strength (40). This latter result shows that movement of bone marrow through the porous trabecular bone plays a role and at displacement rates similar to or higher than 5 mm/s will also be affected by the movement of bone marrow (40). The axial compression tests performed in this study showed trends indicating that sensitivity to displacement rate may exist. The movement of marrow through the trabecular bone structure of the femur may contribute to this trend.

The trend indicating sensitivity to displacement rate however may be due more to the viscoelastic properties of cartilage than to the viscoelastic properties of the femur in axial

compression. Since the growth plates are composed primarily of cartilage and cartilage is more compliant than bone, it is reasonable to assume that the more compliant of the two materials (bone and cartilage) will undergo large strains possibly leading to fracture. It therefore would be inappropriate to try to correlate femoral densitometry measures and femoral geometry measures to biomechanical response when in fact the fracture did not occur in bone.

A databases of child fractures compiled from Children's Hospital of Pittsburgh cases show that femoral growth plate fractures are not common (37). The inconsistencies between fractures experienced in vivo by children and the growth plate fractures resulting from axial compression may be due to the lack of stabilizing structure for the femoral condyles which the tibia and knee ligaments provide.

Fracture types that resulted from the axial compression tests were not expected and might be do to a secondary loading which may have been introduced inadvertently. The femurs were mounted on the UTS and due to their natural curvature may have introduced a shear load onto the specimens. Lundin et al observed that fracture patterns of mature and immature porcine spines subjected to axial compression differed, suggesting that maturity level of porcine bone has a direct effect on fracture type (41). This would account for the unexpected shearing at the growth plates which are not common fractures observed in children during common falls. Rather, buckle fractures were expected but this study was unable to produce a single buckle fracture. One area of concern for this is the natural in-vivo restraints present in children which may prevent the shearing of the growth plate. Knee ligaments, capsules and meniscus may combine to contribute the necessary restraints to prevent the shearing of the growth plates to occur in-vivo.

Another cause of shearing might be attributed to the level of maturity of the femur. Immature femurs have a separated and highly cartilaginous growth plates which are by nature weaker than the boney structure of the femur. Extrapolating data from a Lunar Corp study ("Bone Growth in Children" in Lunar News, published by G.E. Lunar Corp., Madison, WI October 1993), the BMD of immature porcine femurs tested in this study correspond to the human BMD equivalent of about a 1 to 2 year old child (extrapolated value would be near 0.5 g/cm^2). As a child matures, the growth plates fuse and harden into bone which may reduce the chances of causing a fracture at the growth plate and may lead to buckle fractures.

6.4 CROSS MECHANISM COMPARISON

In order to compare fracture types, one must look at measures which can be computed and compared across all mechanisms of loading. Energy to failure is the only fracture measure which can be compared from one loading mechanism to another. Comparing the observed energies to failure shows that femurs require just over half the energy to cause a spiral fracture resulting from a torsion mechanism when compared to a transverse fracture resulting from three-point bending (figure 5-14). Axial growth plate fractures require more than double the energy as compared to transverse fractures. This higher value for energy to failure for axial compression may be due to the fact that the cartilage is also being loaded in compression, and therefore compressing the cartilage and the bone whereas the other test methods (three point bending and torsion) only loaded the boney part of the femur.

The higher values calculated for energy to failure required to cause transverse fractures in three-point bending compared to the energy required to cause spiral fractures supports the idea that transverse fractures of the femurs occur in higher energy trauma events such as motor vehicle accidents or child abuse, where as spiral fractures may be more common in accidental trauma such as ground based falls. This is supported by databases of child fractures kept from Children's Hospital of Pittsburgh which shows that abuse cases have a higher percentage of transverse fractures than do accidental cases and spiral fractures have a higher percentage of occurrence in accidental cases than in abuse cases.

6.5 LIMITATIONS

A limitation of this study is the use of quasi-static (non-dynamic) nature of the loading mechanism. The UTS used in this study does allow for pseudo-dynamic testing, but displacement rates are limited and may not achieve impact speeds associated with childhood femur fractures. This study also, did not investigate combined loading, but rather focused on simple and pure loading mechanisms. In scenarios when children fall, it is rarely the case that their femur experiences pure loading conditions. However, in order to proceed to combined loading, pure loading must first be understood. The methods used in this study did not allow for the detection of small abnormalities in the geometry or bone mineral density of the femurs. Furthermore, this study assumed that the femur geometry was that of a tube and that the bone mineral density of the femur is homogenous throughout the entire femur. It has been reported

that freezing of bone for a short time does not have a major effect on bone mechanical properties, it has been shown to be greatest in long bones (36). However, after thawing, protease and collagenase may become active and degrade the tissue, in fact enzymatic degradation is not totally halted at 20^{o}C (36).

This study utilized an animal model for developing a predictor of femur fracture strength, while the ideal would have been to use immature human cadaveric femurs. The use of a linear multivariable regression is a limitation because it does not explore the possibilities of a non-linear relationship between BMC, BMD and Z (or J or CSA) to fracture load (or torque), energy to failure and stiffness. However, since the sample size is small, non-linear regression models explored did not fit the data better than a linear multivariable regression. However, a larger sample size might prove useful in exploring the nonlinear relation between BMC, BMD and Z (or J or CSA) to fracture load (or torque), energy to failure or stiffness.

Using porcine femurs of varying age (including mature and immature specimen) would be useful in more effectively understanding the effect of maturity level on fracture pattern of the femurs based upon the differences in fracture patterns observed by Lundin between mature and immature porcine bone specimen (41).

7.0 CONCLUSIONS

Data showed that there are significant differences between when testing immature porcine femurs in three point bending with soft tissue intact (n=6) and devoid of soft tissue (n=6) for stiffness (means = 1607.9 ± 402.9 lbf. and 1981.9 ± 268.2 lbf respectively, p=0.046) and energy to failure (means = 36.9 ± 8.3 lbf and 25.0 ± 2.9 lbf respectively, p=0.046). Torsion tests show significant differences in fracture torque between groups tested at 0.167 degrees per second (n=7) and 90 degrees per second (n=7, means = 30.69 ± 4.58 in-lbf and 46.13 ± 9.42 in-lbf, respectively, p=0.018). Axial compression experiments performed at a displacement rate of 0.04 inches per second (n=5) resulted in fracture load, energy to failure and stiffness of 273.4 ± 68.4 lbf, 70.7 ± 38.9 in-lbf and 829.4 ± 248.1 lbf/in respectively. Axial compression of femurs tested at 2 inches per second (n=2) resulted in trends of higher fracture loads, energy to failure and stiffness (441 lbf, 154.2 in-lbf and 1894 lbf/in respectively).

Development of a predictive model plays an important role in developing an objective tool to aid in the diagnosis of child abuse. In cases where a child presents to the emergency department with a fracture, the model could predict the force and energy needed to cause that fracture and if the account used to explain the fracture is inconsistent with the fracture load or energy to failure, then child abuse can be suspected. Correlations of fracture measures (fracture load or torque) and stiffness show strongest correlations to a radiographic measure which combines femur densitometry data and femur geometric data. This shows promise in developing a model to predict fracture load or torque based on densitometry and radiographic geometric

data. Energy to failure was most strongly correlated to BMD in three point bending and geometric data (J) in torsion. This too shows promise in using both densitometry data and geometric data to develop a predictive model for these measures.

The regression models predicting the fracture measures for femurs with soft tissue intact better fit the data (fracture load $R^2 = 0.74$, Energy to failure $R^2 = 0.66$ and stiffness $R^2 = 0.62$) than the regression models for femurs tested devoid of soft tissue in three point bending (fracture load $R^2 = 0.24$, Energy to failure $R^2 = 0.22$ and stiffness $R^2 = 0.29$). Regressions for torsion testing showed promise in predicting fracture torque (0.167 deg/sec $R^2 = 0.78$ and 90 deg/sec $R^2 = 0.66$). The model for predicting energy to failure in torsion had weaker fits (0.167 deg/sec $R^2 = 0.22$ and 90 deg/sec $R^2 = 0.47$) to the data showing that more is needed in this area.

Data presented shows the completion of the specific aims proposed for this project, showing that displacement rate when testing immature porcine femurs does have a significant effect on fracture torque but not on energy to failure when tested in torsion. Displacement rate appears to have some effect on fracture load, stiffness and energy to failure for specimens tested in axial compression. This supports hypothesis one with the exception of the energy to failure of the torsion tests. Specific aim two, was fulfilled by testing immature porcine femurs in three point bending and hypothesis two was partially supported by the significant effect that soft tissue presence had on the energy to failure and while having no significant effect on fracture load.

Specific aim three was carried out by analyzing the data and performing Wilcoxon matched-pairs signed-ranks tests on the data to correlate fracture measures to geometric and radiographic data. Furthermore, multivariable regressions were performed on the data to develop a regression model for prediction of the fracture measures. Hypothesis three was supported for three point bending and torsion.

Further investigation needs to be performed in order to fully understand the relationship between bone mineral content, bone mineral density and bone geometry as well as to develop a more reliable model for predicting immature femur fracture load, energy to failure and stiffness.

8.0 FUTURE WORK

Future work towards the goal of developing a model for predicting immature femur fracture load, stiffness and energy to failure may include testing femurs in combined loading (compression and bending together for example). Further studies should also focus on testing the immature femurs as close to in-vivo conditions as possible such as developing a way to test these femurs with the hip and knee joints intact.

Future work towards developing a model for predicting immature femur fracture strength may also include the use of a more complex model incorporating the use of finite element methods. However, before this work can proceed, material properties of immature femurs must first be determined. This would include testing immature femoral bone samples in compression in the anisotropic directions. Furthermore, since the periosteum is believed to be a contributor to bone fracture measures of interest, material properties for this tissue should also be mapped for use in the finite element model (42). Perhaps bone mineral density and bone mineral content can be used as predictors of strength and ultimate load of the samples of the immature femur, rather than of the entire femur. A more detailed volumetric bone mineral density may be a key to determining the material properties of bone throughout the entire femur and has been utilized to obtain a more accurate representation of bone mineral density (33,43). This model might be validated by performing virtual three point bending and torsion experiments and comparing the results to the real experiment of the immature femur.

APPENDIX A

LOAD DEFORMATION CURVES FOR THREE POINT BENDING TESTS PERFORMED ON FEMURS WITH SOFT TISSUE INTACT AND RESULTING FRACTURES

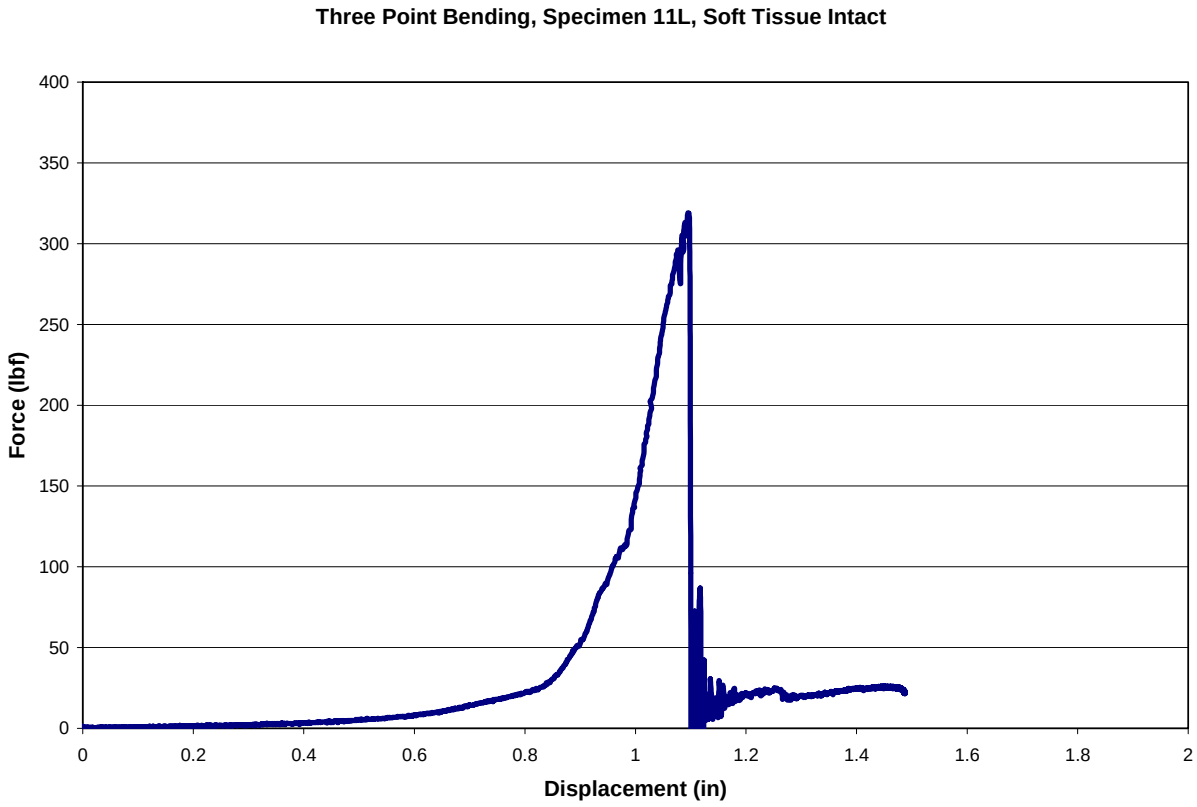

Figure A-1 Force – displacement curve for specimen 11L

Figure A-2 Specimen 11 L post fracture

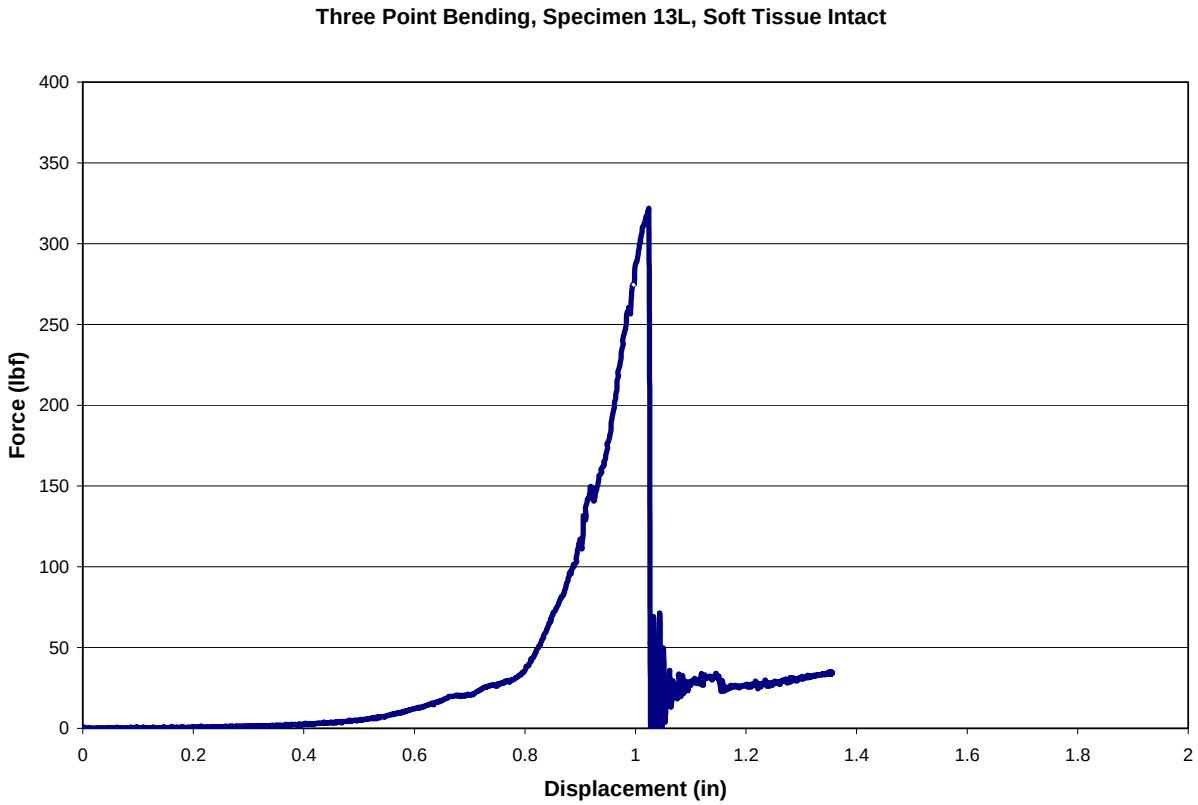

Figure A-3 Force – displacement curve for specimen 13L

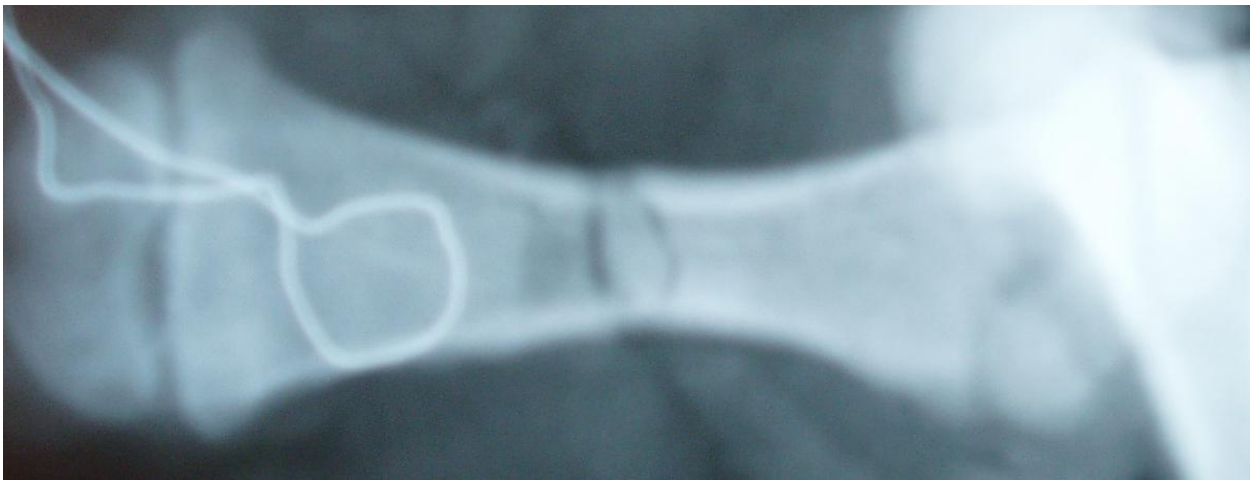

Figure A-4 Specimen 13 L post fracture

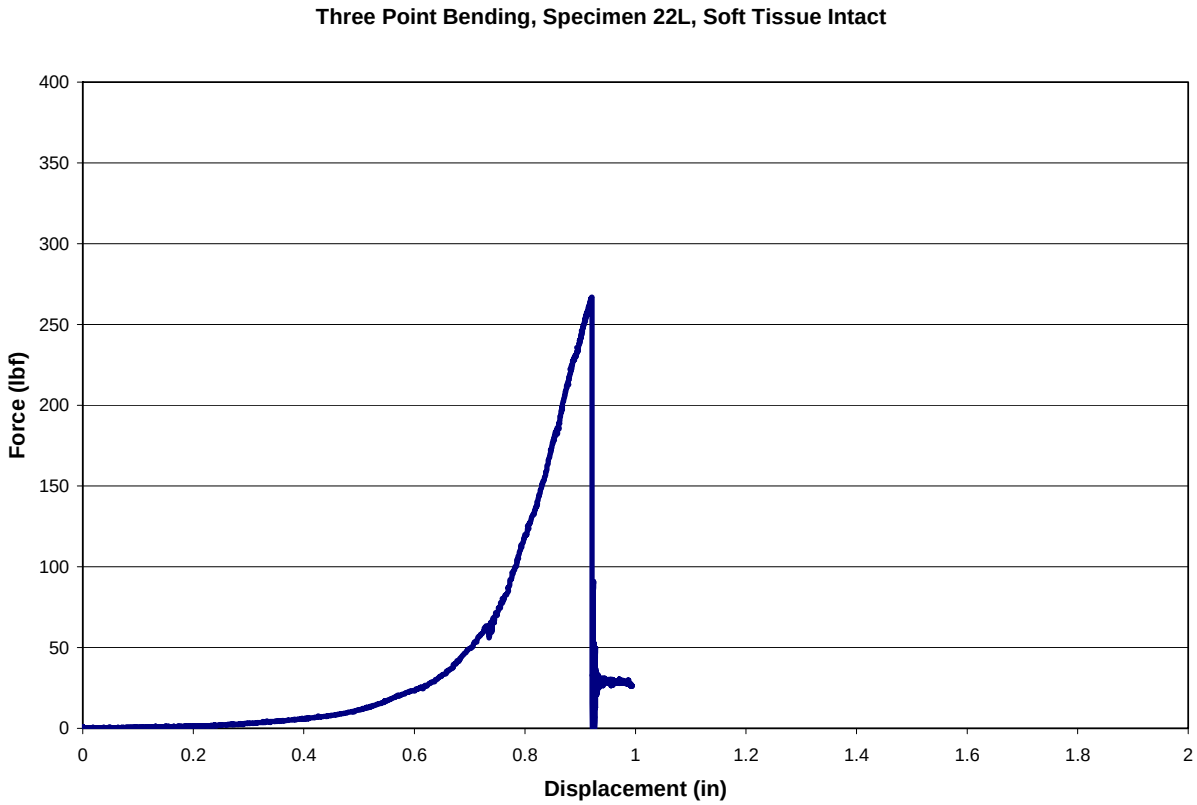

Figure A-5 Force – displacement curve for specimen 22L

Figure A-6 Specimen 22 L post fracture

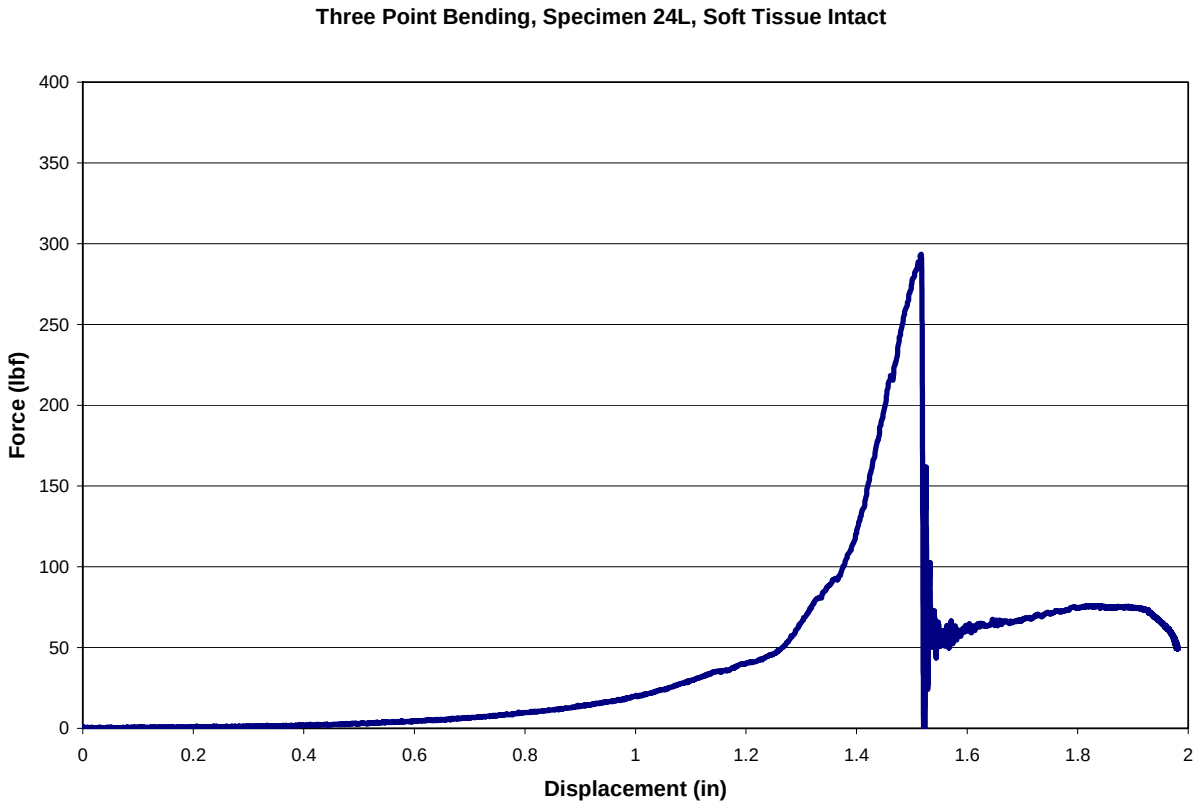

Figure A-7 Force – displacement curve for specimen 24L

Figure A-8 Specimen 24L post fracture

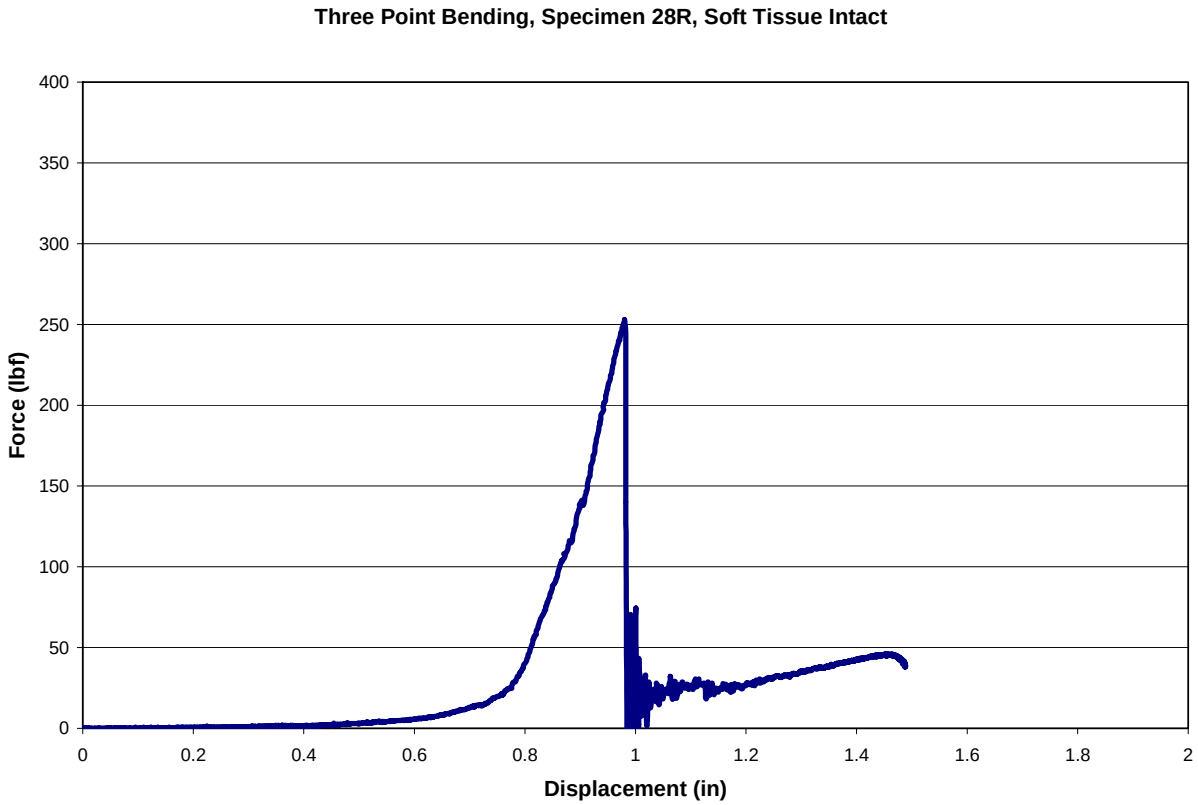

Figure A-9 Force – displacement curve for specimen 28R

Figure A-10 Specimen 28 R post fracture

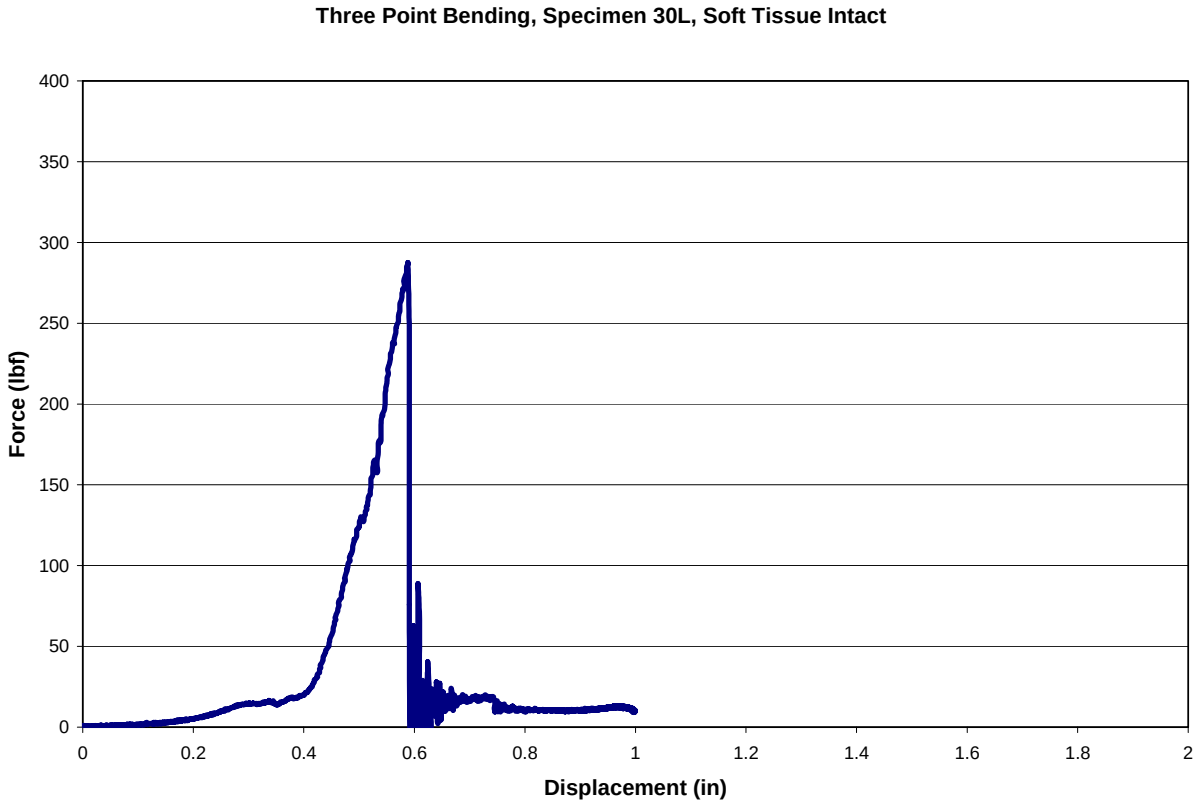

Figure A-11 Force – displacement curve for specimen 30L

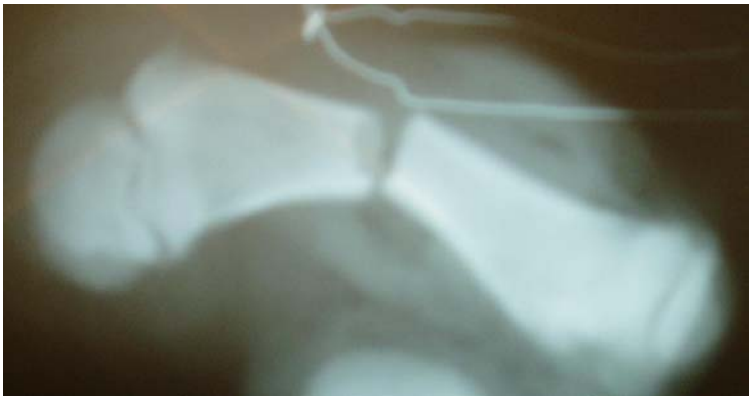

Figure A-12 Specimen 30 L post fracture

APPENDIX B

LOAD DEFORMATION CURVES FOR THREE POINT BENDING TESTS PERFORMED ON FEMURS WITH NO SOFT TISSUE INTACT AND RESULTING FRACTURES

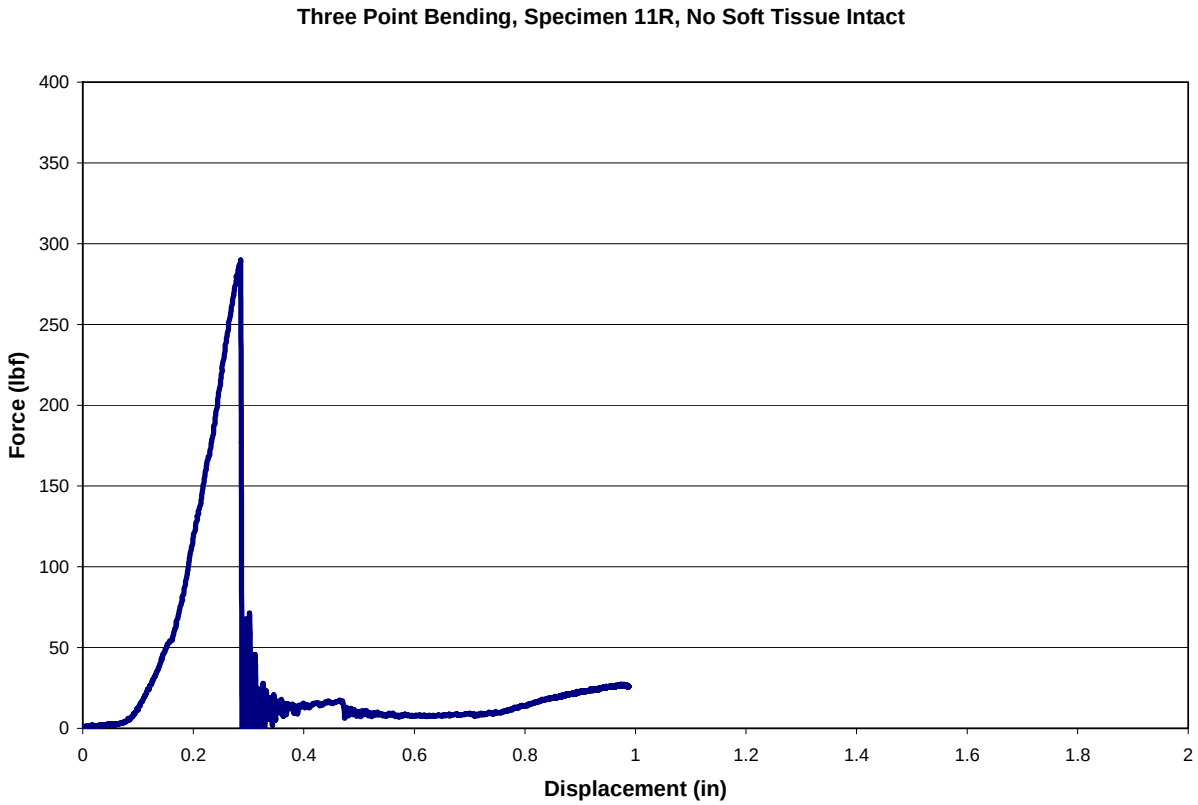

Figure B-1 Force – displacement curve for specimen 11R

Figure B-2 Specimen 11 R post fracture

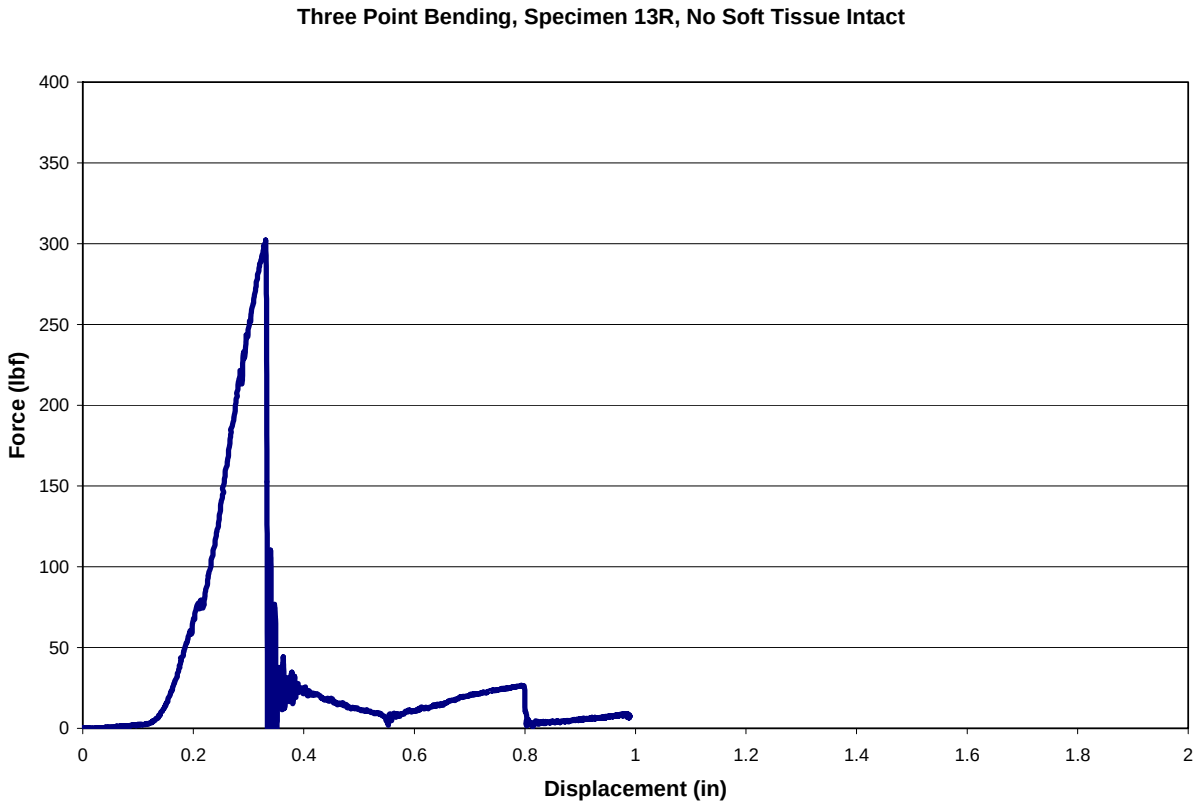

Figure B-3 Force – displacement curve for specimen 13R

Figure B-4 Specimen 13 R post fracture

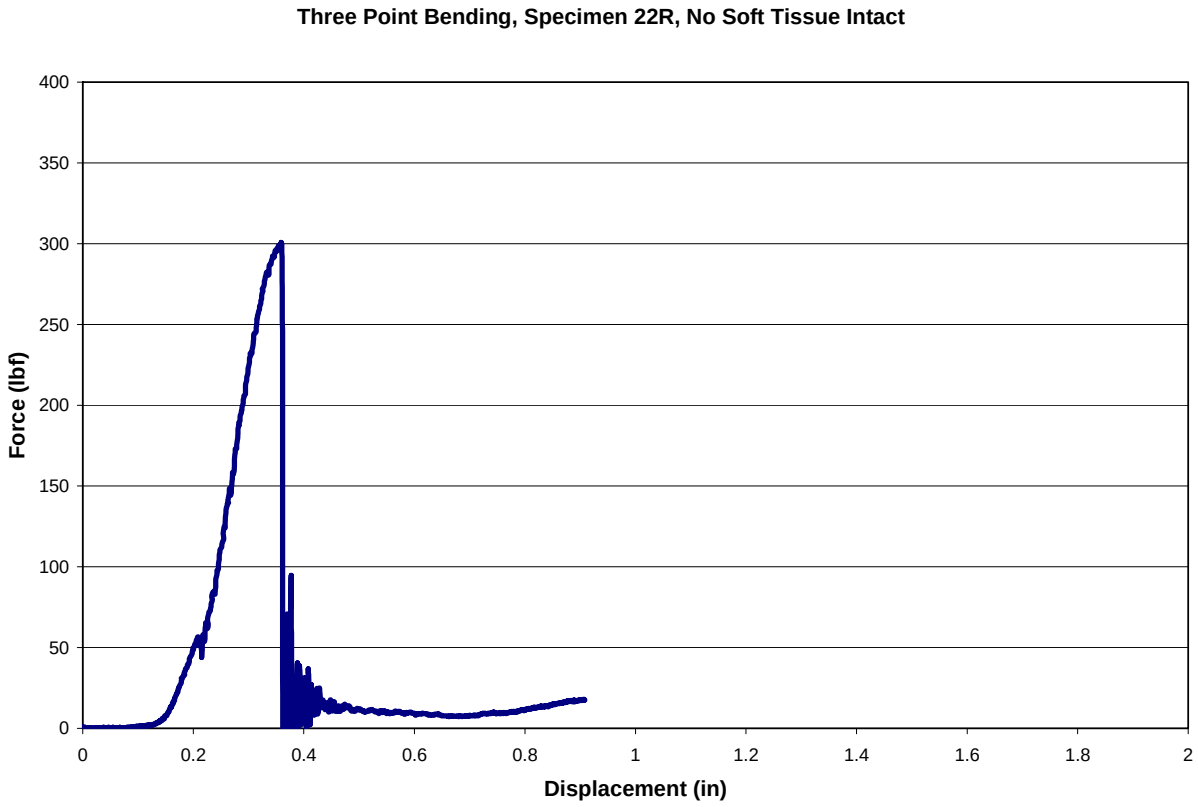

Figure B-5 Force – displacement curve for specimen 22R

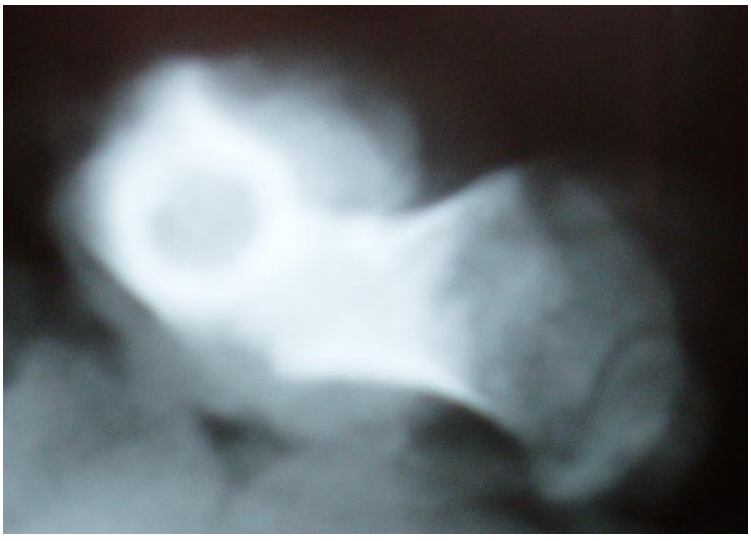

Figure B-6 Specimen 22 R post fracture

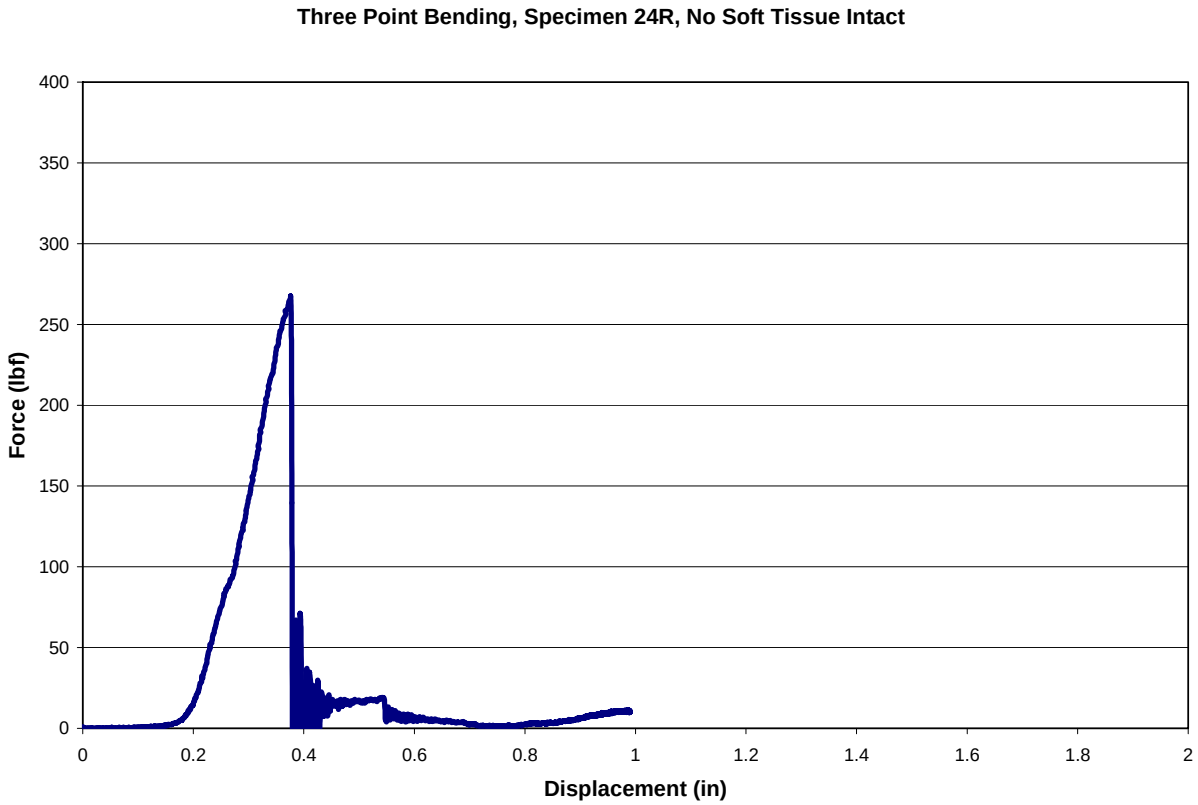

Figure B-7 Force – displacement curve for specimen 24R

Figure B-8 Specimen 24 R post fracture

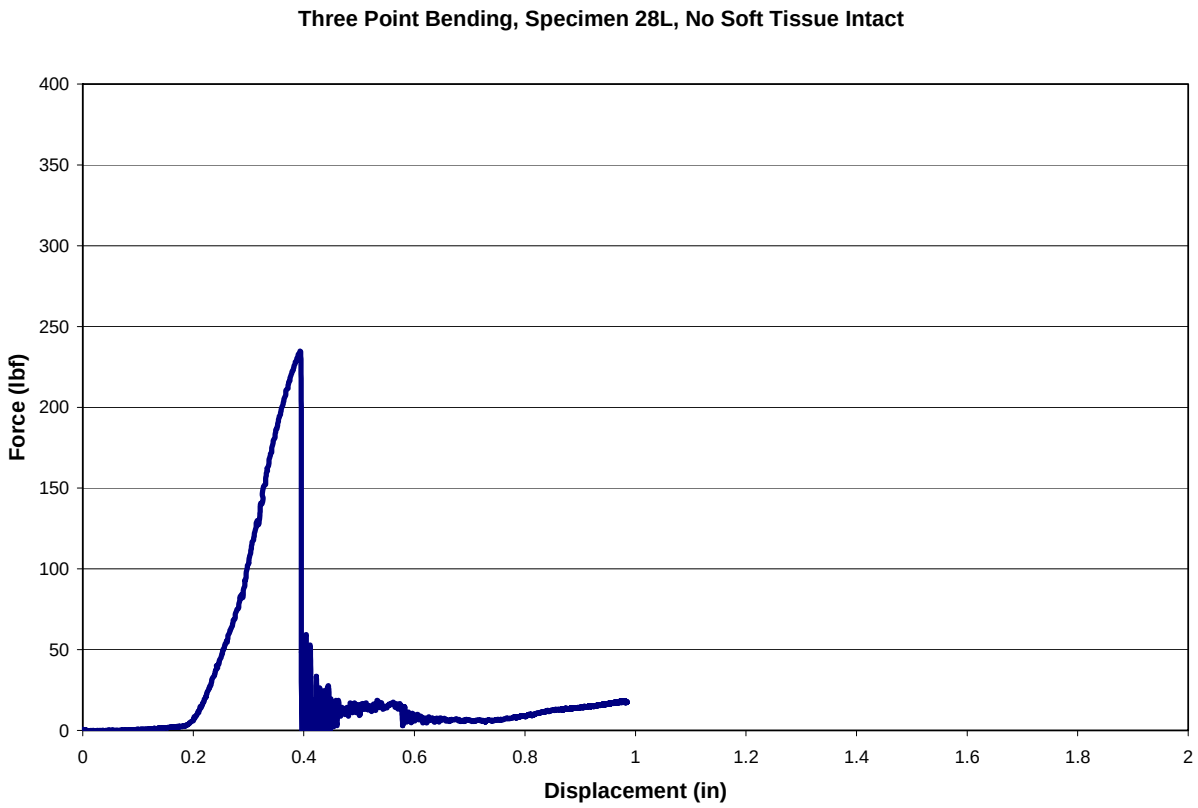

Figure B-9 Force – displacement curve for specimen 28L

Figure B-10 Specimen 28 L post fracture

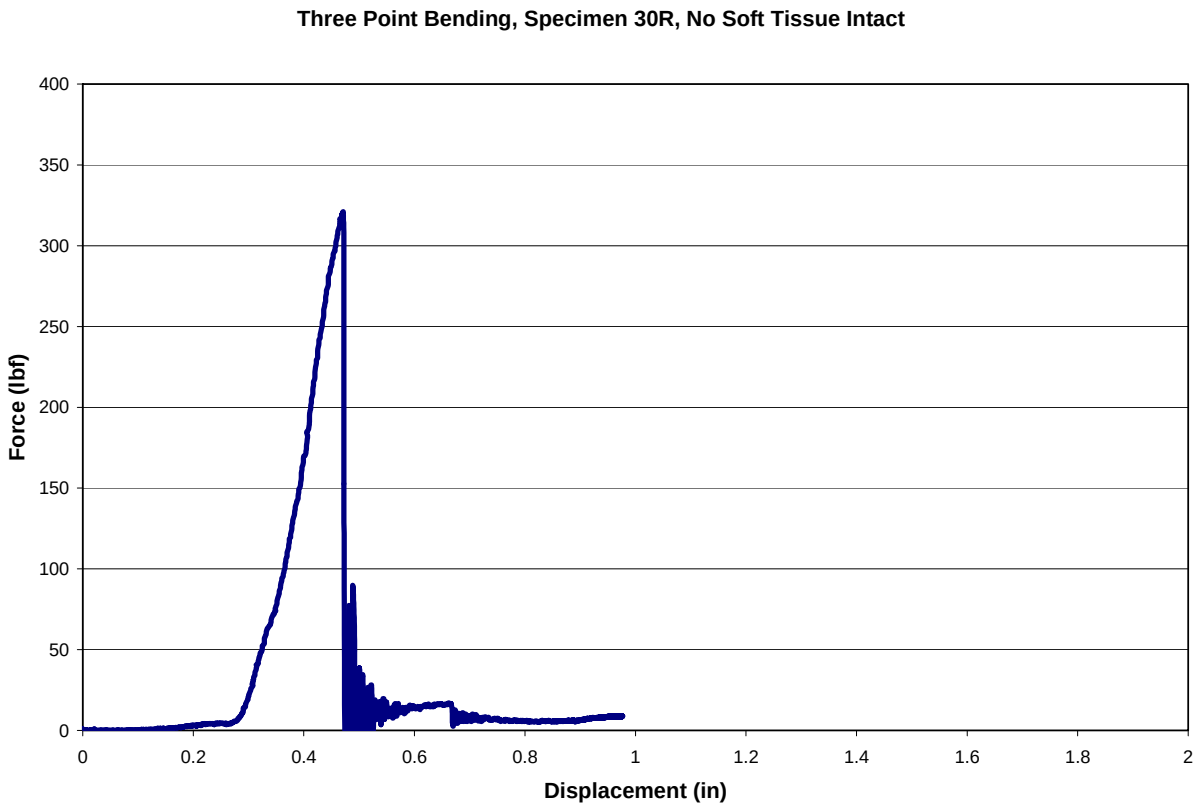

Figure B-11 Force – displacement curve for specimen 30R

Figure B-12 Specimen 30 R post fracture

APPENDIX C

TORQUE VS ANGULAR DEFORMATION CURVES FOR TORSION TESTS PERFORMED ON FEMURS AT 0.167 DEGREES PER SECOND AND RESULTING FRACTURES

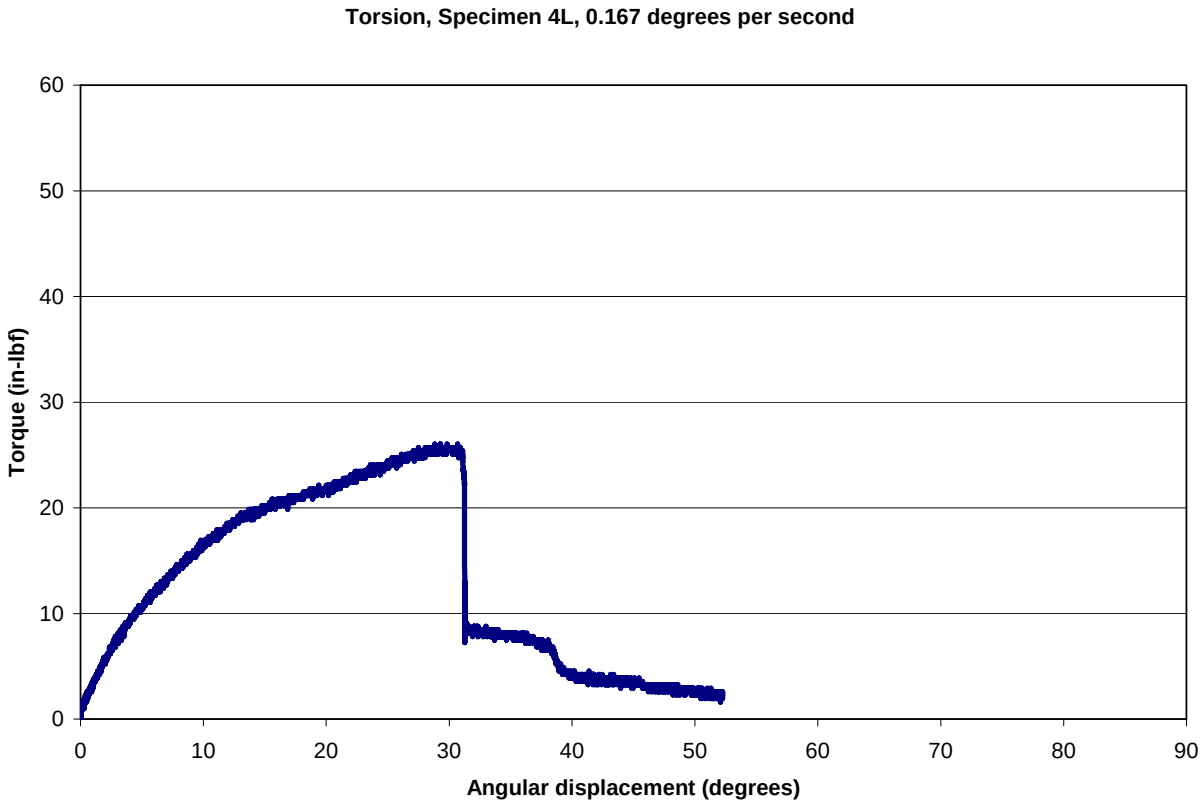

Figure C-1 Torque – angular deformation curve for specimen 4L

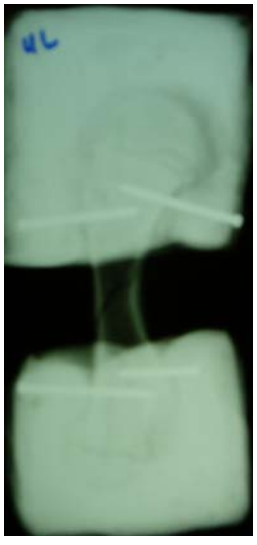

Figure C-2 Specimen 4 L post fracture

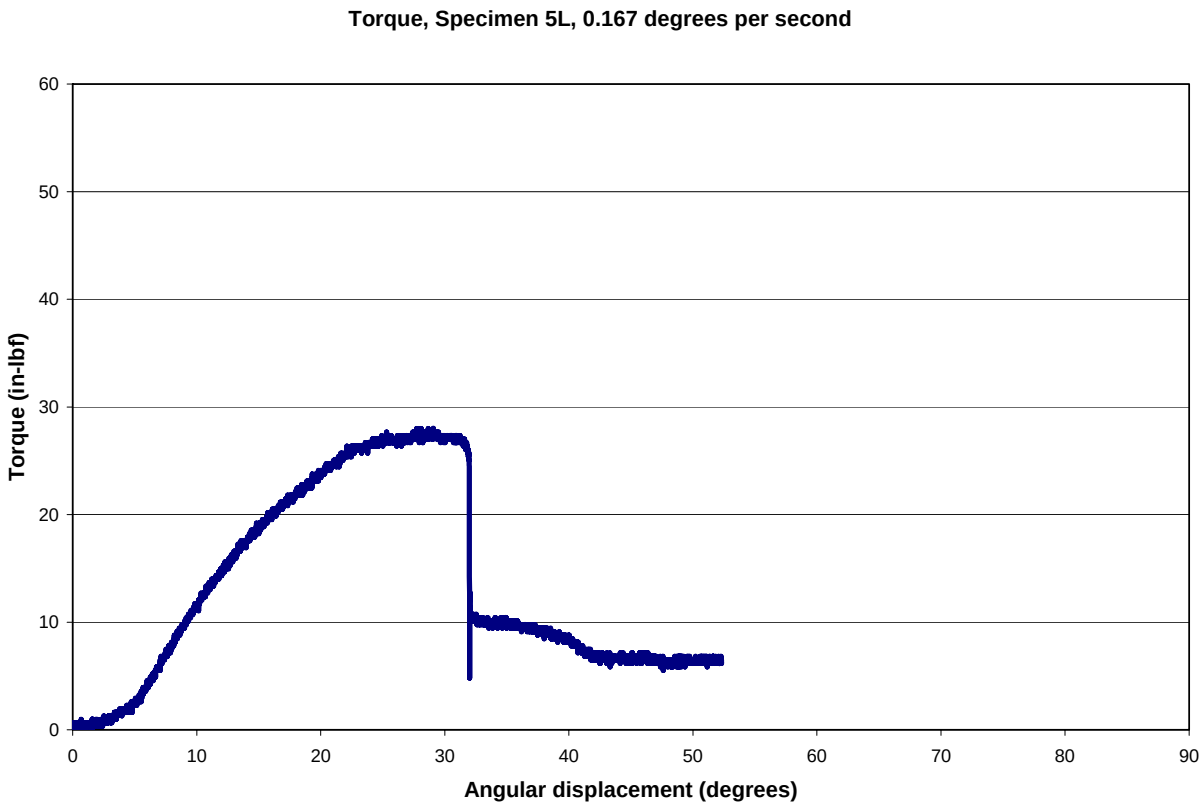

Figure C-3 Torque – angular deformation curve for specimen 5L

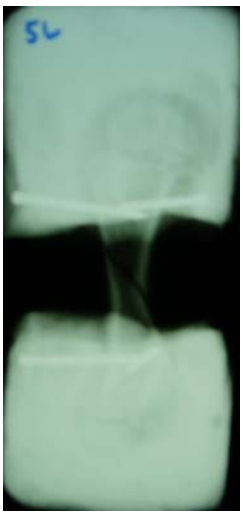

Figure C-4 Specimen 5 L post fracture

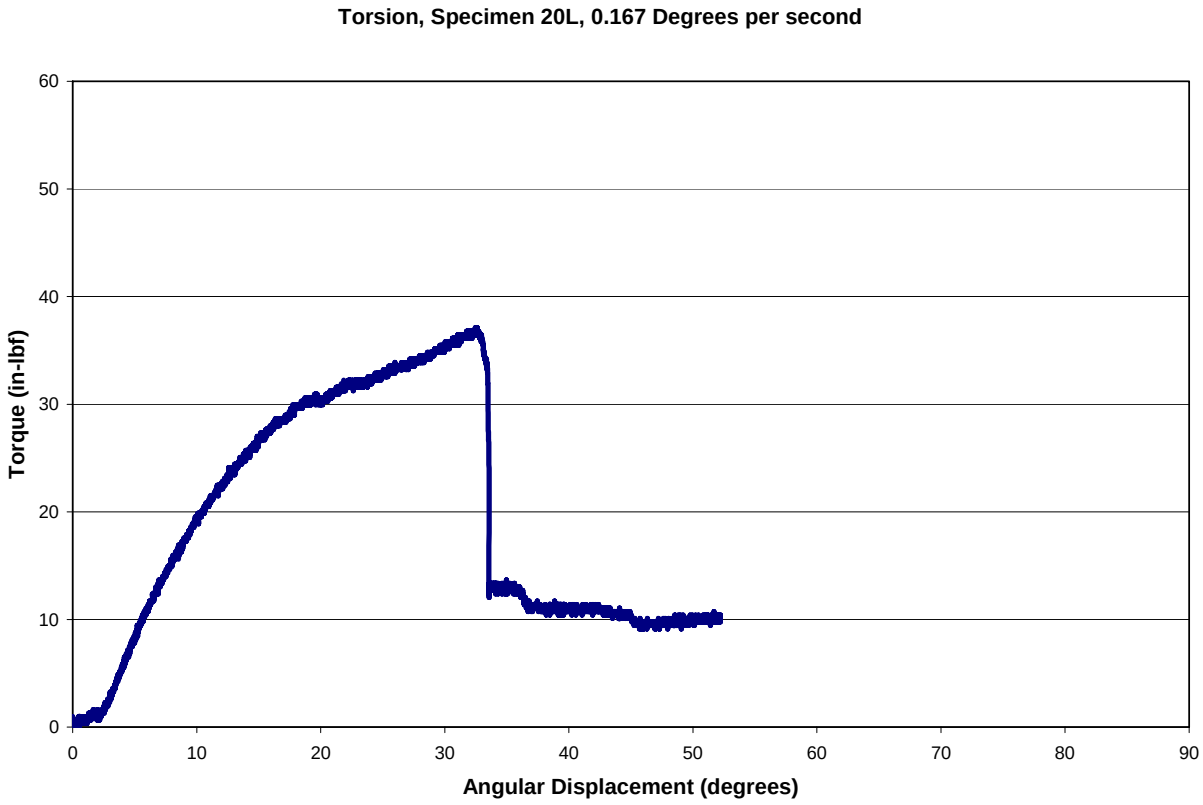

Figure C-5 Torque – angular deformation curve for specimen 20L

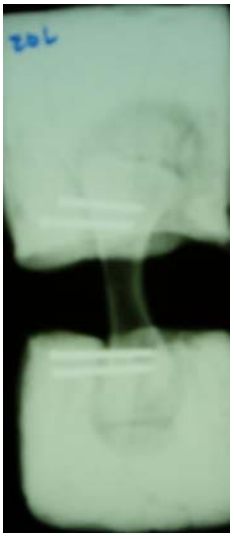

Figure C-6 Specimen 20 L post fracture

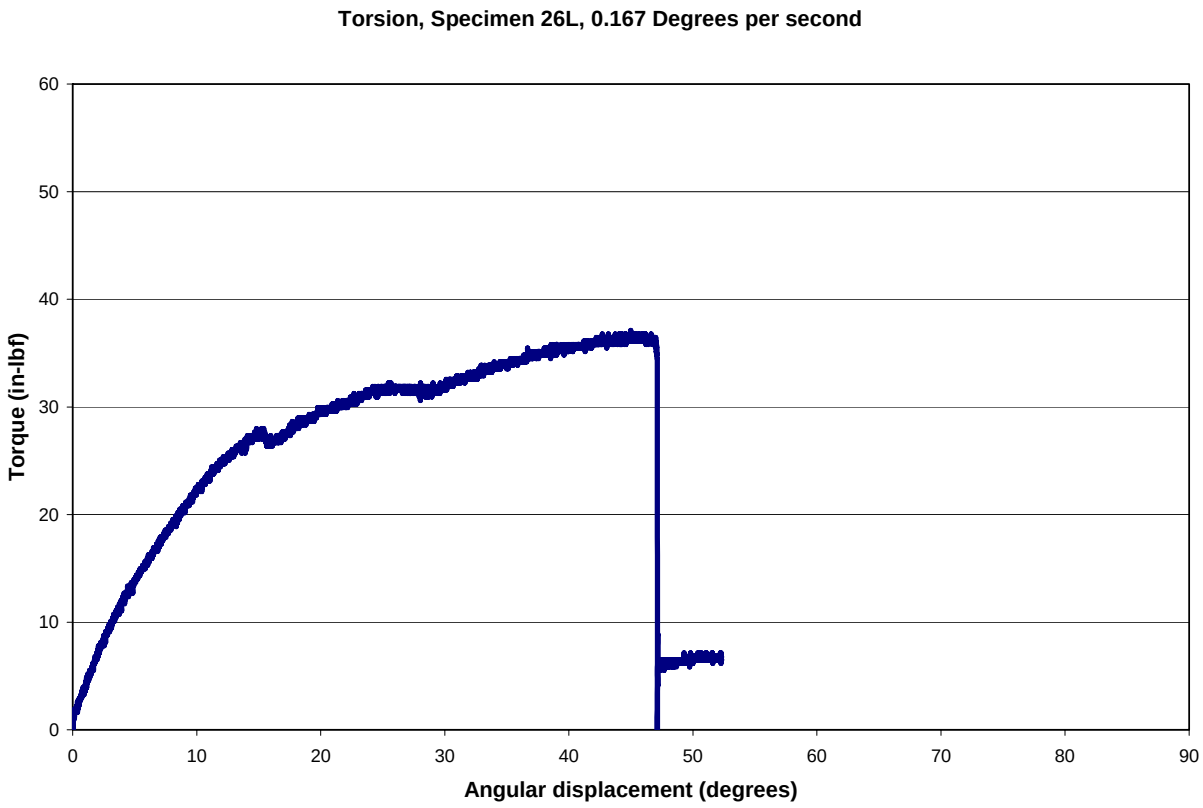

Figure C-7 Torque – angular deformation curve for specimen 26L

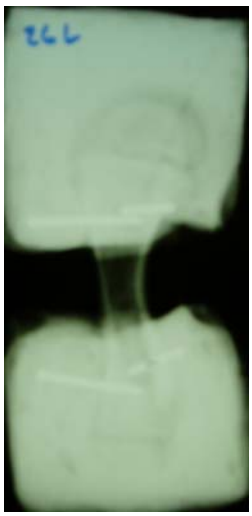

Figure C-8 Specimen 26 L post fracture

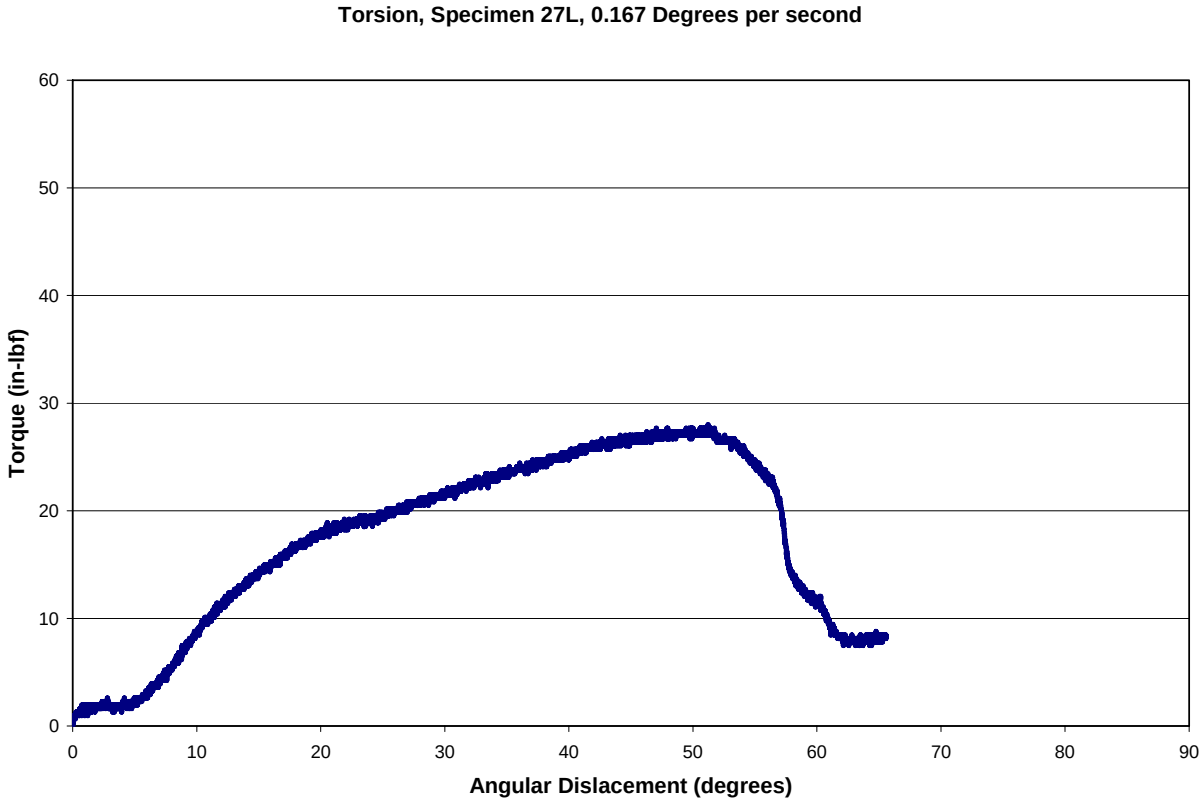

Figure C-9 Torque – angular deformation curve for specimen 27L

Figure C-10 Specimen 27 L post fracture

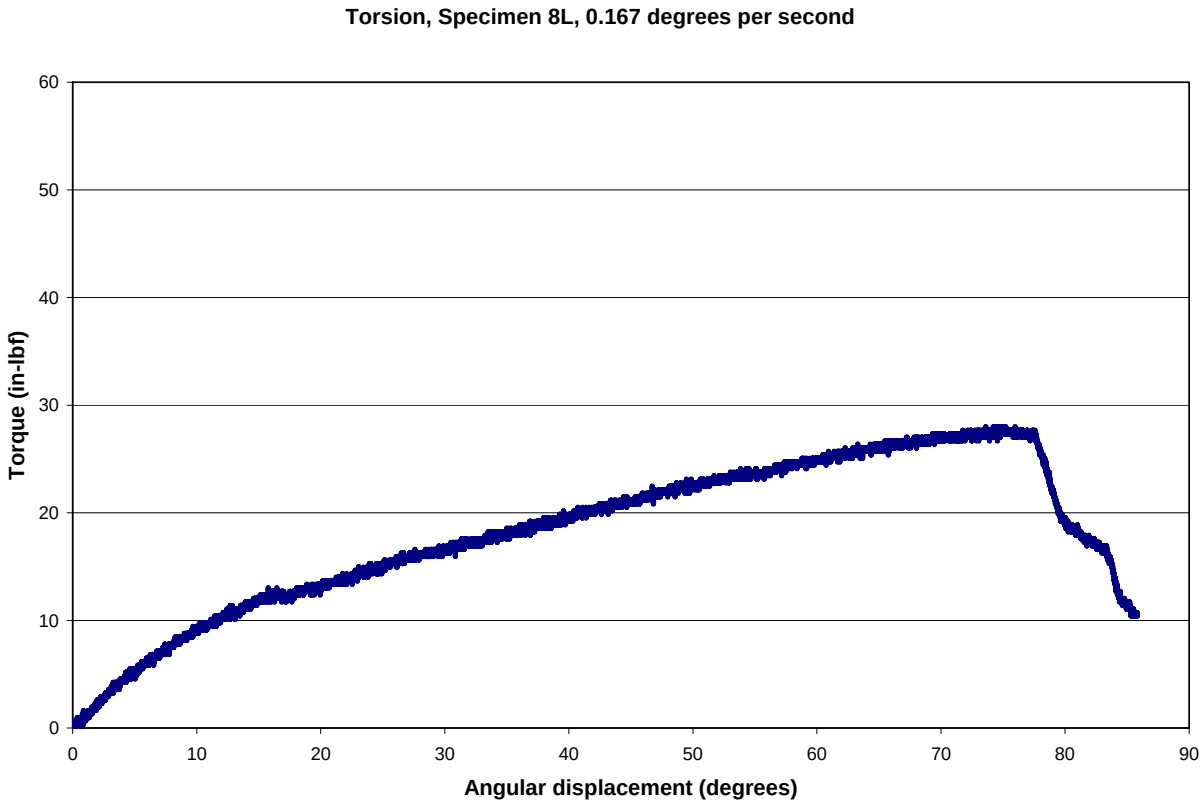

Figure C-11 Torque – angular deformation curve for specimen 8L

Figure C-12 Specimen 8 L post fracture

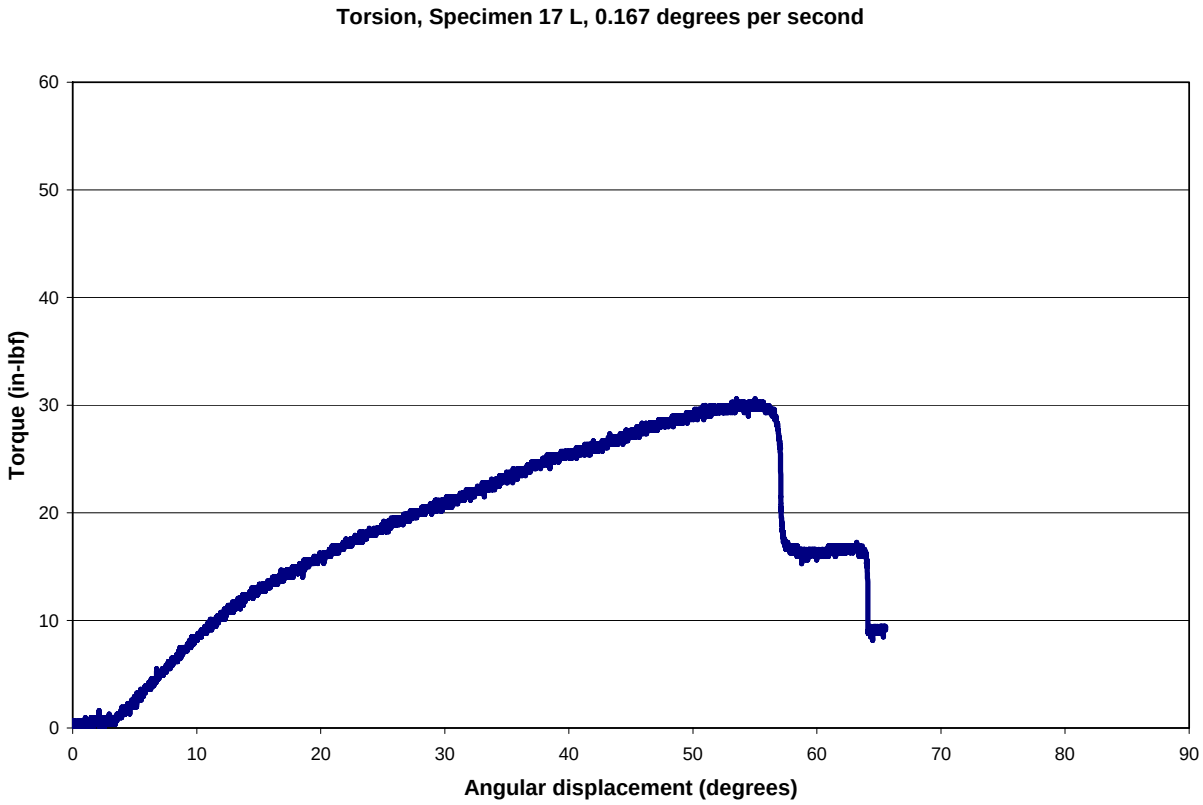

Figure C-13 Torque – angular deformation curve for specimen 17L

Figure C-14 Specimen 17 L post fracture

APPENDIX D

TORQUE VS ANGULAR DEFORMATION CURVES FOR TORSION TESTS PERFORMED ON FEMURS AT 90 DEGREES PER SECOND AND RESULTING FRACTURES

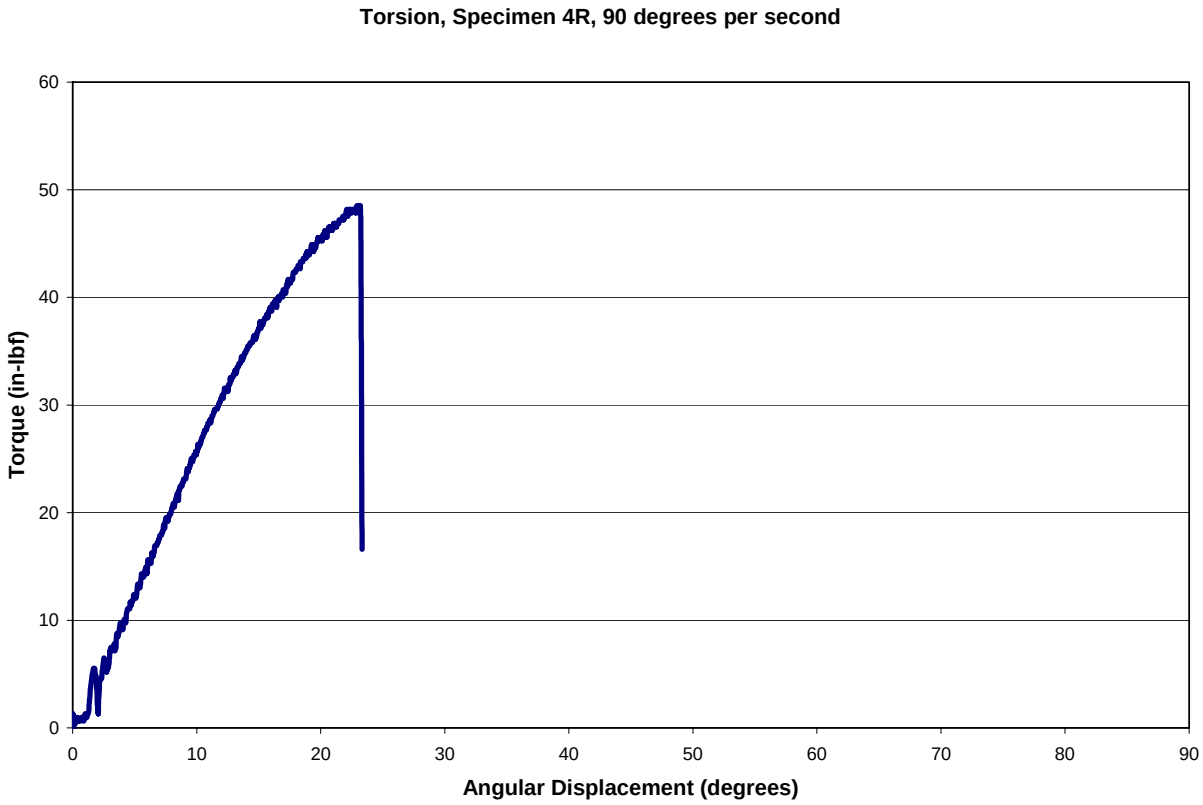

Figure D-1 Torque – angular de formation cur ve for specimen 4R

Figure D-2 Specimen 4 R post fracture

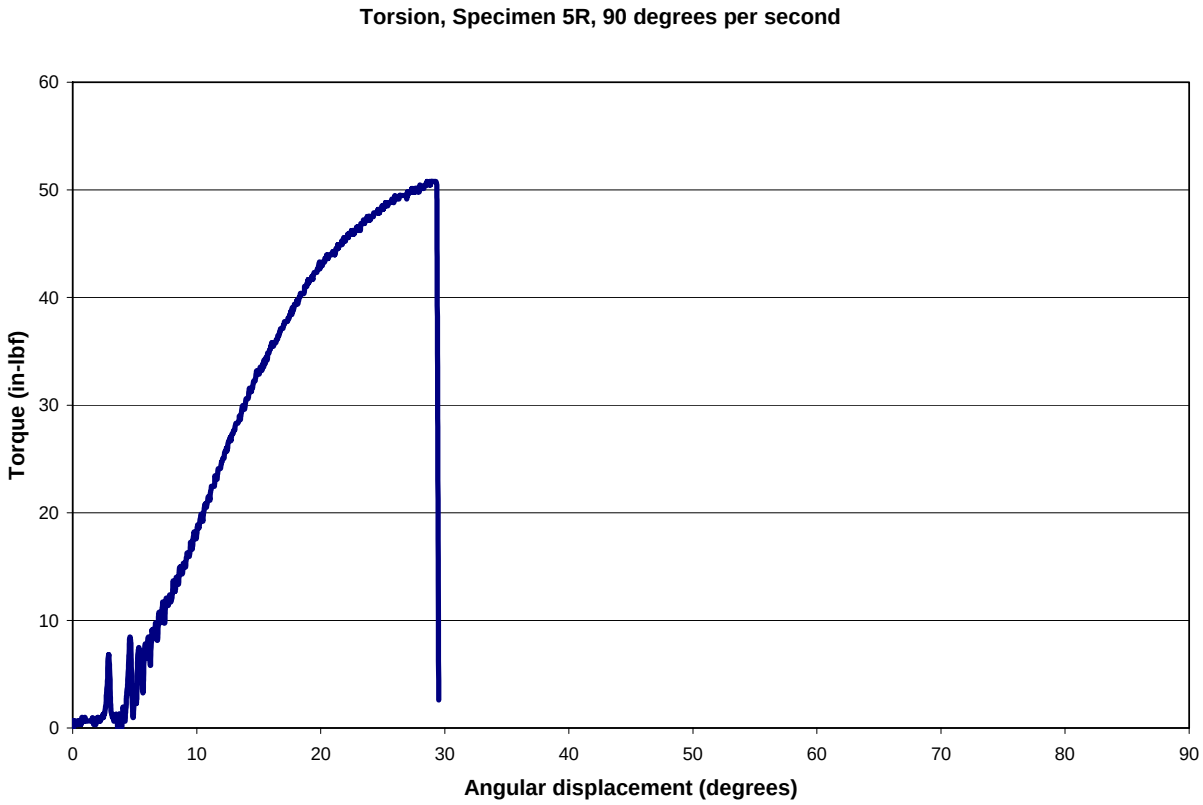

Figure D-3 Torque – angular deformation curve for specimen 5R

Figure D-4 Specimen 5 R post fracture

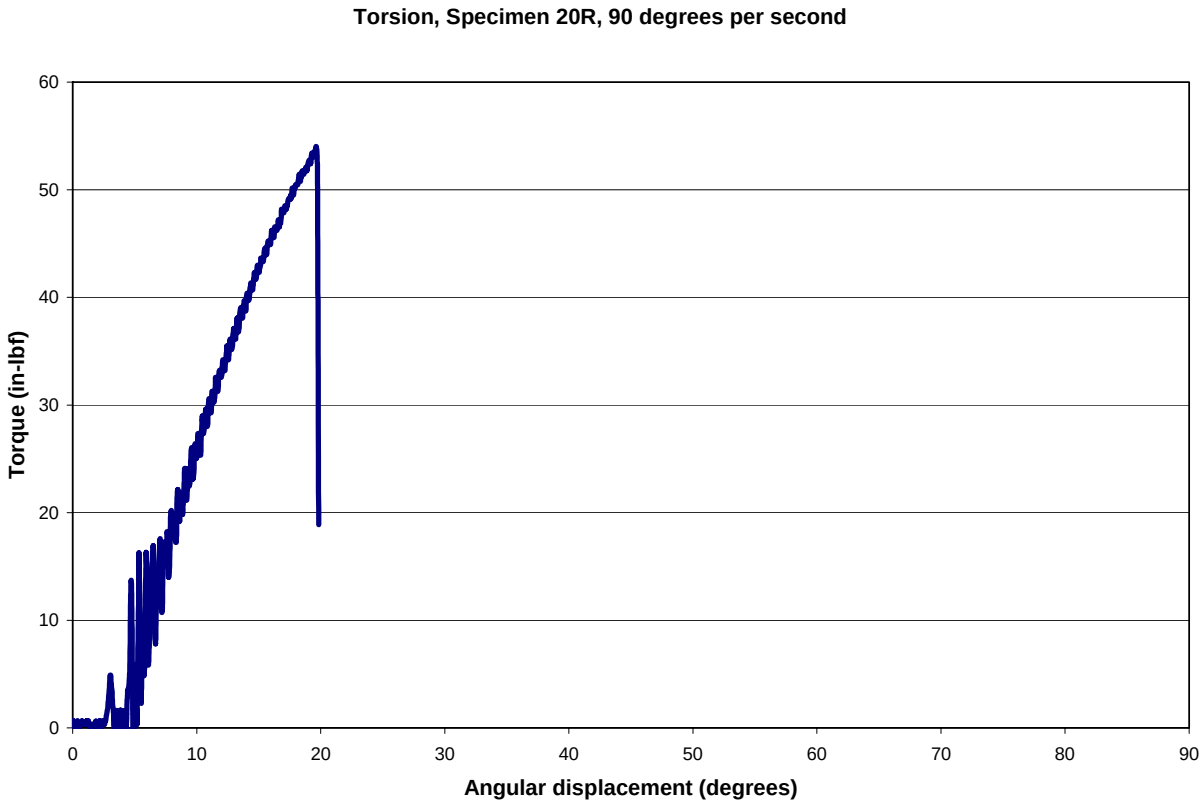

Figure D-5 Torque – angular deformation curve for specimen 20R

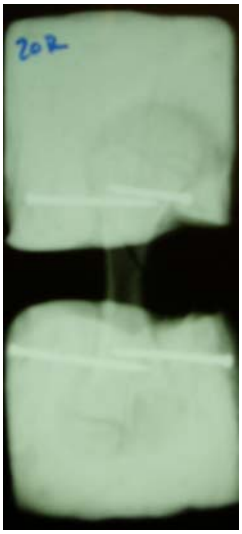

Figure D-6 Specimen 20 R post fracture

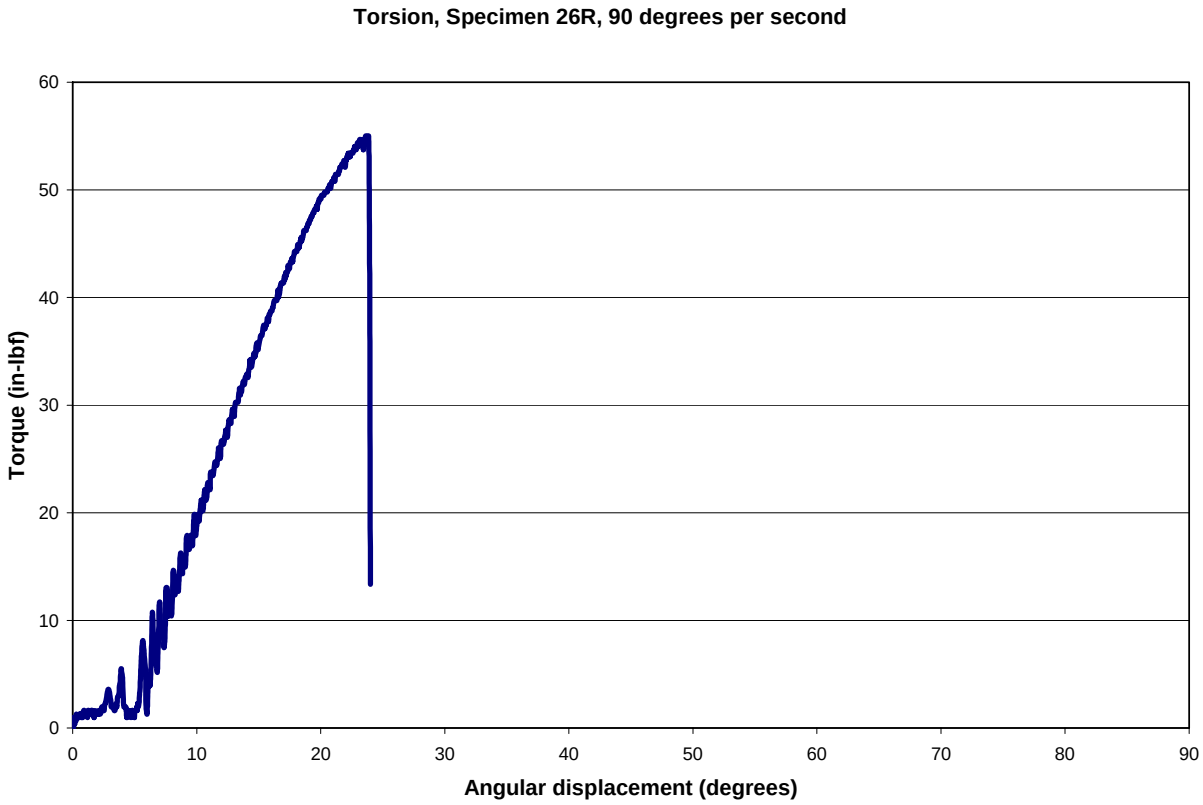

Figure D-7 Torque – angular deformation curve for specimen 26R

Figure D-8 Specimen 26 R post fracture

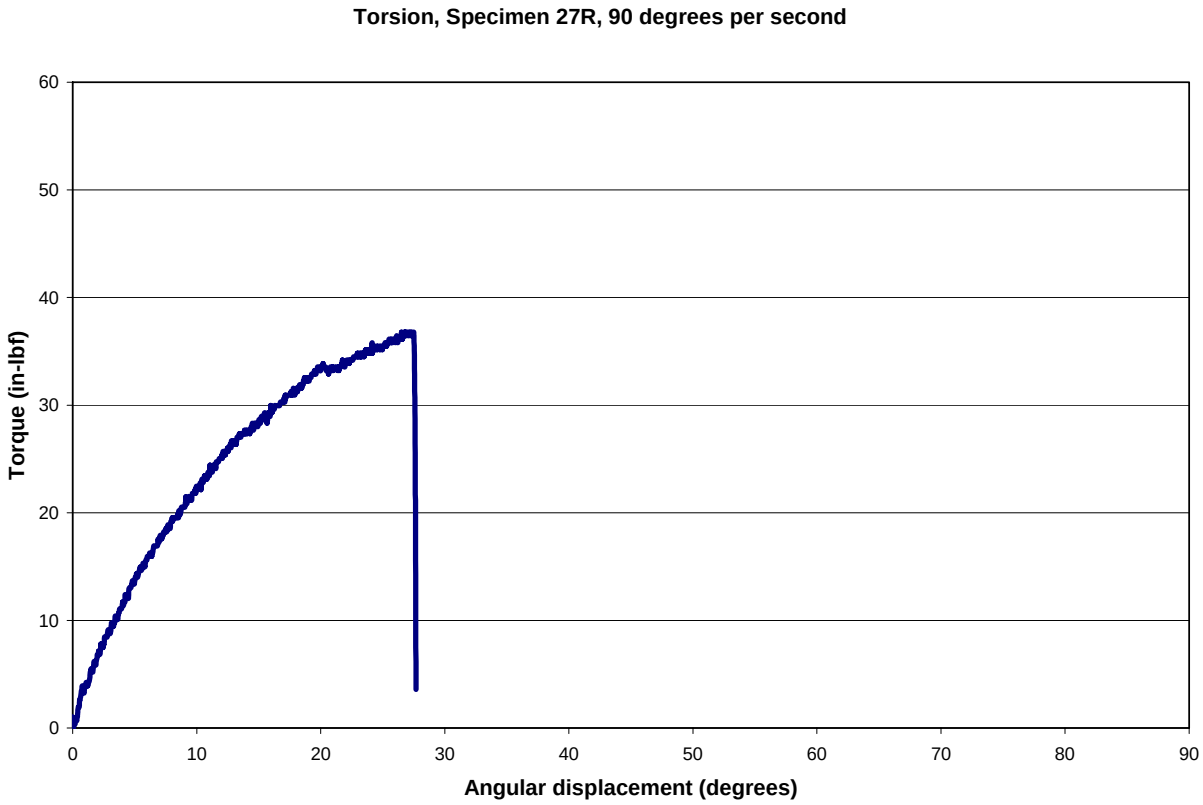

Figure D-9 Torque – angular deformation curve for specimen 27R

Figure D-10 Specimen 27 R post fracture

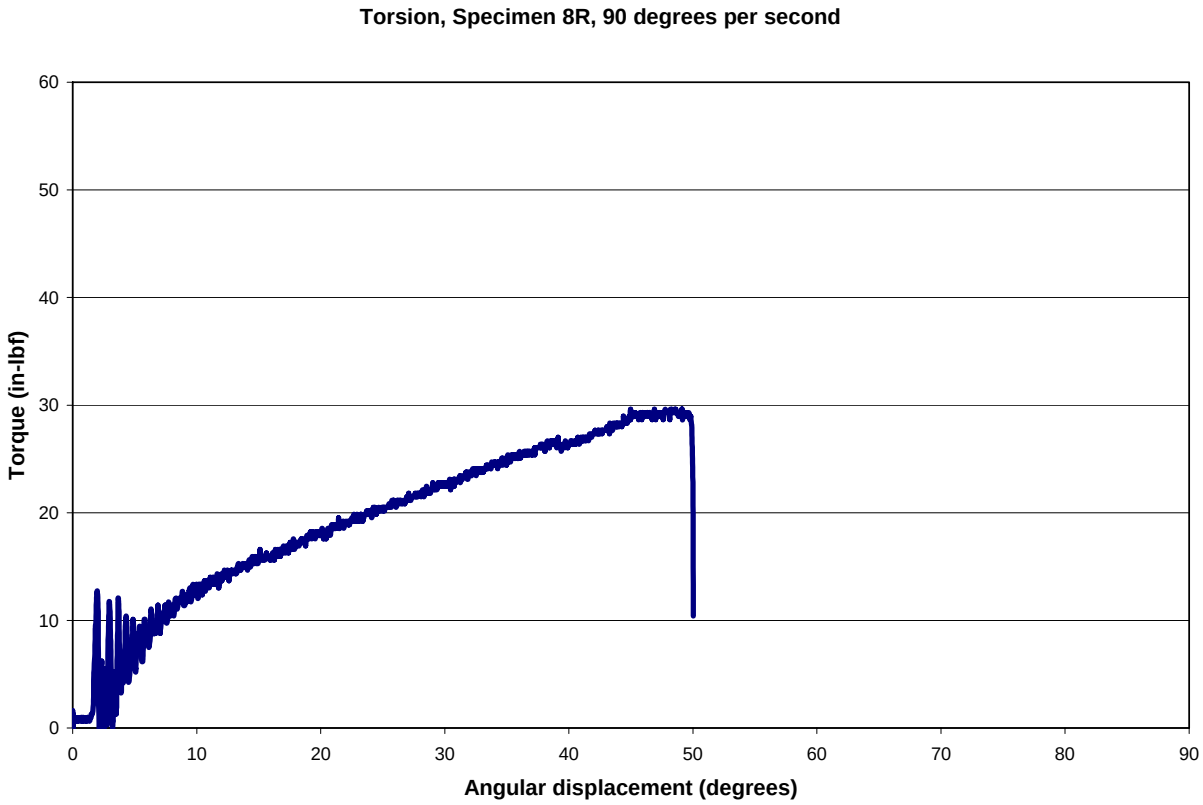

Figure D-11 Torque – angular deformation curve for specimen 8 R

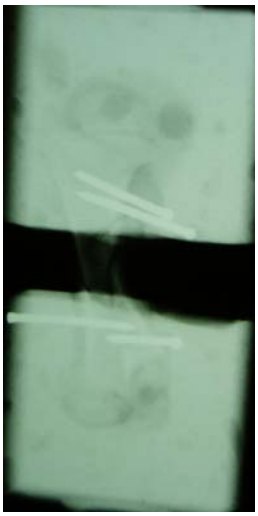

Figure D-12 Specimen 8 R post fracture

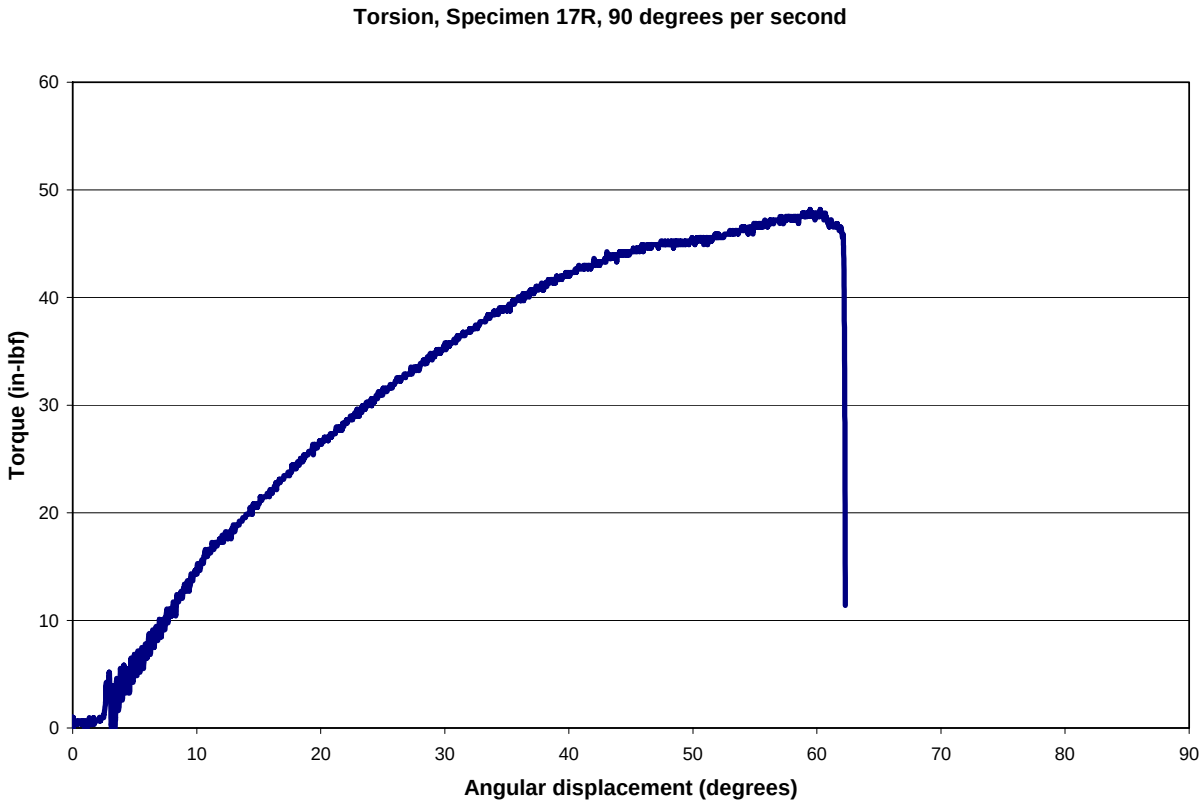

Figure D-13 Torque – angular deformation curve for specimen 17R

Figure D-14 Specimen 17 R post fracture

APPENDIX E

FORCE VS DEFORMATION CURVES FOR AXIAL COMPRESSION TESTS PERFORMED ON FEMURS AT 0.04 INCHES PER SECOND AND RESULTING FRACTURES

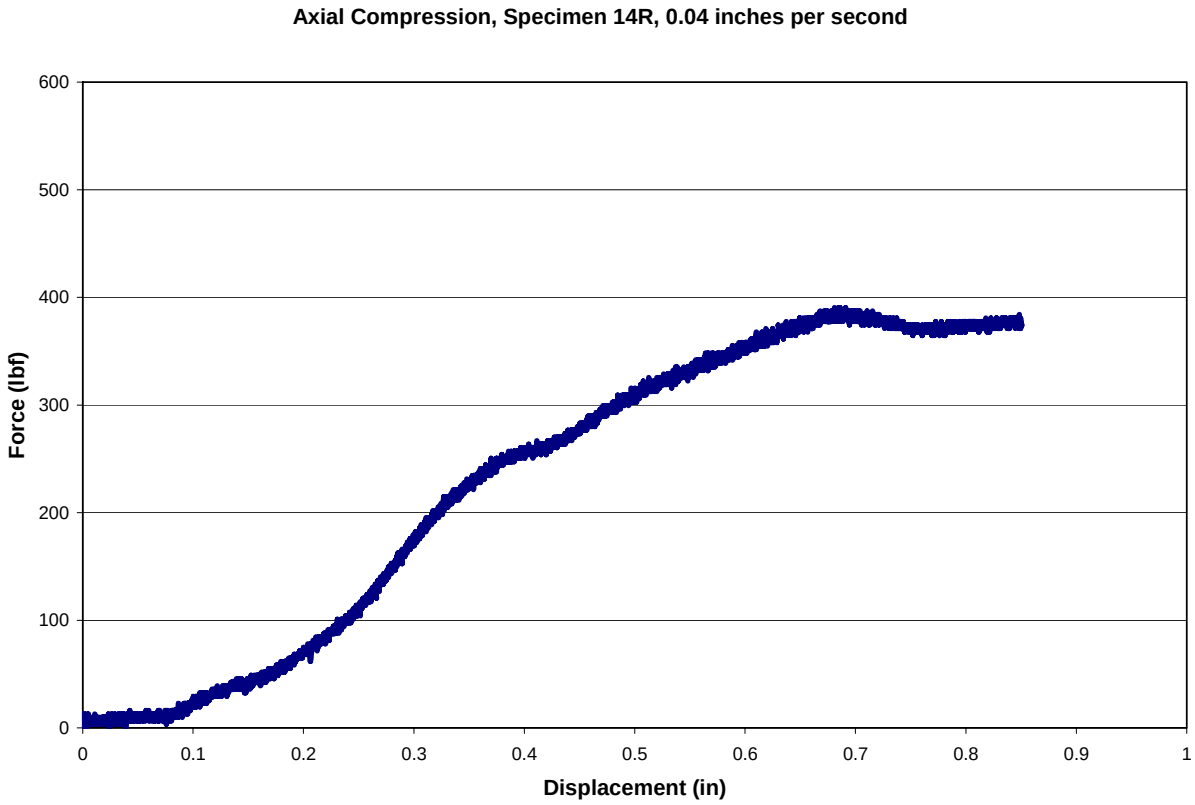

Figure E-1 Force – displacement curve for specimen 14R

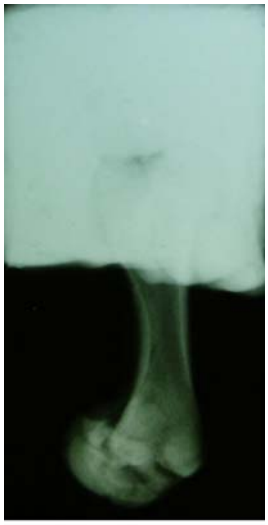

Figure E-2 Specimen 14 R post fracture

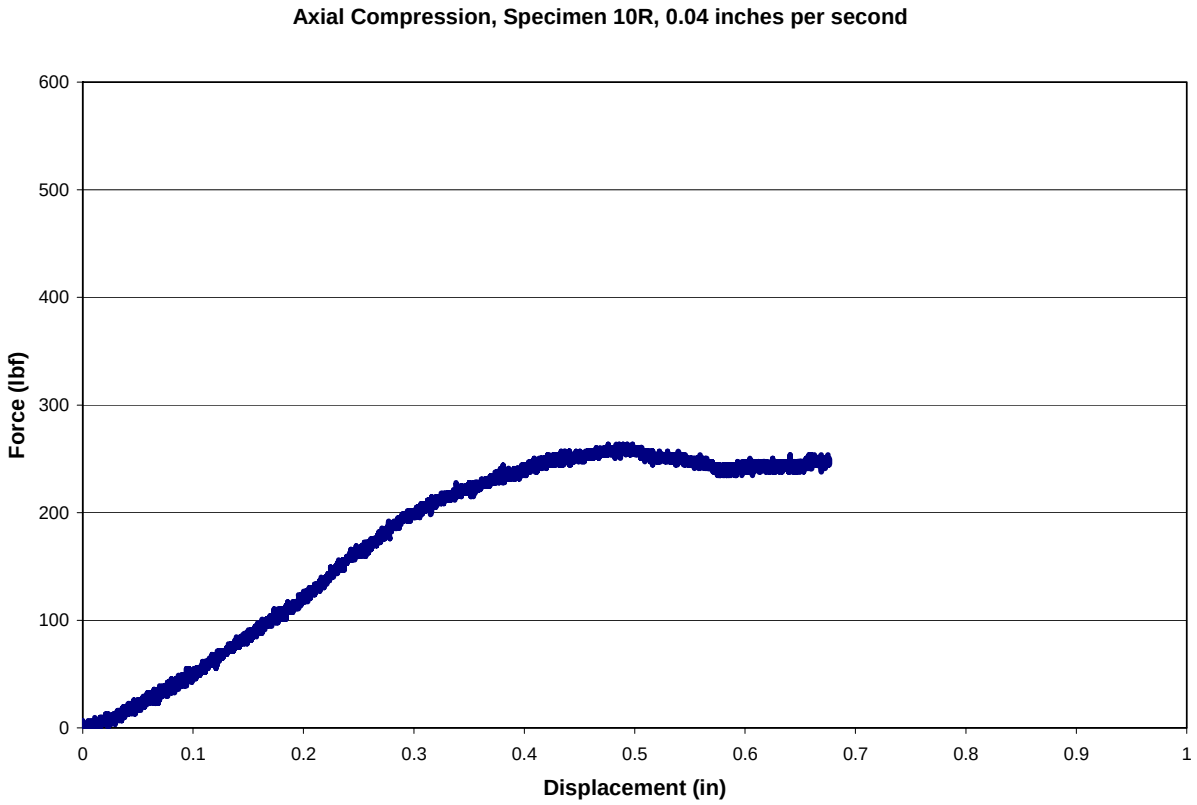

Figure E-3 Force – displacement curve for specimen 10R

Figure E-4 Specimen 10 R post fracture

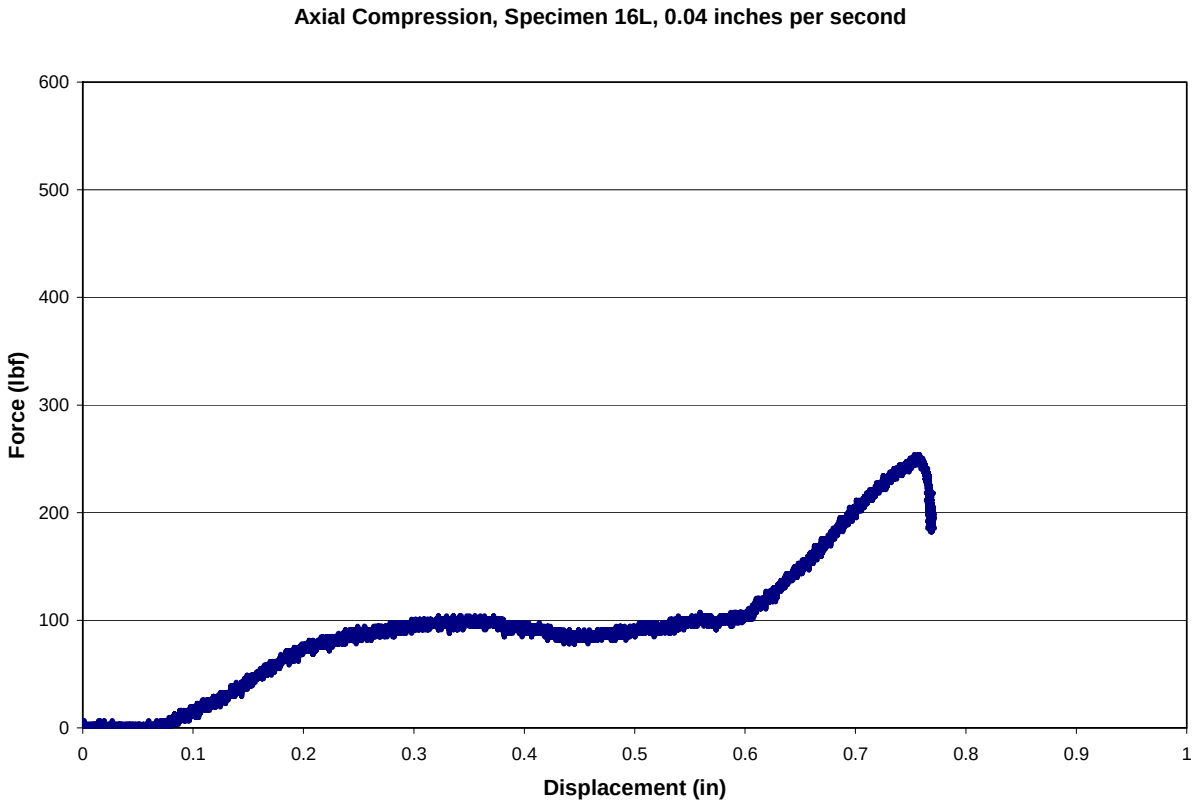

Figure E-5 Force – displacement curve for specimen 16L

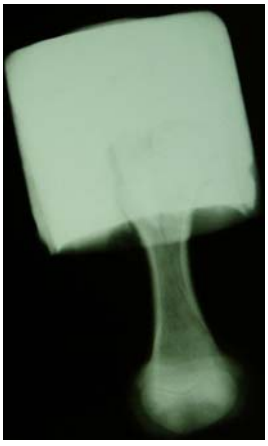

Figure E-6 Specimen 16 L post fracture

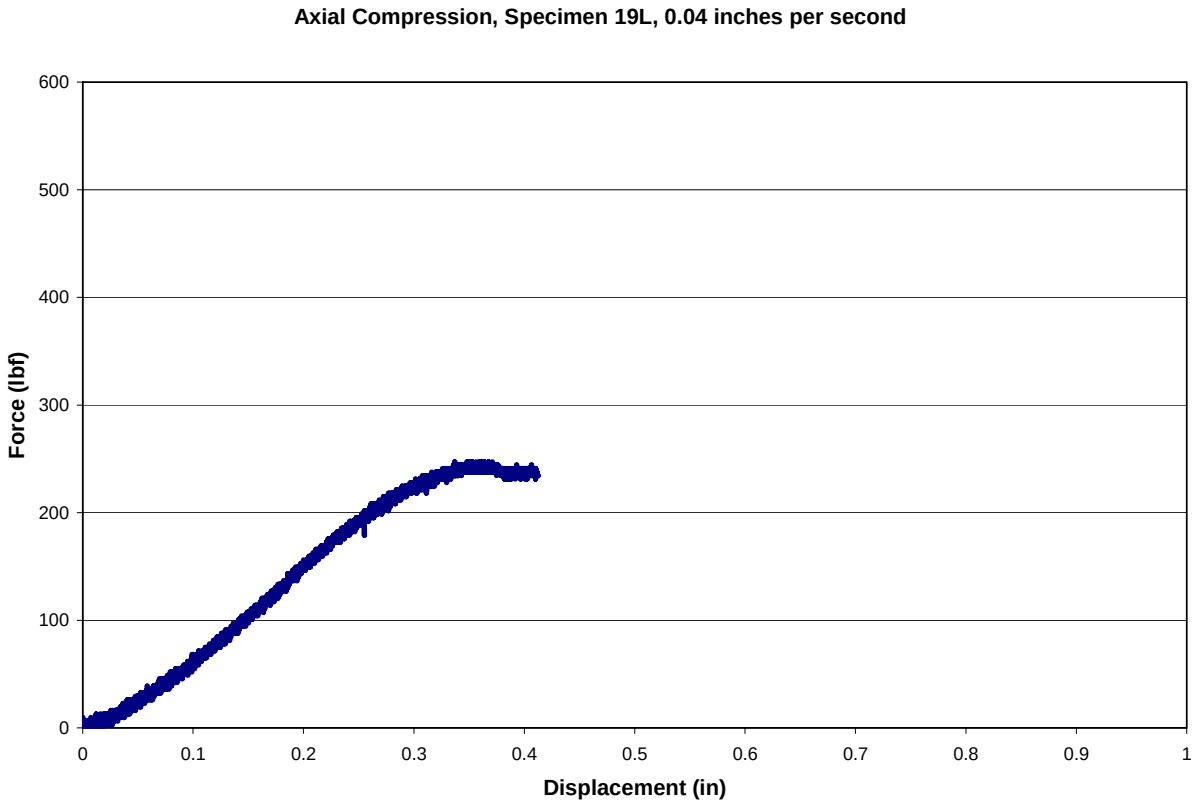

Figure E-7 Force – displacement curve for specimen 19L

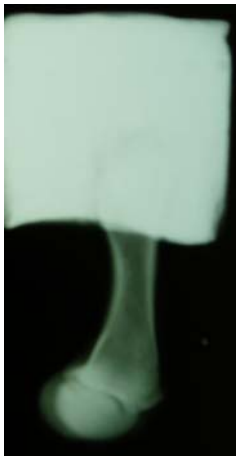

Figure E-8 Specimen 19 L post fracture

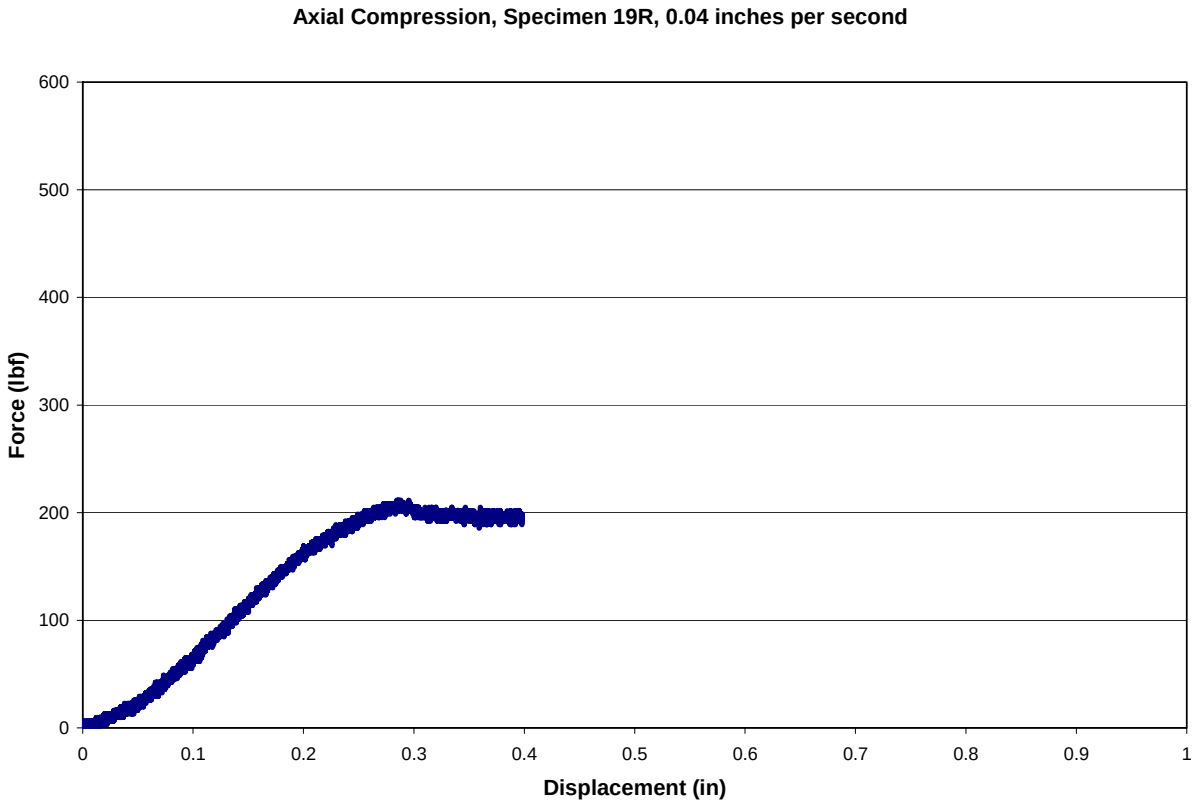

Figure E-9 Force – displacement curve for specimen 19R

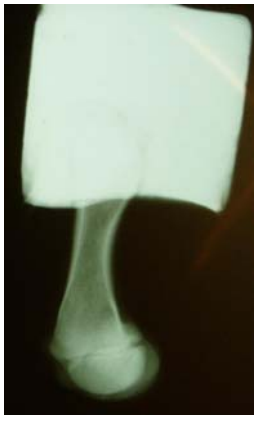

Figure E-10 Specimen 19 R post fracture

APPENDIX F

FORCE VS DEFORMATION CURVES FOR AXIAL COMPRESSION TESTS PERFORMED ON FEMURS AT 2 INCHES PER SECOND AND RESULTING FRACTURES

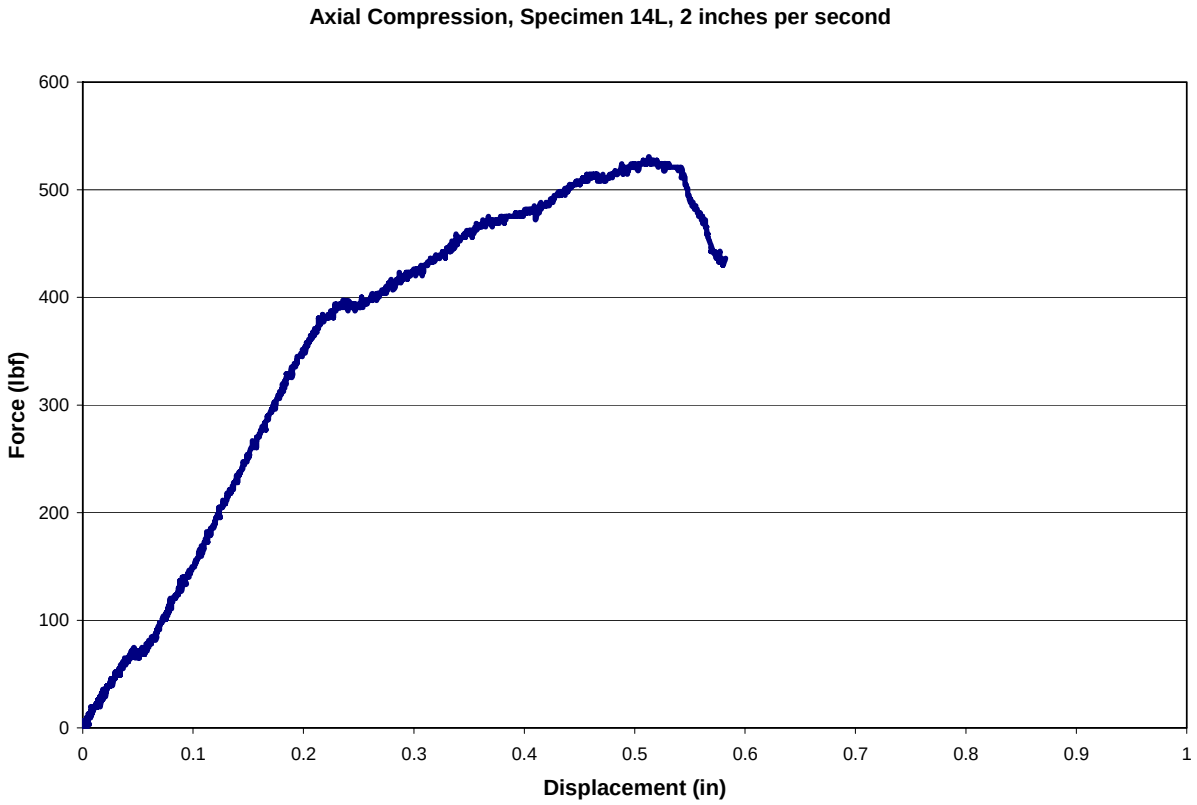

Figure F-1 Force – displacement curve for specimen 14L

Figure F-2 Specimen 14 L post fracture

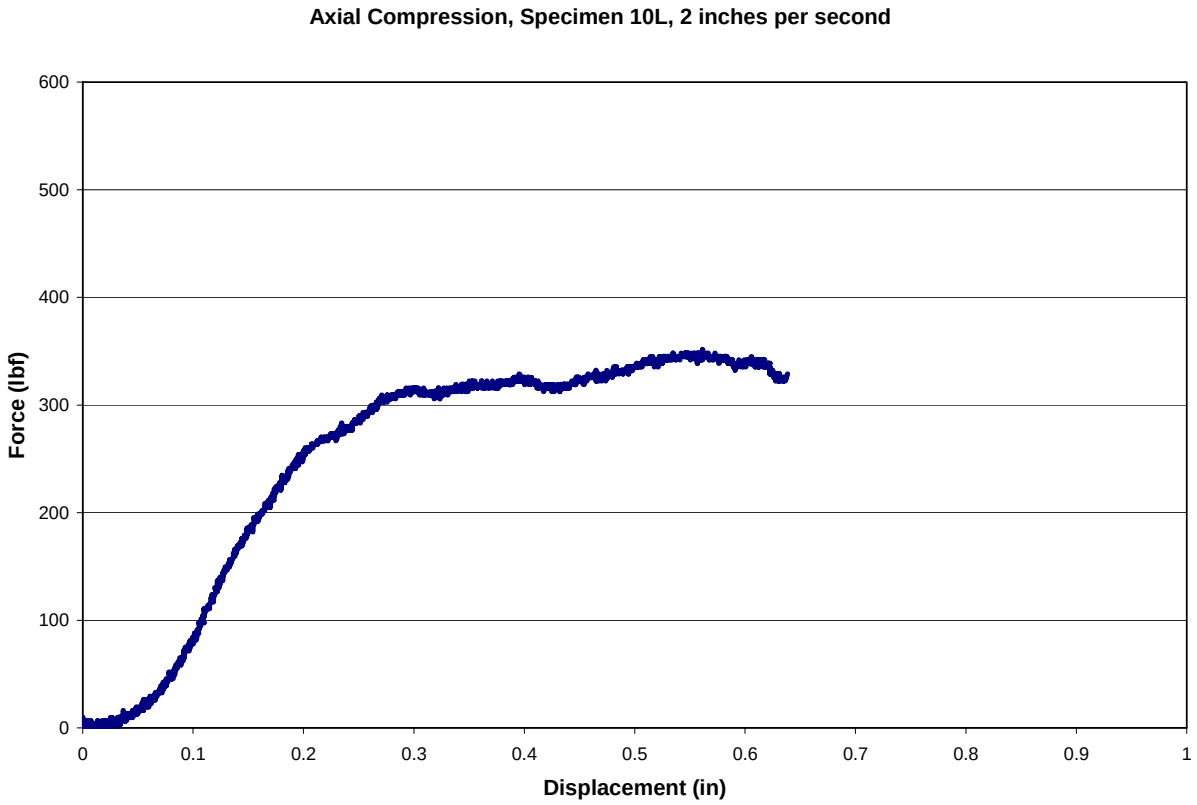

Figure F-3 Force – displacement curve for specimen 10L

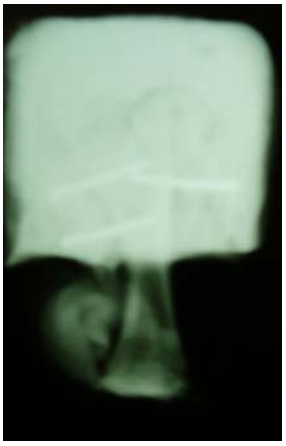

Figure F-4 Specimen 10 L post fracture

BIBLIOGRAPHY

1. Pierce M, Valdevit A, Anderson L, Inoue N, Hauser D 2000 Biomechanical Evaluation of Dual-Energy X-Ray Absorptiometry for Predicting Fracture Loads of the Infant Femur for Injury Investigation: An In Vitro Porcine Model. J of Ortho Trauma **14**(8)**:**571-576.

2. 1995 A Nation's Shame: Fatal Child Abuse and Neglect in the United States. U.S. Advisory Board on Child Abuse and Neglect, fifth report, pp 23-26.

3. 2002 Child Maltreatment 2002: Summary of Key Findings. National Clearinghouse on Child Abuse and Neglect Information, pp 1-2.

4. 2002 Child Abuse and Neglect Fatalities: Statistics and Interventions. National Clearinghouse on Child Abuse and Neglect Information.

5. O'Niell Jr J, Meacham W, Griffin P 1973 Patterns of Injury in Battered Child Syndrome. J of Trauma **12:**332.

6. Leonidas J 1983 Skeletal Trauma in the Child Abuse Syndrome. Pediatr Ann **12:**875-881.

7. Leventhal J, Thomas S, Rosenfield N, Markowitz R 1993 Fractures in Young Children: Distinguishing Child Abuse from Unintentional Injuries. Am J Dis Child **147:**87-92.

8. Loder R, Bookout C 1991 Fracture Patterns in Battered Children. J of Ped Orthop **5:**428-433.

9. King J, Diefendorf D, Apthorp J, Negrete V, Carlson M 1988 Analysis of 429 Fractures in 189 Battered Children. J of Ped Orthop **8:**585-589.

10. Herndon W 1983 Child Abuse in a Military Population. J of Ped Orthop **3:**73-76.

11. Galleno H, Oppenheim W 1982 The Battered Child Syndrome Revisited. Clin Orthop **162:**11-19.

12. Worlock P, Stower M, Barbor P 1986 Patterns of Fractures in Accidedntal and Non-accidental Injury in Children: A Comparative Study. Br Med J **293:**100-102.

13. Wellington P, Bennet G 1987 Fractures of the Femur in Childhood. Injury **18:**103-104.

14. Dalton H, Slovis T, Helfer R, Comstock J, Scheuer S, Riolo S 1990 Undiagnosed Abuse in Children Younger than 3 Years with Femoral Fracture. Am J Dis Child **144:**875-878.

15. Gross R, Stranger M 1983 Causative Factors Responsible for Femoral Fractures in Infants and Young Children. J of Ped Orthop **3:**341-343.

16. Merten D, Radkowski M, Leonidas J 1983 The Abused Child: A Radiological Appraisal. Radiology **146:**337-381.

17. Calero J, Curiel M, Moro M, Carrascal M, Santana J, Avial M 2000 Speed of Sound, Bone Mineral Density and Bone Strength in Ooforectomized Rats. Europ Jour of Clin Inves **30**(3)**:**210-214.

18. Jarvinen T, Sievanen H, Kannus P, Jarvinen M 1998 Dual-Energy X-Ray Absorptiometry in Predicting Mechanical Characteristics of Rat Femur. Bone **22**(5)**:**551-558.

19. Ferretti J, Capozza R, Zanchetta J 1996 Mechanical Validation of a Tomographic (pQCT) Index for Noninvasive Estimation of Rat Femur Bending Strength. Bone **18**(2)**:**97-102.

20. Bramer J, Barentsen R, Elst M, Lange E, Patka P, Haarman H 1998 Representative Assessment of Long Bone Shaft Biomechanical Properties: An Optimized Testing Method. J of Biomech **31:**741-745.

21. Mehta S, Antich P, Daphtary M, Bronson D, Richer E 2001 Bone Material Ultrasound Velocity is Predictive of Whole Bone Strength. Ultasound in Med & Biol **27**(6)**:**861-867.

22. Sarin V, Polefka E, Beaupre G, Kiratli B, Carter D, Meulen M 1999 DXA-Derived Section Modulus and Bone Mineral Content predict Long-Bone Torsional Strength. Acta Orthop Scandinav **70**(1)**:**71-76.

23. Pierce M, Bertocci G, Kambic H, Valdevit A 2001 Prediction of Pediatric Bone Strength Based on Radiographic Geometry and DEXA: An In Vitro Porcine Model for Infant Femur Fracture. Proceedings: Orthopaedic Research Society.

24. Stromsoe K, Hoiseth A, Alho A, Kok W 1995 Bending Strength of the Femur in Relation to Non-Invasive Bone Mineral Assessment. J of Biomech **28**(7)**:**857-861.

25. Koo M, Yang K, Begeman P, Hammami M, Koo W 2001 Prediction of Bone Strength in Growing Animals Using Noninvasive Bone Mass Measurements. Calcif Tissue Int **68:**230-234.

26. Lochmuller E, Lill C, Kuhn V, Schneider E, Eckstein F 2002 Radius Bone Strength in Bending, Compression and Falling and Its Correlation With Clinical Densitometry at Multiple Sites. J of Bone and Min Res **17**(9)**:**1629-1638.

27. Phillips C, Bradley D, Schlotzhauer C, Bergfeld M, Lebreros-Minotta C, Gawenis L, Morris J, Clarke L, Hillman L 2000 OIM Mice Exhibit Altered Femur and Incisor Mineral Composition and Decreased Bone Mineral Density. Bone **27**(2)**:**219-226.

28. Sirois I, Cheung A, Ward W 2003 Biomechanical Bone Strength and Bone Mass in Young Male and Female Rats Fed a Fish Oil Diet. Prostaglandins, Leukotrienes & Essential Fatty Acids **68:**415-421.

29. Camacho N, Raggio C, Doty S, Root L, Zraick V, Ilg W, Toledano T, Boskey A 2001 A Controlled Study of the Effects of Alendronate in a Growing Mouse Model of Osteogenesis Imperfecta. Calcif Tissue Int **69:**94-101.

30. Saban J, Zussman M, Harvey R, Patwardhan A, Scheider G, King D 1996 Heterozygous oim Mice Exhibit a Mild Form of Osteogenesis Imperfecta. Bone **19**(6)**:**575-579.

31. Beer F, Johnston E 1992 Mechanics of Materials, 2 ed. McGraw Hill, New York.

32. http://www.efunda.com 2004 Compression Members, vol. 2004. http://www.efunda.com/formulae/solid_mechanics/columns/intro.cfm.

33. Carter D, Hayes W 1977 The Compressive Behavior of Bone as a Two-Phase Porous Structure. J of Bone & Joint Surg **59-A**(7)**:**954-962.

34. Sturtz G 1980 Biomechanical Data of Children 24th Sapp Car Crash Conference. Society of Automotive Engineers, Inc., Troy, Michigan, pp 511-559.

35. Kress T, Porta D, Snider J, Fuller P, Peihogios J, Heck W, Frick S, Wasserman J 1995 Fracture Patterns of Human Cadaver Long Bones. IRCOBI**:**155-169.

36. An YH DR 2000 Mechanical Testing of Bone and the Bon-Implant Interface. CRC Press, New York.

37. Pierce M, Bertocci G, Vogeley E, Deemer E, Aguel F, Szczepanski J 2001 Result Fracture Types from Known Injury Mechanisms: Development of a Database for Identification of Potential Child Abuse Fractures. Pediatr Academ Soc Conf Proceedings.

38. Battaglia TC TA, Taylor EA, Mikic B 2003 Ash Content Modulation of Torsionally Derived Effective Material Properties in Cortical Mouse Bone. J of Biomech Eng **125:**615-619.

39. Lochmuller EM LC, Kuhn V, Schneider E, Eckstein F 2002 Radius Bone Strength in Bending, Compression and Falling and Its Correlation with Clinical Densitometry at Multiple Sites. J of Bone & Min Res **17**(9)**:**1629-1638.

40. Carter DR HW 1977 The Compressive Behavior of Bone as a Two-Phase Porous Structure. J of Bone & Joint Surg **59-A**(7)**:**954-962.

41. Lundin O, Ekstrom L, Hellstrom M, Holm S, Sward L 2000 Exposure of the Porcine Spine to Mechanical Compression: Differences in Injury Pattern Between Adolescents and Adults. Eur Spine J **9:**466-471.

42. Kitaoka K, Furman B, Saha S 1998 Periosteum: Its Biomechanical Role in Bone Fracture. Proceedings: North American Congress on Biomechanics.

43. Center J, Nguyen T, Pocock N, Eisman J 2004 Volumetric Bone Density at the emoral Neck as a Common Measure of Hip Fracture Risk for Men and Women. J of Clin Endocrin & Metab **89**(6)**:**2776-2782.